All-Optical Signal processing using Highly Nonlinear Photonic Crystal Fiber

Andersen, Peter Andreas; Jeppesen, Palle; Peucheret, Christophe; Clausen, Anders

Publication date:
2006

Document Version
Også kaldet Forlagets PDF

All-Optical signal processing using highly nonlinear photonic crystal fiber

Peter Andreas Andersen

Delivery Date
17^{th} of May 2005

Research Center COM
Technical University of Denmark
Building 345V
2800 Kgs. Lyngby
DENMARK

Contents

Resumé

Denne afhandling studerer optisk signal processering ved hjælp af ulineære fotonisk krystal fiber (UFKF). Studiet er fokuseret på at benytte UFKF i optiske komponenter som bølgelængde konverter, regeneratorer og en undersøgelse af superkontinuum generation og dets brug i et komplet optisk kommunikations system.

Dispersions indflydelse på generationen af et superkontinuum centreret omkring 1550 nm er undersøgt. Forskellige værdier af dispersion er eksperimentelt testet når et superkontinuum skabes. Ved at benytte forskellige UFKF, forskellige superkontinuum er opnået, hvor det bredeste har en 20 dB båndbrede på 210 nm centreret omkring telekommunikations regionen.

Et superkontinuum er genereret og spektralt filtreret til fem kanaler, hvor hver kanal er moduleret til 10 Gbit/s før signalerene er transmitteret over 5.6 km transmissions krystal fiber. De fem kanaler er desuden i et andet eksperiment transmitterede over 2×44 km dispersions kompenseret standard single mode fiber spoler. Bit fejl målinger er udført.

Et bølgelænge konverterings eksperiment af et optisk klokke signal er udført ved hjælp af superkontinuum generation. Superkontinuet er spektralt skåret ved hjælp af et tunebaret optisk bånd pas filter, der både dækker C og L båndet.

En fuldstændig optisk 3R-regenerator, der virker ved 80 Gbit/s og 160 Gbit/s er undersøgt. Regenerationen er udført i en opsætning bestående af tre NOLMer, der alle benytter ulineære fibre som det ulineære medium.

Komplet optisk bølgelængde konvertering ved hjælp af fire bølge blanding (FBB) i en UFKF er blevet undersøgt. Et bølgelængde konverterings eksperiment af et 40 Gbit/s RZ-DPSK signal er blevet udført.

Bølgelængde konvertering over 31 nm med en konvertering effekt, der er bedre end -21 dB blev observeret.

Bølgelængde konvertering ved hjælp af FBB i en UFKF af 6×40 Gbit/s DPSK signal præsenteres. En konversions effektivitet der er bedre end -21 dB er opnået. En modtager effekt forringelse for alle 6 kanaler er målt - foringelserne variere men alle er mindre end 4.1 dB.

Et bølgelængde konverterings eksperiment af et 80 Gbit/s RZ-DPSK-ASK signal præsenteres. Signal bit raten er opnået ved hjælp af 40 Gbit/s udstyr. Signalet er bølgelængde konverteret ved hjælp af FBB in en UFKF.

Det er yderligere vist hvordan en UFKF virker som en optisk fase konjugator, hvor det sledes tillades at transmittere et 40 Gbit/s signal over 5.6 km transmissons krystal fiber. Uden optisk fase konjugation er transmissionen ikke mulig på grund af den høje dispersionen i transmission krystal fiberen.

To metoder til at karakterisere en fiber er diskuteret. En metode til måling af dispersion i korte fiber stykker og en metode til måling af ulinearitets koefficienten af en fiber er vist. Begge teknikker benyttes til at karakterisere krystal fibre.

Det er således vist i denne afhandling hvordan UFKF kan benyttes i forskellige optiske komponenter i et komplet optisk system. UFKF med forskellige ulineære koefficienter og dispersions profiler er benyttet og evalueres.

Acknowledgements

I would first of all thank my supervisors, Palle Jeppesen, Christophe Peucheret, Anders T. Clausen and Claus Friis, for great support and letting me follow my dreams. The doors have always been open when I needed it.

The systems Competence Area at Research Center COM has been a good place to perform this study, with great possibilities in the laboratories and with great help from my colleagues. I have enjoyed the company and friendship of past and present colleagues. Special thanks goes to my office mates Pablo, Andrea and Michael for keeping the mood light and always being helpful. Found memories also go to Leif, Jorge and Christophe for the trips to conferences in various parts of the world.

I would also like to thank all the colleagues that I have had cooperation with both in the systems group and at the University of Aarhus. I have enjoyed working with you all, Yan, Beata, Torker, Michael, Henrik, Jacob, Karen Marie and Christophe. I would also like to thank Mirco for choosing the systems group and coming to Denmark to do research. I enjoyed our time watching football.

I would also like to thank Kim at Crystal Fibre A/S for supplying the fibers.

Thank you for the good company in the Fridays bar when I finally showed up.

Peter Andreas Andersen
May 17, 2005

Ph.D. Publications

The following publications have resulted from this Ph.D. project.

[1] Y. Geng, P. A. Andersen, T. Tokle, C. Peucheret and P. Jeppesen, "Wavelength conversion of a 6 40 Gb/s DPSK WDM signal using FWM in a highly non-linear photonic crystal fiber, in *Proceedings European Conference on Optical Communication, ECOC05*, Glasgow, Scotland, U.K., paper Tu3.3.4, vol. 2, pp. 205-206, 2005.

[2] Y. Geng, P. A. Andersen, T. Tokle, C. Peucheret, and P. Jeppesen, "Broadband wavelength conversion of a 40 Gbit/s RZ-DPSK signal using dispersion flattened highly nonlinear photonic crystal fibre," in *Proceedings Optoelectronics and Communications Conference, OECC05*, Seoul, Korea, 2005, p. P1142.

[3] T. Tokle, P. A. Andersen, Y. Geng, B. Zsigri, C. Peucheret, and P. Jeppesen, "Generation, transmission and wavelength conversion an 80 Gbit/s RZ-DBPSK-ASK signal," in *Proceedings Conference on Lasers & Electro-Optics*, Baltimore, Maryland, USA, 2005, p. CMQ4.

[4] M. Scaffardi, P. A. Andersen, L. K. Oxenløwe, D. Larsson, K. Yvind, P. Jeppesen, A. Bogoni, P. Ghelfi, and L. Potì, "Experimental characterisation of a highly non-linear fibre based 3-stage NOLM scheme for regeneration at 160 Gb/s," in *Proceedings European Conference on Optical Communication, ECOC'04*, vol. 3, Stockholm, Sweden, September 2004, pp. We4.P.030, 530–531.

[5] M. Scaffardi, P. A. Andersen, L. K. Oxenløwe, M. Galili, D. Larsson, K. Yvind, P. Jeppesen, A. Bogoni, P. Ghelfi, and L. Potì, "Perfor-

mance evaluation of a highly non-linear fibre based NOLM for regeneration up to 160 Gb/s," in *Proceedings IEEE Laser and Electro-Optics Society Annual Meeting*. Puerto-Rico: LEOS'04, 2004, pp. ThBB4, 979–980.

[6] P. A. Andersen, T. Tokle, Y. Geng, C. Peucheret, and P. Jeppesen, "Wavelength conversion of a 40 Gbit/s RZ-DPSK signal using four-wave mixing in a dispersion flattened highly nonlinear photonic crystal fiber," *IEEE Photonics Technology Letters*, vol. 17, no. 9 pp. 1908–1910, 2005.

[7] P. A. Andersen, B. Zsigri, C. Peucheret, P. Jeppesen, K. P. Hansen, and M. Dybendal Nielsen, "Photonic Crystal Fibers used in a Multi-Wavelength Source and as a Transmission Fiber in a WDM system," in *Proceedings Conference on Lasers & Electro-Optics*. CLEO, May 2004.

[8] C. Peucheret, B. Zsigri, P. Andersen, K. Berg, A. Tersigni, P. Jeppesen, K. P. Hansen, and M. D. Nielsen, "40 Gbit/s transmission over photonic crystal fibre using mid-span spectral inversion in highly nonlinear photonic crystal fibre," *Electronics Letters*, vol. 39, no. 12, pp. 919–921, 2003.

[9] P. A. Andersen, C. Peucheret, K. M. Hilligsøe, K. S. Berg, K. P. Hansen, and P. Jeppesen, "Supercontinuum generation in a photonic crystastal fibre using picosecond pulses at 1550 nm," in *5th International Conference on Ttansparent Optical Networks*, vol. 1, Warsaw, Poland, June 2003, p. Mo.C1.6.

[10] L. K. Oxenløwe, A. I. Siahlo, P. A. Andersen, K. S. Berg, A. T. Clausen, P. Jeppesen, K. P. Hansen, J. R. Folkenberg, K. Hoppe, and J. Hanberg, "Complete transmission system with a highly non-linear dispersion shifted photonic crystal fibre as the demultiplexer," in *Technical Digest Conference on Lasers and Electro-Optics, CLEO'03*, Baltimore, Maryland, U.S.A, 2003, p. CFJ1.

[11] C. Peucheret, B. Zsigri, P. A. Andersen, K. S. Berg, A. Tersigni, P. Jeppesen, K. P. Hansen, and M. D. Nielsen, "Transmission over

photonic crystal fiber at 40 Gbit/s using mid-span spectral inversion in a highly nonlinear photonic crystal fiber," in *Technical Digest Conference on Lasers and Electro-Optics, CLEO'03*, Baltimore, Maryland, U.S.A, 2003, pp. post–deadline paper CThPDB4.

[12] A. Siahlo, L. Oxenlowe, K. Berg, A. Clausen, P. Andersen, C. Peucheret, A. Tersigni, P. Jeppesen, K. Hansen, and J. Folkenberg, "A high-speed demultiplexer based on a nonlinear optical loop mirror with a photonic crystal fiber," *IEEE Photonics Technology Letters*, vol. 15, no. 8, pp. 1147–1149, August 2003.

[13] P. A. Andersen, H. N. Paulsen, and J. J. Larsen, "A photonic crystal fiber with zero dispersion at 1064 nm," in *Proceedings European Conference on Optical Communication, ECOC'02*, vol. 2, Copenhagen, Denmark, 2002, p. 3.4.6.

[14] P. A. Andersen, C. Peucheret, P. Jeppesen, K. P. Hansen, and J. R. Jensen, "Supercontinuum generation in a photonic crystal fiber around 1550 nm," in *Annual Meeting 2002 Danish Optical Society book of abstracts*. DOPS 2002, 2002.

List of acronyms

ASK	Amplitude Shift Keying
AWG	Arrayed Waveguide Grating
BER	Bit Error Rate
CW	Continuous Wave
DCF	Dispersion Compensating Fibre
DSF	Dispersion Shifted Fibre
EAM	Electro Absorption Modulator
ECMSL	External Cavity Mode-Locked Semiconductor Laser
EDFA	Erbium Doped Fibre Amplifier
ERGO-PGL	Erbium-Glass Oscillator Pulse Generating Laser
FSK	Frequency Shift Keying
FWHM	Full-Width Half-Maximum
FWM	Four-Wave Mixing
GVD	Group Velocity Dispersion
HNL-PCF	Highly Nonlinear Photonic Crystal Fiber
HNLF	Highly Nonlinear Fiber
MLFRL	Mode-Locked Fibre Ring Laser

MMLL	Monolithic Mode-Locked Laser
MZ	Mach-Zehnder
NOLM	Nonlinear Optical Loop Mirror
NRZ	Non Return-to-Zero
OBPF	Optical Band-pass Filter
OOK	On-Off Keying
OSNR	Optical Signal-to-Noise Ratio
OTDM	Optical Time Division Multiplexing
PBG	Photonic Bandgap
PCF	Photonic Crystal Fiber
PD	Photo-Diode
pdf	Probability Density Function
PMD	Polarisation Mode Dispersion
PRBS	Pseudo-Random Binary Sequence
PWM	Power Meter
RZ	Return-to-Zero
RZ-DPSK	Return-to-zero Differential Phase Shift Keying
SBS	Stimulated Brillouin Scattering
SMF	Standard single Mode Fibre
SNR	Signal-to-Noise Ratio
SPM	Self-Phase Modulation
SRS	Stimulated Raman Scattering
TLS	Tunable Laser Source

WDM	Wavelength Division Multiplexing
XGM	Cross Gain Modulation
XPM	Cross-Phase Modulation

Chapter 1

Introduction

Since the discovery of transmission in optical fibers in 1970 optical communication has boomed. One of the first commercial steps towards an all-optical network was taken in 1988 when the first optical fiber was installed between Europe and America. Since then the telecommunication industry has been through a major economic boom and a crash and is now on the road to recovery.

Since the first installation of optical fibers between the continents several companies and network providers have installed more fibers leading to a massive increase in capacity. With the increased internet traffic through the 90'ties the demand for more capacity kept raising and network providers kept delivering. The bandwidth was supplied with the aid of the newest advances in research such as wavelength division multiplexing (WDM). WDM lead to an explosion in data capacity in one single fiber [1]. Instead of only transmitting one data signal in one fiber the possibility of transmission of several data signals in one fiber became a reality.

With the increase in capacity the network providers had supplied much more capacity than needed and a killer application using optical communication was needed in order for the continued growth in transmission capacity. Such an application was not found and the capacity supplied for optical communication was several times higher than needed. After all the investments companies had performed in order to deliver that massive capacity the lack of a killer application became a disaster for many companies and the telecommunication crash became a reality

[2]. An application and service that will make use of the huge bandwidth offered is still missing before further investment in optical fiber links are likely to be performed. The internet traffic keeps growing [3] and the future for the telecommunication industry looks bright.

The use of WDM demands a number of components since two signals can not occupy the same wavelength in the same WDM fiber link. Some of the components include wavelength converters, regenerators and switches. The data rate for commercial systems has been 2.5 Gbit/s or 10 Gbit/s per channel, but new and faster electronics has made it possible for vendors to get a channel rate as high as 40 Gbit/s [4]. The first commercial investment from networks vendors is still not performed.

Traditionally components such as wavelength converters and regenerators have been working using electronics hence converting the optical signal to an electronic signal for processing in the electrical domain. A traditional wavelength converter works by receiving the optical signal and transforming it to an electrical signal that is used to modulated an optical signal at the new wavelength. Likewise, a regenerator works by receiving the distorted optical signal and transforming it into an electrical signal that is used to modulate an undistorted optical signal.

The need for even higher channel bit rates in a WDM system has forced the channel bit rate into the range 80 to 160 Gbit/s. Since commercial electronic components do not work at these bit rates (May 2005) only all optical solutions will help avoid bottlenecks coursed by electronic processing. In the search of achieving all-optical components such as wavelength conversion and regenerators various different methods have been used [5]. One of the ways of obtaining all-optical signal processing has been by using nonlinear effects. Using HNLF is an attractive method for all-optical signal processing in modern optical communication systems.

1.1 Photonic crystal fiber and telecommunication

Photonic crystal fibers (PCF) have been the focus of increasing technical interest since the first working example was reported in 1996 [6, 7, 8]. PCFs have a unique microstructure consisting of an array of microscopic holes that runs along the entire length of the fiber. These holes act as an optical barrier for light within the central core (either hollow or made

of solid glass) and makes guiding light in the core a possibility. The holes can range in diameter from $\sim$ 25 nm to $\sim$ 50 μm [8]. Most PCFs are constructed of pure silica but using polymers [9] and non-silica glass [8] has been shown, although that will not be investigated in the work presented.

PCF supports two guiding mechanisms. Total internal reflection, in which case the core must have a higher average refractive index than the cladding. Another guiding mechanism is a two-dimensional photonic bandgap (PBG), where the index of the core is uncritical, it can be hollow or filled with material [8]. PCFs guiding by the PBG effect has contributed to the field of gas based nonlinear optics. Using a hollow core fiber and filling the core with a gas supply a long interaction length between the light and the gas and increases the effectiveness of the experiments considerably.

The design of PCF made the fabrication a challenge since no helpful precedent existed. A stack of glass tubes are arranged in the pattern of the PCF design before drawing the fiber. The preform is heated and a fiber can be drawn on to a spool [8]. A schematic of the drawing process is seen in figure 1.1.

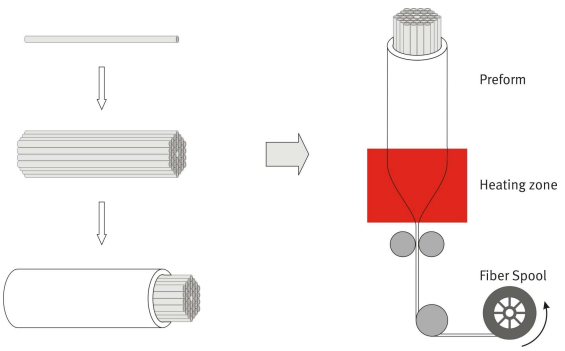

Figure 1.1: A schematic of the drawing process. Glass tubes are ordered in the appropriate pattern and inserted into the preform (The figure is supplied by Kim P. Hansen at Crystal fibre A/S).

This stack and draw method provides a high degree of freedom in the design of a PCF. Doping in the fiber can be achieved by using doped

glass tubes in the drawing of a fiber. HNL-PCFs can be achieved by this method of drawing.

HNL-PCFs have been used in various experiments such as investigation of supercontinuum generation [10, 11], as well as using a supercontinuum in an optical communication system [12, 13]. Other nonlinear effects have also been investigated in PCFs and used in optical communication systems such as wavelength conversion using FWM [14] and as part of an optical demultiplexer for optical time division multiplexing (OTDM) systems [15]. HNL-PCF used in telecommunication networks is a new field of research and a number of related research areas have only been scratched, so further investigation is needed.

1.2 Structure of the Thesis

The work presented in this thesis concentrates on HNL-PCF applications in optical communication systems. The work is focused on experimental results using HNLF or HNL-PCF in all optical components in system experiments. The components and key building blocks focused on in this thesis are all optical wavelength conversion, all optical regeneration and the use of supercontinuum generation in modern all optical communication systems.

In Chapter 2 methods of measuring the dispersion and the nonlinear coefficient are discussed and results obtained from different PCFs are shown. In modern optical communication systems dispersion management and nonlinearities are difficult to completely separate due to the intensity dependence of the refractive index of silica. Erbium doped fiber amplifiers (EDFAs) are often used to amplify the signal, whereby fiber nonlinearities are introdued in the system. In designing fibers for optical systems different aspects of the fiber can be emphasized. A number of different fiber types exists, SMF, dispersion compensating fiber (DCF) and HNLF just to mention a few used in this thesis. The work reported in this chapter is performed in cooperation with Christophe Peucheret, Henrik Nørregaard Poulsen and Jacob Juul Larsen.

In Chapter 3 the use of supercontinuum generation in system experiments is investigated. Supercontinuum generation has the potential of being a cheap solution to a multi-wavelength pulse source for WDM systems. Supercontinua generated by different HNL-PCF are shown. The depen-

dence of dispersion profile of the HNL-PCF when generating a supercontinuum spectrum is also discussed. An experiment showing a HNL-PCF as the medium for a WDM source and the comparison of two different HNL-PCFs with respect to which is best suited as a source for WDM systems is performed. Supercontinuum generation as a wavelength converter of optical clock signals is also mentioned. The experimental work done in this chapter was done with assistance from Beata Zsigri and Christophe Peucheret.

In Chapter 4 all optical regeneration and all optical demultiplexing experiments are reported. The fibers used in this chapter are mainly HNLFs. An all optical regenerator based on three NOLMs is tested. An evaluation of a HNLF in a NOLM is also performed. The work is performed in cooperation with Mirco Scaffardi, Leif Oxenløwe and Michael Galili.

In Chapter 5 an extensive study of HNL-PCF used to wavelength convert DPSK signals is presented. Both wavelength conversion of single channel and of multi-channel signals are studied. A combination of different modulation formats and all optical wavelength conversion is also studied. All optical wavelength conversion of DPSK using a HNL-PCF is shown. An experiment using a HNL-PCF as an optical phase conjugator in a complete crystal fiber system is also discussed. The work done in this chapter is performed in cooperation and assistance by Yan Geng, Torker Togler, Beata Zsigri and Christophe Peucheret.

Chapter 6 concludes the thesis.

Chapter 2

Photonic Crystal Fiber properties

2.1 Introduction

PCF technology has come a long way since the discovery of the PBG effect in 1987 [16, 17]. PCFs have been associated with two different ways of guiding light, namely the PBG effect and the more traditional total internal reflection technique. The PCFs used in this thesis do all guide light according to the same principle as step index or graded index fibers, namely total internal reflection. The PCFs can therefore be considered as a new variation to step index fibers with the possibility of having large differences between the index of refraction in the core and the effective index of refraction of the cladding. All the investigated PCFs have a solid core (as opposed to air core).

This chapter consists of two sections. In both sections methods of measuring fiber characteristics are described.

The first section describes a low coherence method suitable for measuring dispersion on a short length of fiber. Dispersion measurement obtained on PCFs are shown. The second section describe a method of measuring the nonlinear coefficient of a fiber based on the nonlinear phase shift induced through self phase modulation (SPM). Experimental results using the method are also shown.

2.2 Dispersion measurements

The dispersion of a fiber is an important parameter to know if fiber experiments are to be made. Different fiber types possess different dispersion profiles for example constant with wavelength, negative or positive over all wavelengths [18, 19], just to name a few. The zero dispersion wavelength of a fiber can also vary depending on the fiber and is also an important parameter to know. With the development of PCF technology the zero dispersion wavelength of a fiber can now be located between 700 nm to 1550 nm [20, 19]. Dispersion measurements are therefore an important measurement in the characterization of fiber properties.

A number of different methods are used to measure dispersion [21, 22, 23, 24, 25]. The advantage of the one described in this section is that it is a one shot technique. A single path length scan of light is all that is needed to obtain the dispersion profile in a range covering 1100 nm. Both part of the visible spectrum and part of the infrared spectrum are achieved. The dispersion is only measured on a short piece of fiber about 25 mm long. The zero dispersion wavelength and the dispersion profile can change slightly during the drawing process. The assumption that the dispersion of the fiber does not change during the drawing process has to be accommodated for the measurement of the dispersion in a short piece of fiber to be identical to the dispersion of the entire spool.

2.2.1 Experimental setup for dispersion measurements

The experimental setup used to measure dispersion is a white light interferometer [21] built at the University of Aarhus. A sketch of the apparatus is seen in figure 2.1.

White light from a halogen light bulb is transported to a Mach-Zehnder interferometer through a standard optical fiber and collimated by a microscope objective. Before the light is input to the beam-splitter at the input of the interferometer, the beam is sent through a polarizer. In one of the interferometer arms the light is coupled through a short piece of fiber (typically 25 mm) using microscope objectives. The dispersion in the microscope objectives is compensated with a block of glass in the reference arm. A translation stage provides control of the optical delay. The optical delay is calibrated with a Mach-Zehnder HeNe interferometer (not shown) overlaying the white light interferometer. The white light

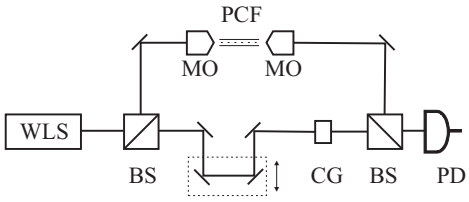

Figure 2.1: Schematic of the experimental setup. WLS: white light source, BS: beam-splitter, MO: microscope objective, CG: compensating glass, PCF: photonic crystal fiber, PD: photo-detector.

interferograms (intensity as a function of delay) are recorded using two photo-detectors and lock-in detection. The visible part of the spectrum is measured with a silicon avalanche photo-detector whereas the infrared part is covered with an InGaAs photodiode. With these two detectors the wavelength range 500-1700 nm can be covered. Experimentally, interferograms with and without the fiber present are recorded. By Fourier transforming the interferograms, the spectrum and relative phase of the spectral components of the white light is found. The phase imposed on the white light by passing through the fiber is found by substraction of the two data sets. The phase is fitted to a polynomial and the fitting coefficients are directly related to the dispersion of the fiber [21]. When evaluating the measurements, short pieces of fiber from both ends of the PCF spool are used in order to check the uniformity of the dispersion profile.

2.2.2 Dispersion results

The photonic crystal fiber investigated is made from fused silica. A scanning electron microscope (SEM) picture of the central region of the fiber is shown in the inset of Figure 2.2. The core diameter is D = 5.8 μm and the surrounding air-holes have a diameter of d = 1.1 μm with an inter-hole spacing (pitch) of 2.5 μm.

To test the fiber for single mode operation, a short piece of the fiber is placed in the interferometer and a HeNe laser is used as the light source. A resulting clear interference pattern with high fringe visibility indicates that only a single mode has been excited in the fiber [9].

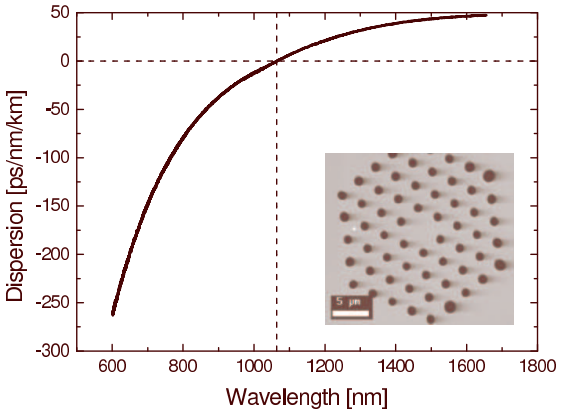

Figure 2.2: Measured dispersion profile of the investigated PCF. The zero dispersion wavelength is 1064 nm. The inset shows a SEM picture of the PCF central cross section.

Figure 2.2 shows the measured dispersion curve. The zero dispersion wavelength is found to be 1064 nm with an uncertainty of ±3 nm. In the telecommunication region at 1550 nm the dispersion is 46 ps/(nm·km). In the visible region the dispersion is dominated by material dispersion [26]. By rotating the polarizer in front of the interferometer the dispersion dependence on polarization of light is measured. Throughout the entire IR region and well into the visible the dispersion profiles along the two axes are identical within the experimental uncertainty.

A zero dispersion wavelength of 1064 nm indicates that this fiber is well suited for generating a nonlinear response when pumped with a Nd:YAG laser (e.g. at 1064 nm). Slight modifications of the fiber design can allow for a fiber with the same dispersion properties but with either a smaller or a larger core. A smaller core will increase the intensity of the light in the fiber thus enhancing the nonlinear response whereas a larger core will decrease the nonlinear response and making the fiber useful for other purposes i.e. transportation of pulses from mode-locked Yb fiber lasers with a minimum influence from dispersion.

Figure 2.3 shows the dispersion of a fiber with slightly different design parameters. The core diameter is D = 5.6 μm and the surrounding air-hole diameter is d = 1.25 μm with a pitch of 3.0 μm. The zero dispersion

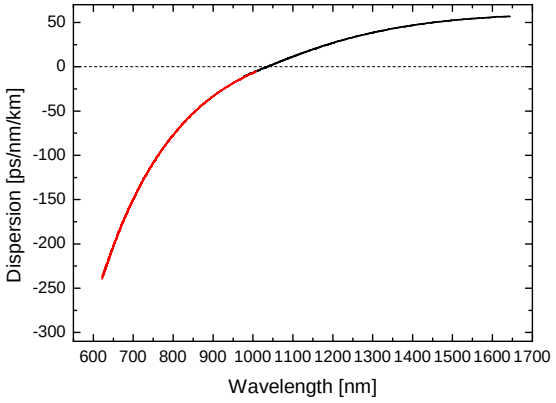

Figure 2.3: Measured dispersion profile of PCF with zero dispersion wavelength at 1035 nm.

wavelength is found to be 1035 nm with an uncertainty of 4 nm. The fiber is again tested for single mode operation using a HeNe laser. This fiber is also found to be single mode operated.

A slight difference between the two states of polarization is observed below 750 nm. Figure 2.4 shows the polarization dependence of the fiber piece for short wavelengths. It can be seen from the figure that the dispersion changes depending on the polarization of the light by as much as 48 ps/(nm·km) or 18 % at 600 nm. The figure shows the biggest dispersion difference when changing the polarization of the light.

The uncertainty of the measurements are mostly dependent on the measurement of the length of the fiber. This measurement is done by a normal measuring stick and can therefore only be precise within 1 mm.

2.2.3 Conclusion on dispersion measurements

The dispersion profiles obtained when investigating both ends of the fiber show good agreement of the results and suggest that the drawing of the PCF is performed under uniform conditions with no significant changes to the dispersion profile. The method used is a reliable and efficient way of obtaining the dispersion of a short length of fiber over a wide wavelength range. The fact that two photodiodes are used to cover the range

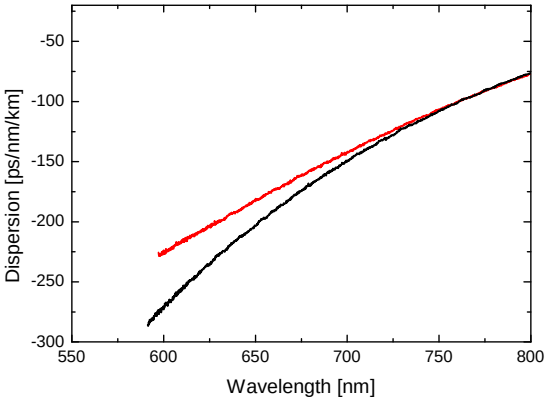

Figure 2.4: Measured dispersion profile and polarization dependence in the range 550 nm to 800 mn. The zero dispersion wavelength is 1035 nm.

from 500-1700 nm the method obtain dispersion results over a 1100 nm wavelength range. Two PCFs with the same structure, but with slightly different core diameter, pitch and air-hole diameter of the surrounding holes have been tested and their dispersion profiles obtained. The zero dispersion wavelengths for the two PCFs tested is found to be 1064 nm and 1035 nm.

2.3 Non-linear coefficient measurements

Nonlinear coefficient measurements are reported in this section. The method used for the measurements of the nonlinear coefficient is described in [27, 28].

The method is based on measuring the nonlinear phase shift induced through self phase modulation (SPM). Two continuous wave (CW) lasers form the pump signals and by assuming negligible dispersion in the nonlinear fiber the nonlinear phase shift of the pump signal when propagating along the fiber can be expressed as

$$\phi_{SPM} = \frac{2\omega_0}{c}\frac{n_2}{A_{eff}}L_{eff}P_{in} = 2\gamma L_{eff}P_{in} \tag{2.1}$$

where P_{in} is the total power of the signal into the fiber, L_{eff} is the effec-

tive length of the fiber, n_2 is the nonlinear refractive index, A_{eff} is the effective mode area and γ is the nonlinear coefficient. In obtaining the nonlinear coefficient, the nonlinear phase shift is measured as a function of fiber input power. The nonlinear phase shift is measured in the spectral domain by considering the electric field and Fourier transforming it. The intensities of the two pump signals and SPM (FWM) products are measured on an optical spectrum analyzer. Only the first order sidebands of the SPM product and the original pump signals are used when obtaining the phase shift given by

$$\frac{I_0}{I_1} = \frac{J_0^2(\phi_{SPM}/2) + J_1^2(\phi_{SPM}/2)}{J_1^2(\phi_{SPM}/2) + J_2^2(\phi_{SPM}/2)} \tag{2.2}$$

where I_0 and I_1 are intensities of the zero- and first-order harmonics of the SPM process and J_n is the Bessel function of the n^{th} order.

The experimental setup is shown in figure 2.5. The polarization controller at the output of one the lasers is used to obtain the most intense first order sidebands. The EDFA delivers 18 dBm output power.

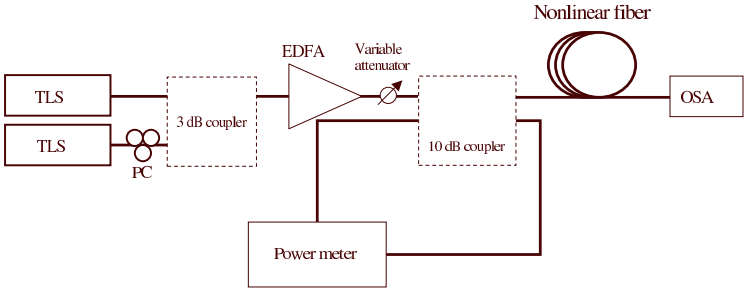

Figure 2.5: Experimental setup used to measure the nonlinear coefficient of a fiber. TLS: tunable laser source, PC: polarization controller, OSA: optical spectrum analyzer.

The power meter is calibrated to measure the input power to the nonlinear fiber and also monitor the backscattered light to detect possible occurrence of stimulated Brillouin scattering (SBS). The power of the two lasers are equalized at the input to the nonlinear fiber. The two lasers are tuned to 1549.668 nm and 1549.906 nm.

Since the splice loss in the fiber is not known the power at the input

Table 2.1: Measured nonlinear coefficient dependence on splice loss. Resolution bandwidth 0.05 nm.

splice loss (dB)/splice	0	0.3	0.5	1
γ_{13} ($W^{-1}km^{-1}$)	18.2	16.0	14.7	11.9
γ_{24} ($W^{-1}km^{-1}$)	19.6	17.3	15.9	12.8

of the PCF can be expressed as

$$P_{in} = SLP_{meas} \tag{2.3}$$

where SL is the splice and connector loss and P_{meas} is the measured power. The correct value of $2\gamma L_{eff}$ is still obtained if the slope of the phase shift ϕ_{SPM} vs SLP_{meas} curve is used.

$$\phi_{SPM} = 2\gamma L_{eff} P_{in} = 2\gamma L_{eff} SLP_{meas} \tag{2.4}$$

2.3.1 Results and discussion

The fiber investigated is a 50 m long PCF with a zero dispersion wavelength at 1552.5 nm and a dispersion slope of $S = -0.26$ ps/(nm^2·km) at 1550 nm. This fiber will be used extensively in chapter 3 for supercontinuum generation and in chapter 5 for optical phase conjugation of an optical signal.

Figure 2.6 shows the phase shift versus the measured finer input power (before splice). Two different sets of measurements are seen and they correspond to the zero and first order product so that the peaks marked 1 and 3 and the peaks marked 2 and 4 in figure 2.7 each form a data set.

The slope of the linear fit made in figure 2.6 determines the nonlinear coefficient. The nonlinear coefficient is determined by measuring intensities from an OSA. Table 2.1 show the nonlinear coefficients based on the measurements of intensity of the peaks when the input power to the fiber is changed.

Since the splice loss of the "pigtails" of the PCF is not known the table show the nonlinear coefficient of the fiber with different values of splice loss. It is clear that the PCF investigated is a highly nonlinear (HNL)-PCF. Without knowing the exact value of the splice loss a specific value for the nonlinear coefficient can not be extracted, but with a splice

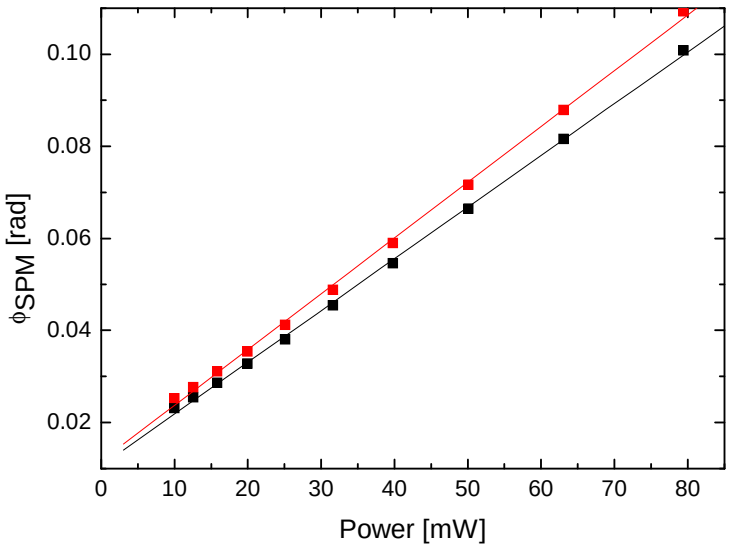

Figure 2.6: Phase shift as a function of the measured input power of the HNL-PCF.

loss of 0.3 dB [19] the nonlinear coefficient is found in the range 16 to 17.3 $W^{-1}km^{-1}$.

2.3.2 PCF with zero dispersion at 1064 nm

Nonlinear measurements have also been performed on the PCF with the dispersion curve shown in figure 2.2. The fiber is 66 m long and has a loss at 1550 nm of 8.5 dB. The two lasers are again tuned to 1549.668 nm and 1549.906 nm. Figure 2.8 shows the measured nonlinear phase shift for the PCF with zero dispersion wavelength at 1064 nm.

From the figure it can be seen that the measured points do not coincide with the linear fit. The linear fit is not appropriate for the calculation of the nonlinear coefficient based on the method described in this section. The assumption of zero dispersion in the fiber is clearly not satisfied in this case and a nonlinear coefficient can not be found.

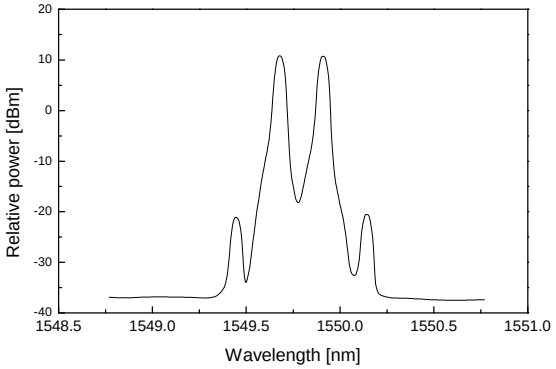

Figure 2.7: Measured OSA spectrum for 19 dBm total input power. The peaks are numbered so number 1 and 3 form one data set and 2 and 4 form another data set.

2.3.3 Conclusion of nonlinear coefficient measurements

A nonlinear coefficient measurement technique based on SPM in the fiber has been used to obtain the nonlinear coefficient of a 50 m long HNL-PCF. The nonlinear coefficient is found to be between 16 and 17.3 $W^{-1}km^{-1}$ if the splice loss in the fiber is 0.3 dB per splice. The method was also used in an attempt to measure the nonlinear coefficient of a 66 m long PCF with 46 ps/(nm·km) dispersion at 1550 nm. It was clear that the assumption of negligible dispersion at the wavelength of the pump used in measuring the nonlinear coefficient was not satisfied and therefore a value for the nonlinear coefficient could not be obtained.

2.4 Summary

In this chapter two methods for measuring fiber characteristics have been explained and used in order to obtain dispersion curves and nonlinear coefficient.

The method used for measuring the dispersion curve of a fiber is a low coherence method suitable for obtaining dispersion from 500 to 1700 nm. The technique covers a large wavelength region, but only measures the dispersion in a small piece of fiber ($\sim$ 25 mm). The method achieve good

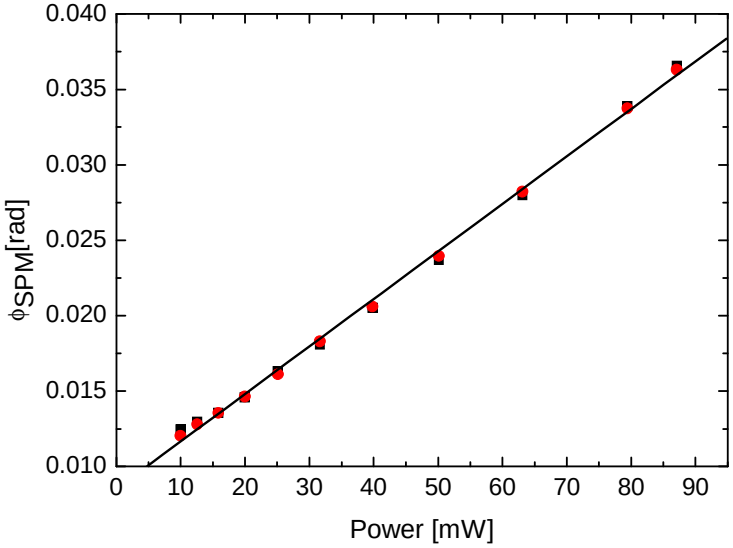

Figure 2.8: Measured nonlinear phase shift for the PCF with zero dispersion at 1064 nm. A linear fit is made but the measured points do not fit to a straight line.

results based on the assumption that the dispersion is the same for the entire fiber spool as for the 25 mm used. The method is therefore linked very closely to the drawing process of the fiber. If the drawing is stable then only a small piece of fiber will be enough to obtain the dispersion of the entire fiber spool. This can be difficult to satisfy for PCFs with small core dimensions.

A simple setup was used for measuring the nonlinear coefficient of a HNL-PCF. The method is based on the nonlinear phase shift experienced by the pump. The nonlinear phase shift is caused by SPM. In obtaining the nonlinear coefficient it is assumed that the dispersion of the fiber is negligible. A number of different fiber parameters play an important role in the characterization of a fiber like, the dispersion, the length and the dispersion slope. If the method described in this chapter for measuring the nonlinear coefficient is used then the zero dispersion wavelength of a fiber becomes an important parameter to know before characterizing the fiber in more detail.

Chapter 3

Supercontinuum generation in a HNL-PCF at 1550 nm and system applications.

3.1 Introduction

The generation of supercontinuum has been of interest for several reasons. First of all, it is not always clear what a supercontinuum is and which physical effects contribute to a supercontinuum [29]. A supercontinuum is a spectrum covering a large wavelength region with preferably uniform power distribution in the entire region. A supercontinuum can be applied in areas such as metrology [30], optical coherence tomography [31] or as a white light source.

Secondly, it is interesting to investigate its potential for use in an optical communication system. Supercontinuum generation has been proposed as a way to realize multi-wavelength pulse sources for WDM systems [32, 12, 33, 34]. The potential for a cheap multi-wavelength source has been the driving force behind the supercontinuum generation research in system experiments. One pulse source is used to generate a broad supercontinuum spectrum which in turn is sliced into several channels generating a WDM signal. The design of the fiber is an important part in achieving a broad supercontinuum and thereby which physical effects are responsible for the creation of the supercontinuum [35, 36].

In recent years supercontinuum has been used in system experiments for a number of different components such as a pulse source for WDM [13, 37, 12, 38], as a medium for wavelength conversion [39] and as part of an optical 3R-regenerator [40].

New advances in fiber technology have made it possible to manufacture HNL-PCF as well as dispersion flattened HNL-PCF to generate supercontinuum [19, 18]. The PCF technology allows a wide freedom in the design of the fiber. It is possible to change the zero dispersion wavelength from ∼700 nm [41, 42] to telecommunication wavelength ∼1550 nm [18, 19] and the dispersion profile as well as the nonlinear coefficient of the HNL-PCF. All these degrees of freedom allow for a very unique fiber design and the possibility of fulfilling very strict demands on the fiber.

The many design degrees of freedom of PCF have resulted in a number of speciality fibers with i.e. large core ($> 20\mu m$), endlessly single mode and small core ($\sim 1\mu m$) fibers. Due to the many possible designs of PCF they are believed to be able to contribute significantly to the supercontinuum generation area of research.

Before even considering what a supercontinuum can contribute to in a telecommunication system [5], basic demands on the properties of the supercontinuum must be identified. The most important demand is the stability of the supercontinuum. Furthermore a set of practical limitations for supercontinuum generation, the medium in which the supercontinuum is generated, i.e. a fiber or a crystal, should be compatible with fiber optical technology, e.g. spliced to connectorized fiber pigtails. The average power demanded for the generation of a supercontinuum should be of the order 25-30 dBm.

In this chapter a study of supercontinuum generation and its use in optical communication systems are presented. First a brief overview of the physical mechanisms responsible for supercontinuum generation is given.

The experiments in this chapter have been done according to four major principles. The use of laser sources with telecommunication wavelengths around 1550 nm, the use of picosecond pulses at a repetition rate of 10 GHz or above, the use of relatively low average power of ∼30 dBm for the generation of the supercontinuum and compatibility of the medium where supercontinuum is generated with fiber optics tech-

nology. These principles constitute minimum requirements for a supercontinuum to function in a telecommunication system.

An experimental characterization of supercontinuum generation using a HNL-PCF with different dispersion values of the fiber at the pump wavelength is also presented.

The use of supercontinuum in system experiments as a WDM source and as a medium for wavelength conversion are reported. The demands imposed on a supercontinuum for it to work in an optical system is discussed. A comparison of two HNL-PCFs with different dispersion profiles and the generated supercontinuum used as a WDM source is performed.

3.1.1 Overview of supercontinuum generation

In recent years many studies have attempted to develop a theory for supercontinuum generation [43, 20, 10, 42, 44, 41, 11, 45]. A big part of the work has been focused on using femto-second pulses with a temporal width of 100 fs or smaller, and a repetition rate up to 1 GHz. The experiments and simulations performed have typically been using PCFs with a zero dispersion wavelength between 600 nm and 1000 nm [8, 20, 46].

It is found that supercontinuum generation both depends on the parameters of the input pulses (temporal width and peak power) and the parameters of the PCF (dispersion profile, effective modal area and birefringence)[46, 47]. The optical nonlinear processes contributing to the generation of a supercontinuum can be divided into two categories photon-photon interactions and photon-phonon interactions. For the photon-photon interactions no energy exchange occurs between the medium and the photon and the processes include SPM, XPM, FWM [48] and third harmonic generation [48] with the two latter requiring phase matching to be efficient. The photon-phonon interaction leads to energy exchange between the medium and the photon. Such effects include SRS and SBS [48].

In recent years there has been much investigation into which effects are responsible for the creation of supercontinuum [49, 46, 35]. The creation of a supercontinuum depends on a number of parameters such as the length and nonlinear coefficient of the fiber. That makes a general theory on supercontinuum generation a difficult task that still remains [29]. Many of the studies are using pulses with femto-second pulse width

and repetition rate of the laser in the MHz region far from the demands set forth by telecommunication systems.

Several studies [47, 46] have tried to explain the optics behind supercontinuum generation and all of them have found that the dispersion profile of the fiber plays an important role in determining which effects contribute to the creation of a supercontinuum.

A lot of work has been put into making a reliable simulation [11] of a supercontinuum in the positive dispersion domain and many [47, 50, 49, 46] believe that soliton decay is an important effect to take into account in some cases. Another process is SRS which is not so effected by the dispersion of the fiber [44].

This section is split into two parts namely pumping in positive and negative dispersion regions.

Pumping in positive dispersion region

A very general explanation of what happens when pumping with ∼100 fs pulses in the positive dispersion region of a PCF relies on soliton decay [50]. At the input of the fiber the pulse corresponding to a N^{th} order soliton is compressed by SPM. The perturbation of this N^{th} order soliton by SRS and higher order dispersion leads to breaking up of the N^{th} order soliton into multiple 1^{st} order (fundamental) solitons. That process is called soliton decay [49, 46].

N is an integer given by [48]:

$$N^2 = L_D/L_{NL} = \gamma P_0 T_0^2/|\beta_2| \tag{3.1}$$

where L_D and L_{NL} are the dispersion length and nonlinear length, respectively. P_0 is the peak power, T_0 is the temporal width, γ is the nonlinear coefficient and β_2 is the second derivative with respect to frequency of the propagation constant in the Taylor series of the dispersion.

Increasing the pulse width but keeping the energy constant changes the creation of the supercontinuum and the effects mostly responsible for the generation. The soliton N-value increases with the pulse width (T_0) leading to the splitting of the input pulse into more 1^{st} order solitons. They have broader temporal widths which results in a decrease of the interaction between the soliton and the Raman gain from the SRS process [50] leading to a more narrow supercontinuum spectrum.

Using pico- or nano-second pulses for the generation of a supercontinuum the peak power of the pulses are often much lower and SRS, FWM and SPM [42, 44, 51] are the major contributors to supercontinuum generation.

Pumping in negative dispersion region

When pumping in a negative dispersion region the process generating supercontinuum is different from the process when pumping in a positive dispersion region [52]. Solitons are not able to propagate in the normal dispersion region [48]. The supercontinuum generation is due to SPM and SRS processes. Since SPM is the driving effect behind the generation of supercontinuum, the change of pulse width and energy will also change the supercontinuum spectrum. When a broader pulse with the same average power is used it will result in smaller peak power of the input pulse and the spectrum broadened by SPM becomes more narrow which transfers into a more narrow supercontinuum spectrum [53]. The opposite happens if the pulse width is kept constant, but the average power is increased. The spectrum based on SPM will broaden and the same will happen to the supercontinuum spectrum due to higher peak power of the pulse.

3.2 Characterization of supercontinuum

Due to the fact that supercontinuum generation has a strong dependence on the dispersion of the fiber [35] several different pump wavelengths have been used in order to investigate the different supercontinuum spectra that can be generated.

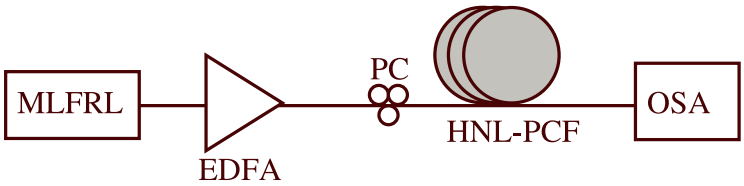

Figure 3.1: Experimental setup used to characterize supercontinuum. MLFRL: mode locked fiber ring laser, EDFA: Erbium doped fiber amplifier, PC: polarization controller, OSA: optical spectrum analyzer.

Figure 3.1 shows the setup used in the characterization of supercontinuum generation in a HNL-PCF. The laser used is a mode locked fiber ring laser (MLFRL) generating pulses with a FWHM equal to 2.9 ps. The EDFA delivers an output power of up to 30 dBm. A polarization controller is placed before the HNL-PCF to control the polarization of the light since the HNL-PCF is birefringent. The output from the HNL-PCF is recorded using an optical spectrum analyzer (OSA). One polarization state of the light is chosen and not changed as the average input power to the fiber is increased.

The laser is tuned to several different wavelengths around the zero dispersion wavelength of the fiber in order to determined the effect dispersion has on supercontinuum generation.

3.2.1 Fiber parameters

The HNL-PCF is 50 m long and has a nonlinear coefficient, $\gamma = 18\text{W}^{-1}\cdot\text{km}^{-1}$, and the birefringence is estimated to 1.1×10^{-4} [19]. Figure 3.2 shows the dispersion curve of the HNL-PCF where it is seen that the zero dispersion wavelength is at 1552.5 nm. The inset shows a microscopic picture of the cross section of the fiber. The HNL-PCF has a negative dispersion slope of $S = -0.26$ ps/(nm^2·km) at 1550 nm.

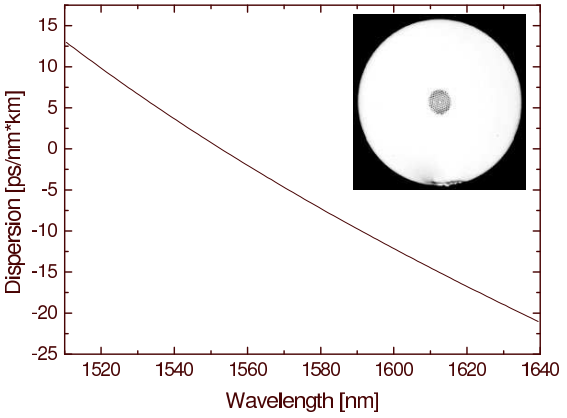

Figure 3.2: Dispersion of the 50 m long HNL-PCF with zero dispersion wavelength at 1552.5 nm. The inset shows a microscopic picture of the HNL-PCF.

3.2.2 Supercontinuum generation characterization results

In attempting to explain the supercontinuum spectra several different variables have to be considered like the wavelength of the pump, the pulse width and the peak power as well as the chirp of the pulse [54]. The different spectra can be divided into two categories according to pumping in the positive or negative dispersion region of the fiber.

Pumping in the positive dispersion region

When the pump is placed at wavelengths shorter than 1552.5 nm it is considered pumping in the positive dispersion region as seen from figure 3.2.

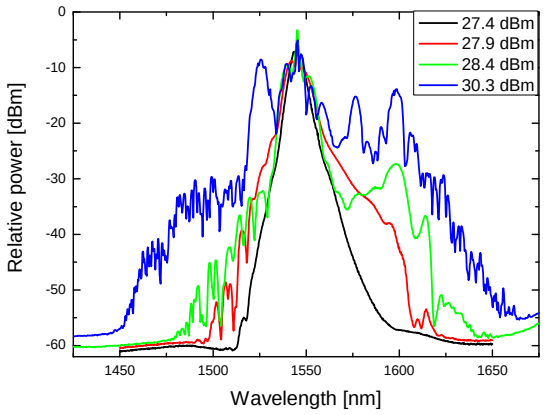

Figure 3.3: Measured supercontinuum spectra when pumping at 1545.5 nm with a FWHM = 2.9 ps and varying the average input power from 27.4 dBm to 30.3 dBm with a 20 dB bandwidth of 87 nm. The fiber zero dispersion wavelength is 1552.5 nm. Resolution bandwidth 0.5 nm.

Figure 3.3 shows the build up of a supercontinuum when pumping is performed at 1545.5 nm and different average input power to the fiber is used. It is seen how an average input power of 27.4 dBm slightly broadens the spectrum and also how increasing the input power leads to an increase in the spectrum width.

The 20 dB width of the broadest spectrum seen in figure 3.3 is measured to be 91 nm.

The soliton order N can be calculated using equation 3.1 and is found to be $N = 27$ for the spectrum generated with 30.3 dBm average power.

From the figure it can be seen how the spectrum broadens with increasing power and that the spectrum broadens towards longer wavelengths into the negative dispersion region of the HNL-PCF. Several major peaks are observed in the region between the pump and 1625 nm and they are seen to become predominant as the input power to the fiber increases. One major peak is also observed at a shorter wavelength namely at 1525 nm. To determine exactly which effects are responsible for those peaks would require comparison with extensive simulation results.

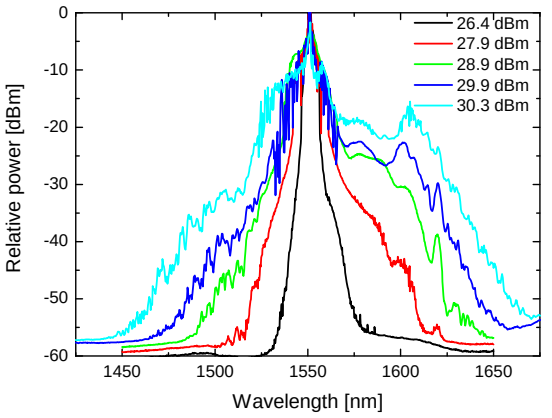

Figure 3.4: Measured supercontinuum spectra when pumping at 1551.5 nm with a pulse width FWHM = 2.9 ps and varying the average input power from 26.4 dBm to 30.3 dBm. The fiber zero dispersion wavelength is 1552.5 nm. Resolution bandwidth 0.5 nm.

Figure 3.4 shows the evolution of a supercontinuum when pumping close to the zero dispersion wavelength of the fiber. The pumping is performed at 1551.5 nm. It is seen from figure 3.4 how the supercontinuum evolves and broadens toward longer wavelengths as observed in figure 3.3. A shoulder like structure is observed around 1610 nm and a notch is also seen around 1585-1590 nm. The 20 dB width of the supercontinuum is measured to be 87 nm. A comparison of the two figures shows fewer major peaks toward longer wavelengths when pumping close to the zero dispersion wavelength and no major peaks at the short wavelength side

of the pump as opposed to what is seen in figure 3.4. The soliton order is calculated to be $N = 76$.

Pumping in negative dispersion region

Figure 3.5 shows the generation of supercontinuum when pumping at 1554.3 nm. It can be observed how a shoulder like structure appears and how smaller peaks are shifted towards longer wavelengths as the input power is increased. The shoulder like structure located around 1625 nm could be due to SRS since it is located 70 nm from the pump where the SRS gain becomes significant. The spectrum is more narrow than the two spectra shown in figure 3.3 and figure 3.4, having a 20 dB width of 37 nm.

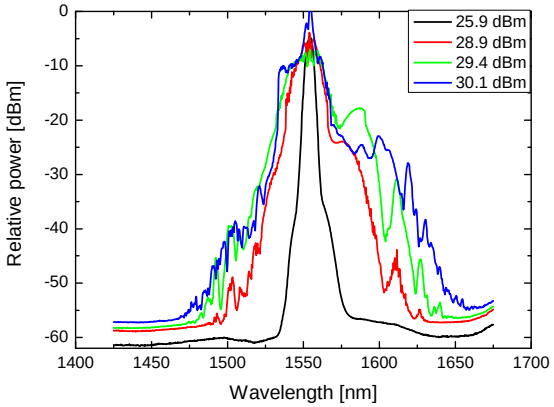

Figure 3.5: Measured supercontinuum spectra when pumping at 1554.3 nm with pulse width FWHM = 2.9 ps and varying the average input power from 25.9 dBm to 30.1 dBm. The fiber zero dispersion wavelength is 1552.5 nm. Resolution bandwidth 0.5 nm.

Figure 3.6 shows the supercontinuum generation when the input power into the HNL-PCF is increased and when a pumping wavelength of 1559.4 nm is used. This spectrum is even more narrow than the one shown in figure 3.5 and it has a 20 dB width of 35 nm. One peak at around 1610 nm and two peaks around 1508 nm and 1504 nm, are observed in figure 3.5. When pumping in negative dispersion region it is

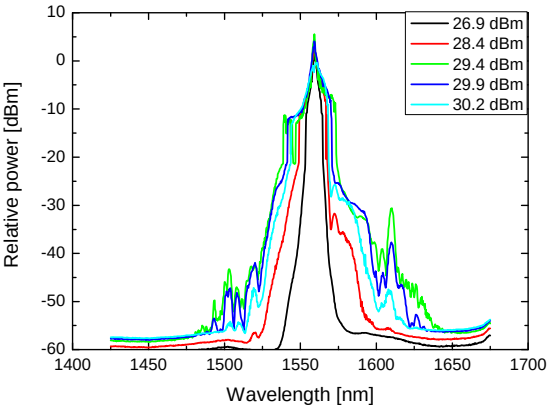

Figure 3.6: Measured supercontinuum spectra when pumping at 1559.4 nm with pulse width FWHM = 2.9 ps. The average input power varies between 26.9 dBm to 30.2 dBm. Resolution bandwidth 0.5 nm.

believed that SRS and SPM [44, 42, 51] are the main processes behind supercontinuum generation.

By using pulses with a FWHM in the pico-second region ($\sim 1-50$ ps) the contribution from soliton decay becomes small even when the soliton order is high. In comparing the spectra when pumping in the negative and positive dispersion region it is believed that SPM and SRS are the major contributors to the supercontinuum generation in both pumping domains.

All the measured spectra are asymmetrically shaped with spectral broadening towards longer wavelengths. This asymmetry is believed to be due to SRS since the Raman gain provides amplification at longer wavelengths than the pump wavelength.

Based on the results shown it can be concluded that a broader supercontinuum spectrum is obtained by pumping in the positive dispersion region of the fiber and that pumping close to the zero dispersion wavelength leads to a more "smooth" spectrum (fewer peaks).

It can also be seen that more negative dispersion leads to a more narrow supercontinuum spectrum. It has been experimentally confirmed that the dispersion of the fiber at the pumping wavelength plays a crucial role in how broad a supercontinuum can become. A good rule of thumb

is that the higher the dispersion of the fiber, the narrower the generated supercontinuum.

3.2.3 Supercontinuum in a dispersion flattened HNL-PCF

A new design in PCF technology has produced a HNL-PCF with a flattened dispersion profile. The fiber used in this experiment is a 100 m long dispersion flattened HNL-PCF with a nonlinear coefficient of $\gamma = 11.2\ \mathrm{W}^{-1}\cdot\ \mathrm{km}^{-1}$ [18]. The dispersion curve can be seen in figure 3.7 where it should be noted that the fiber does not have a zero dispersion wavelength in the range $1500-1600$ nm. It exhibits a dispersion flattened profile with a dispersion slope of 1.0×10^{-3} ps/nm^2/km at 1550 nm and an insertion loss of 5 dB. It can also be seen that the fiber only has positive dispersion in the telecommunication window. The maximum dispersion point is seen at 1570 nm and has a value of 2.9 ps/(km·nm). The inset in figure 3.7 shows a picture of the microstructured region of the HNL-PCF.

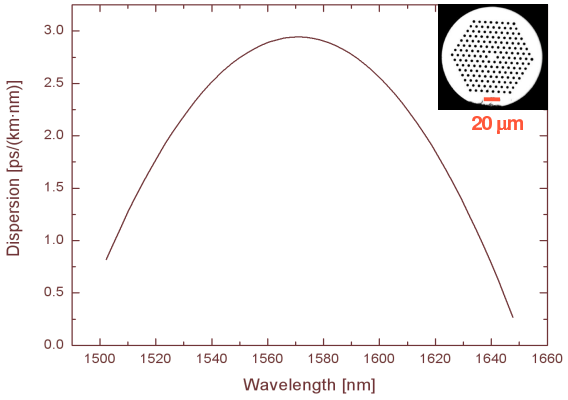

Figure 3.7: Dispersion curve of 100 m long HNL-PCF. The inset shows the microstructured region of the HNL-PCF.

The setup is the one shown in figure 3.1. The pulse width is FWHM = 2.9 ps and the pulse is Gaussian shaped. The laser is tuned to 1559.5 nm. The generated supercontinuum is seen in figure 3.8 and its 20 dB width is measured to be at least 210 nm when an average input power of 30 dBm is used.

The spectrum broadens towards longer wavelengths which is partly

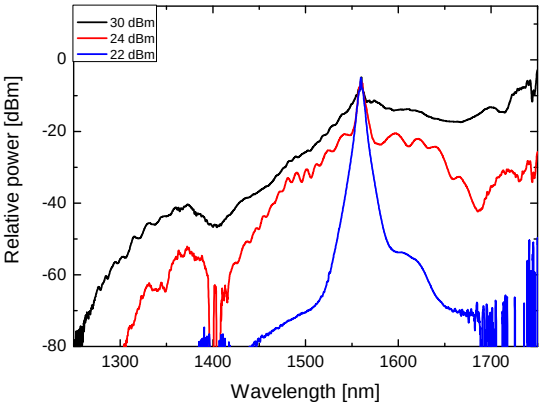

Figure 3.8: Supercontinuum generated in a dispersion flattened HNL-PCF. Pumped at 1559.5 nm. The 20 dB width is measured to be at least 210 nm. The pulse width is FWHM = 2.9 ps.

due to SRS. The broadening towards shorter wavelengths is not so pronounced and a deep notch is seen around 1400 nm which is ascribed to the OH absorption. The HNL-PCF with the flat dispersion profile favors supercontinuum generation much more than the HNL-PCF used in the previous experiments. For a determination of how exactly the different nonlinear effects contribute to the supercontinuum generation in a fiber requires extensive computer simulations such as those performed in [20, 53].

Based on the earlier results a combination of SPM, SRS and FWM is expected to contribute significantly to the generation of the supercontinuum.

3.3 Supercontinum as a WDM source for systems

In this section a supercontinuum generated in a dispersion flattened HNL-PCF used in a system experiment is presented. The generated supercontinuum is used as a source for a multi-wavelength system. It is shown how the supercontinuum is spectrally sliced into 5 channels all transmit-

ted over 2×44 km of standard single mode fiber (SMF) and 13 km of dispersion compensating fiber (DCF). The channels are modulated one at a time with a 10 Gbit/s data signal before multiplexing and transmission. Transmission over 5.6 km of PCF without dispersion compensation is also described.

3.3.1 Experimental setup

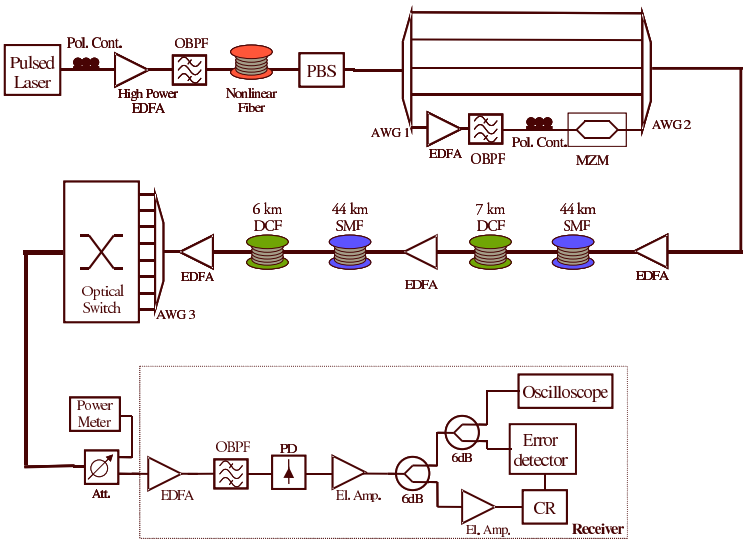

Figure 3.9: Experimental setup for supercontinuum as a multi-wavelength pulse source for a WDM system. PBS: polarization beam splitter, AWG: arrayed waveguide grating, MZM: Mach-Zehnder modulator.

A schematic of the experimental setup is shown in figure 3.9. A pulse train is generated by a MLFRL with repetition rate of 10 GHz at the wavelength of 1554.5 nm. The pulse train is polarization controlled before being amplified by an EDFA delivering 27 dBm average output power. The OBPF after the high power EDFA has a 3 dB bandwidth of 2.8 nm. The pulses have a FWHM of 2.9 ps before entering the HNL-PCF with an average power of 24.5 dBm. The polarization beam splitter (PBS) is used to select one polarization axis of the supercontinuum generated in the birefringent HNL-PCF. The supercontinuum generated in the HNL-PCF

is then sliced into 5 channels by an arrayed waveguide grating (AWG) with 200 GHz channel spacing (channel 1 at 1552.52 nm and channel 5 at 1558.96 nm) and a 3 dB bandwidth of 0.8 nm. The channels are modulated one by one with a 10 Gbit/s pseudo-random bit-sequence (PRBS) (2^{31}-1) giving the WDM scenario with one modulated channel and the adjacent channels all transmitting strings of 1-bits. The WDM signal is transmitted over two dispersion compensated fiber spans consisting of 44 km SMF and 6 and 7 km DCF, respectively.

Figure 3.10 shows the pulse shape and development of channel 1 and it can be seen how the transmitted pulse retained the pulse shape after transmission over two dispersion compensated SMF spans. The sliced pulses are measured using an autocorrelator and are found to be Gaussian shaped with a FWHM pulse width of 5 ps that is increased to 8.5 ps after modulation.

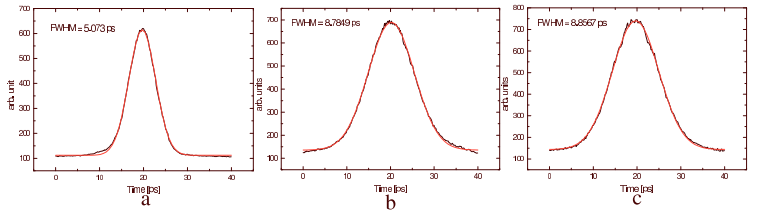

Figure 3.10: Autocorrelation traces and pulse width (FWHM) evolution of channel 1 (a) after slicing 5 ps (b) after modulation 8.8 ps (c) after transmission on two dispersion compensated SMF spans 8.8 ps. The traces show the measured data and the Gaussian fit. The 4 other channels have the same performance.

After transmission the 5 channels are wavelength demultiplexed before being input to a pre-amplified receiver. The pre-amplified receiver consists of an EDFA followed by an OBPF with a 3 dB bandwidth of 0.9 nm and a 45 GHz photodiode (PD). The signal quality is quantified by measuring the bit error rate (BER) of the received signal using a 10 Gbit/s error detector.

Table 3.1: Receiver sensitivity penalty of the 5 channel WDM signal transmitted over 2×44 km of SMF and 13 km of DCF.

Channel number	Transmitted signal dBm	Back-to-back dBm	Power penalty dBm
1	-31.4	-31.5	0.1
2	-34.3	-34.9	0.6
3	-35.9	-35.3	-0.6
4	-34.7	-34.6	-0.1
5	-32.3	-31.4	-0.9

3.3.2 Results

Transmission on SMF

Figure 3.11 shows BER curves of all the 5 transmitted channels. The figure shows the results of the transmitted signal and from figure 3.11(b) the receiver sensitivity of each channel after transmission can be seen. Figure 3.11(a) shows the receiver sensitivity when the transmission spans are omitted (defined, as the back-to-back case). The receiver sensitivity is defined as the power at the input of the receiver when the BER is 1.0×10^{-9}. It is seen that the receiver power penalty between the back-to-back and transmission varies from negative, meaning improvement in performance, to a small positive power penalty, meaning degradation in the performance. Table 3.1 shows the receiver power penalty obtained from each channel. It is seen that the receiver power penalty varies from channel to channel with a difference of 1.5 dB between the best and worst channels.

It is believed that the difference in sensitivity between the channels is partly due to noise generated in the supercontinuum [55, 56, 57, 58] which leads to noise variations from channel to channel depending on where in the supercontinuum spectrum the spectral slicing is performed. The noise generated in the supercontinuum is mainly due to the amplitude and timing jitter in the pulse source. The variation in power penalty is also due to the instability of the system. The system is very dependent on the stability of the laser and the incoming pulses. It is very important that the fluctuations in pulse shape, width and peak power stay small or

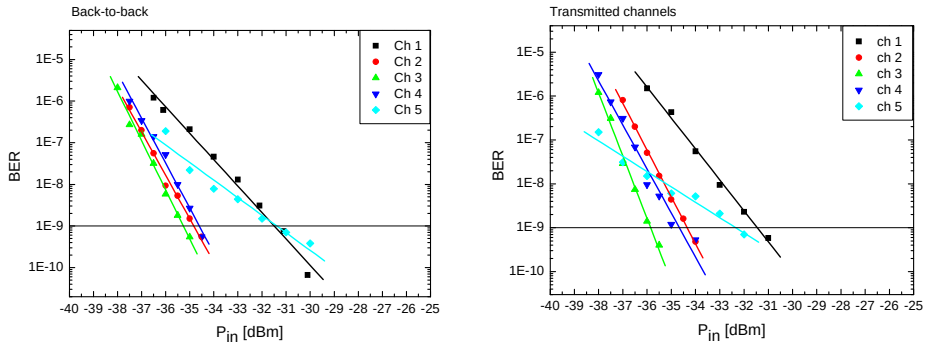

(a) (b)

Figure 3.11: BER curves for (a) the back-to-back signal and (b) the transmitted signal. The channel bit-rate is 10 Gbit/s and the transmission is over 88 km of SMF and 13 km of DCF.

the generated supercontinuum will change and thereby the performance of the entire system.

The generated supercontinuum is shown in figure 3.12 when an average output power of 27 dBm from the high power EDFA is used and a Gaussian pulse with FWHM = 2.9 ps. The 10 dB bandwidth is measured to 11 nm. The continuum generated is wide enough for the creation of a 5 channel WDM signal with wavelength between 1552.52 nm and 1558.96 nm. The slicing of the spectrum is shown in figure 3.13 where the channels are numbered according to increasing wavelength. Channel 3 is the channel with the wavelength that is closest to the wavelength of the pulse source generating the supercontinuum and is located in the middle of the supercontinuum spectrum. It is believed that SPM is responsible for the two shoulder structures seen in the spectrum in figure 3.12 [32, 48].

Transmission on PCF

A WDM experiment with a transmission link of 5.6 km PCF has also been performed. The setup used in this experiment is the same as the one shown in figure 3.9 where the transmission link consists of two spools of transmission PCF of 2.6 km and 3.0 km length, respectively [59]. The 5.6 km long transmission PCF has 1.7 dB/km loss, 32 ps/nm/km dis-

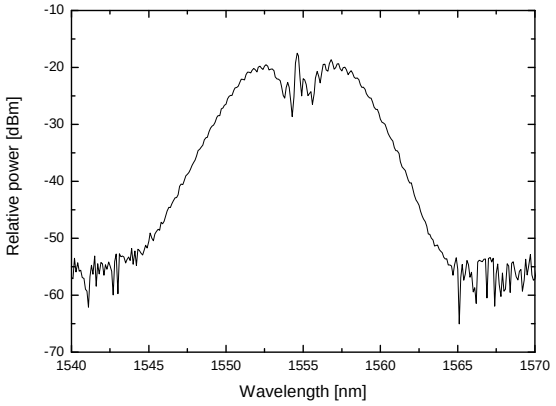

Figure 3.12: Generated supercontinuum used as a WDM source. The pulse width used is FWHM = 2.9 ps and an average power of 27 dBm. The fiber used is a dispersion flattened HNL-PCF with the dispersion curve shown in figure 3.7.

persion at 1550 nm and 0.067 ps/nm^2/km dispersion slope. The results are quantified by measuring BER curves and the power penalty for each channel. The BER curves of the transmission for all 5 channels are seen in figure 3.14 with the back-to-back curves being the same as shown before in figure 3.11(a).

The power penalty is seen in table 3.2. It is noted that the power penalty varies between -0.2 and 3.4 dB for the best and worst case.

The negative power penalty is believed to be due to instability in the system and within the uncertainty of the measurements. The instability can be observed in figure 3.11(a) where the BER of channel 5 in the back-to-back configuration shows a big deviation between some of the measured points and the linear fit. The uncertainty due to instability in the system helps explain the negative power penalty observed. The major reason for the high uncertainty is ascribed to the instability of the laser pulse width and thereby of the peak power of the pulses generating the supercontinuum.

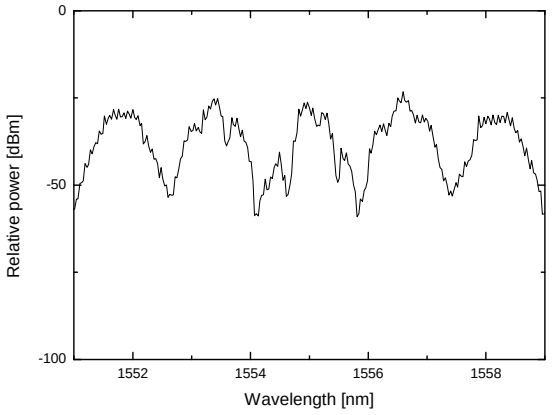

Figure 3.13: Sliced supercontinuum. The five different channels are clearly seen with channel number 1 to the left and number 5 to the right.

3.3.3 Pulse source comparison for WDM source

In a comparison between two pulse sources used in the setup from the previous experiments it is seen that the different channels have different receiver sensitivities. The comparison shows the importance of a stable pulse source in a supercontinuum generation experiment. A stable pulse source makes for a stable supercontinuum that does not change with time when it is spectrally sliced into 5 channels with the same pulse shape. The experimental setup used is the back-to-back setup from the

Table 3.2: Receiver sensitivity penalty for WDM transmission over 5.6 km of PCF.

Channel number	Transmitted signal dBm	Back-to-back dBm	Power penalty dBm
1	-28.1	-31.5	3.4
2	-33.8	-34.9	1.1
3	-34.3	-35.3	1.0
4	-34.5	-34.6	0.1
5	-31.6	-31.4	-0.2

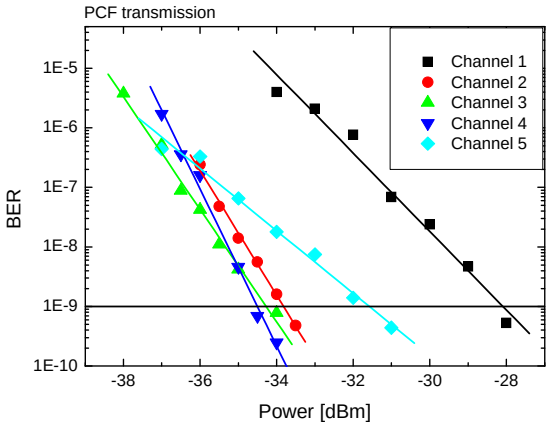

Figure 3.14: PCF Transmission BER curves. The bit-rate of each channel is 10 Gbit/s.

experiment shown in figure 3.9 and the pulsed laser is either a MLFRL or an Erbium-Glass oscillator pulse generating laser (ERGO-PGL) [60]. The sliced channels are modulated one by one with a 10 Gbit/s PRBS $2^{31} - 1$ sequence and BER measurements are performed.

Figure 3.15 shows a comparison of the back-to-back BER measurements of all 5 channels based on the two different pulse sources. Both lasers were tuned to the same wavelength 1554.5 nm and they both have Gaussian shape with a FWHM pulse width of 2.9 ps for the MLFRL and 2.2 ps for the ERGO-PGL. The input pulses to the HNL-PCF have an average power of 24.5 dBm into the HNL-PCF in both cases. In spite of the slight difference in pulse width which is expected to generate different supercontinua the comparison still shows the importance of the laser source in WDM experiments.

It is clear to see a large difference in the sensitivity of the channels depending on which of the two lasers is used. The stability of the lasers can be estimated by considering the quality of the linear fit made in figure 3.15. The BER measurements based on the MLFRL has a bigger uncertainty compared to the BER measurements based on the ERGO-PGL. The uncertainty difference is ascribed to the intensity and timing jitter of the laser. Small fluctuations in the pulse parameters can change

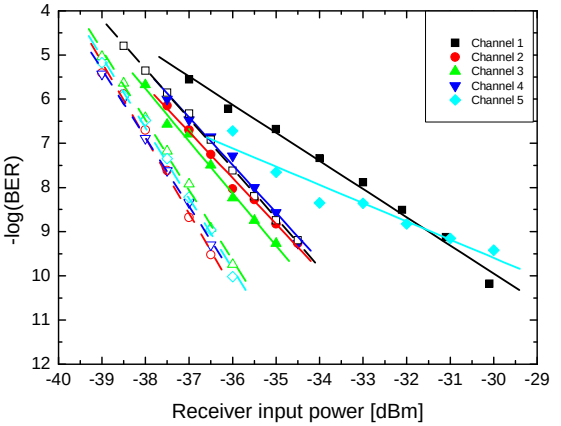

Figure 3.15: Comparison of the BER curves between the 5 WDM channels generated using MLFRL (solid) and ERGO-PGL (dashed) laser.

the generated supercontinuum significantly. The importance of the laser source and the pulse parameters are seen by considering the big improvement in the system performance by changing lasers.

3.4 Comparison of two HNL-PCFs with flattened dispersion profile for a WDM source

A comparison between two HNL-PCFs and the supercontinuum they generate under identical circumstances is made. Both of the HNL-PCFs have a flattened dispersion profile and no zero dispersion wavelength between 1500 nm and 1600 nm.

3.4.1 Fiber parameters

The HNL-PCF used in this experiment is 50 m long and has a nonlinear coefficient of $\gamma = 11$ W^{-1}·km^{-1} [18]. The cross-section is represented in figure 3.16. The dispersion of the fiber is also seen in figure 3.16 where it can be seen that the dispersion is negative in the entire region and it has a variation smaller than 1.5 ps/nm/km between 1500 and 1650 nm. Such a fiber structure has been reported earlier to provide the lowest

value of dispersion slope (less than 10^{-3} ps/nm^2/km) for a HNL-PCF [18]. For the specific sample used in this experiment, the dispersion slope is equal to 0.01 ps/nm^2/km at the wavelength 1554.5 nm. The HNL-PCF is spliced to standard-single mode fiber pigtails, leading to a total loss of 3 dB at 1550 nm.

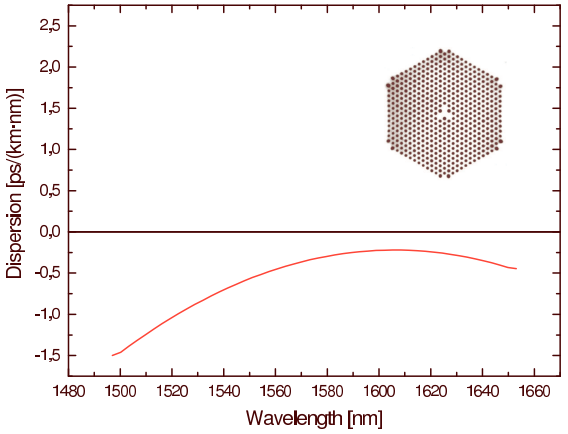

Figure 3.16: Measured dispersion curve of the 50 m HNL-PCF. The inset shows the microstructured region of the HNL-PCF where the three-fold symmetry is obtained from three missing holes.

The other HNL-PCF is described in section 3.2.3 and the dispersion profile of the fiber is seen in figure 3.7. Both fibers have a flattened dispersion profile, but with different sign of the dispersion.

3.4.2 HNL-PCF with positive and negative dispersion

The comparison between the two HNL-PCFs is performed in the back-to-back configuration of the setup shown in figure 3.9 with the laser changed to the ERGO-PGL. Both the supercontinuum generation spectra from the two fibers as well as the slicing of the spectra into 8 channels are monitored. Finally BER measurements are performed on all channels. The AWG used to slice the supercontinuum into 8 channels is the same as the one used in the previous experiment. Channel 1 is located at 1548.6 nm and channel 8 at 1559.6 nm all with 200 GHz spacing and

a 3 dB bandwidth of 0.8 nm. The input pulses to the HNL-PCF are Gaussian shaped and have a FWHM of 3.2 ps.

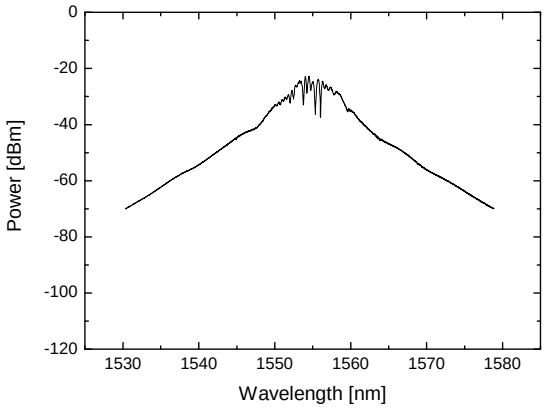

Figure 3.17: Supercontinuum generated by the HNL-PCF described in section 3.2.3. The 10 dB width is 9.3 nm (Resolution bandwidth 0.1 nm).

The supercontinuum generated by the HNL-PCF with a flat positive dispersion profile is shown in figure 3.17 and the 10 dB bandwidth is measured to be 9.3 nm.

The supercontinuum generated using the HNL-PCF with flat negative dispersion profile is seen in figure 3.18 and it has a 10 dB bandwidth of 11 nm. The fringes observed in the spectrum are due to the 10 GHz tones due to the laser repetiotion frequency and they are only seen because of the very high resolution bandwidth of 0.01 nm used in recording the spectrum.

The two spectra from figure 3.17 and figure 3.18 cover the region in which the AWG is centered and slicing of the spectra can be performed. Figure 3.19 shows the slicing of the spectrum seen in figure 3.17. 8 distinct channels are seen with small spectral deteriorations on channel 3, 4 and 5. The spectral lines from the laser can be seen because of the resolution bandwidth of 0.05 nm.

The slicing of the spectrum from the HNL-PCF with flat negative dispersion profile is seen in figure 3.20. All 8 channels are also clearly seen in this case and the laser fringes can again be observed. Channel

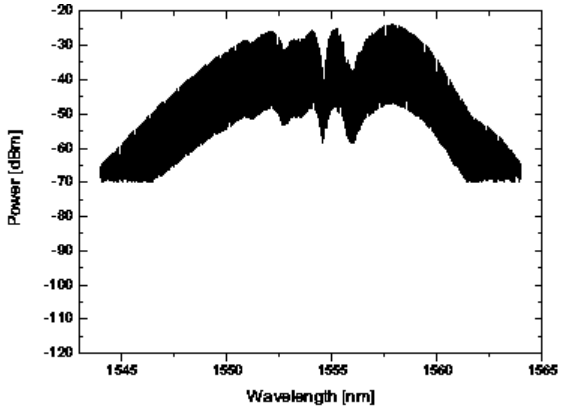

Figure 3.18: Supercontinuum generated by the HNL-PCF described in section 3.4.1. The 10 dB width is 11 nm (Resolution bandwidth 0.01 nm).

6 is modulated. In both sliced spectra the peak power of all 8 channels vary depending on the shape of the supercontinuum that is sliced.

BER measurements have been performed on all 8 channels from each HNL-PCF supercontinuum. All the BER curves obtained when the HNL-PCF with flat positive dispersion profile is used as a WDM source are shown in figure 3.21. The receiver sensitivity from all 8 channels can be seen in table 3.3. A variation of 2.1 dB between the best (channel 4) and worst (channels 3 and 8) channel, is observed.

The BER curves associated with the HNL-PCF with negative flat dispersion profile are shown in figure 3.22. It is seen how all the channels nearly coincide and the difference between the best (channel 7) and worst (channel 5) receiver sensitivity is measured to be 0.6 dB. From the BER curves it can be seen that all the linear fits made nearly have the same slope. Only channel 3 has a more reduced slope than the other channels. Looking at figure 3.21 the variation in slope between the channels are more pronounced. The difference in slope is believed to be due to the generation of the supercontinuum when the HNL-PCF has a positive dispersion profile compared to a negative dispersion profile.

The difference in receiver sensitivity between channels depending on which HNL-PCF is used is seen in table 3.3. The difference varies from 0 dB to 2.2 dB with the HNL-PCF with the flat positive dispersion having

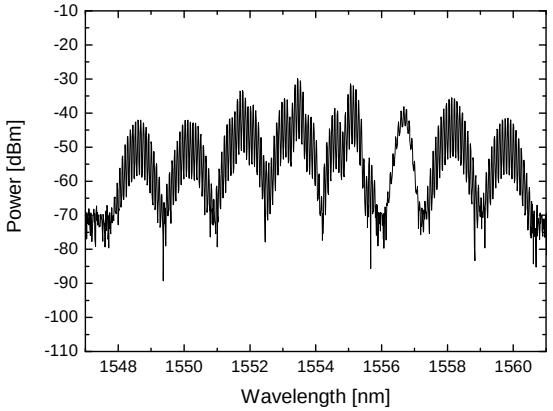

Figure 3.19: Slicing of the supercontinuum generated by the HNL-PCF described in section 3.2.3 with 8 different channels. Channel 1 is located at 1548.6 nm and channel 8 is located at 1559.8 nm. All channels have 200 GHz channel spacing (RB 0.05 nm).

the highest power in order to obtain error free operation (BER = 10^{-9}) for all 8 channels.

A more uniform performance of all 8 channels is found when using the HNL-PCF with a flat negative dispersion profile. The variance in both receiver sensitivity and slope of the linear fit is smaller when the HNL-PCF with a flat negative dispersion profile is used. An overall better receiver sensitivity is found when using the HNL-PCF with a negative dispersion profile. The width of both supercontinuum spectra are limited compared to what has been reported elsewhere [10]. It is believed that in both cases the dominating effect behind the continuum generation is SPM. The slicing of a spectrum generated in a medium with negative dispersion has less contributing effects [32] such as soliton decay and is therefore better suited for optical communication systems. The comparison between the two HNL-PCFs shows a clear advantage in using the HNL-PCF with a flat negative dispersion profile as a source for WDM signals in optical communication systems.

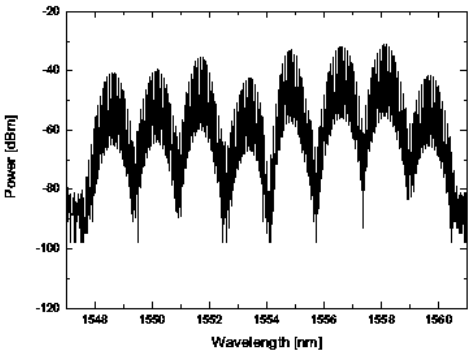

Figure 3.20: Slicing of the supercontinuum generated by the HNL-PCF described in section 3.4.1 with 8 different channels. Channel 1 is located at 1548.6 nm and channel 8 is located at 1559.8 nm. All channels have 200 GHz channel spacing (RB 0.01 nm).

3.5 Wavelength conversion using supercontinuum generation

One of the interesting applications of a supercontinuum is wavelength conversion of an optical signal [61]. The optical signal needs to be intensity modulated, as opposed to phase modulation for example, to work in a wavelength converter based on supercontinuum generation.

An interesting application of a supercontinuum is the realization of a tunable optical clock translator for high speed optical time division multiplexing (OTDM) systems where a clock signal at the base rate is transmitted simultaneously with OTDM data signal in order to ease the clock recovery at the receiving end, as proposed in [62, 63]. The optical clock signal is customarily derived from the pulse source using wavelength conversion in a nonlinear optical loop mirror [64, 65]. Using instead a tunable clock translator based on supercontinuum would save the cost of a tunable laser.

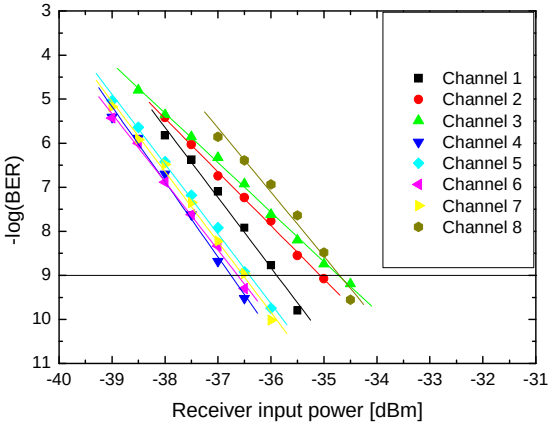

Figure 3.21: BER measurements of the 8 channels sliced from the supercontinuum generated in the HNL-PCF described in section 3.2.3

3.5.1 Experimental setup

The experimental setup is shown in figure 3.23. A pulse train is generated by a MLFRL with a repetition rate of 10 GHz, before being amplified by an EDFA delivering up to 30 dBm average power. The pulses are compressed in a nonlinear pulse compressor (NLPC) made of alternating lengths of HNLF and SMF, before being input to 50 m of HNL-PCF with zero dispersion at 1552.5 nm [19]. The HNL-PCF is described in section 3.2.1. The HNL-PCF is spliced to standard single mode fiber pigtails. Due to the fiber birefringence, a polarization controller (PC) is used before the HNL-PCF. The light at the output of the HNL-PCF is filtered using a tunable OBPF before being amplified, detected by a photodiode (PD) with 50 GHz bandwidth and displayed on a high speed sampling oscilloscope. An optical spectrum analyzer (OSA) is used to monitor the output from the HNL-PCF.

The laser wavelength is fixed at 1550.5 nm and the pulses are compressed from 2.9 to 0.5 ps in the NLPC. The NLPC consists of 200 m HNLF, 10 m SMF, 100 m HNLF and 20 m SMF. The HNLF used in the NLPC has a nonlinear coefficient, $\gamma = 10.3$ W^{-1}·km^{-1}, and zero dispersion wavelength at 1553 nm. The wavelength converted pulse is measured

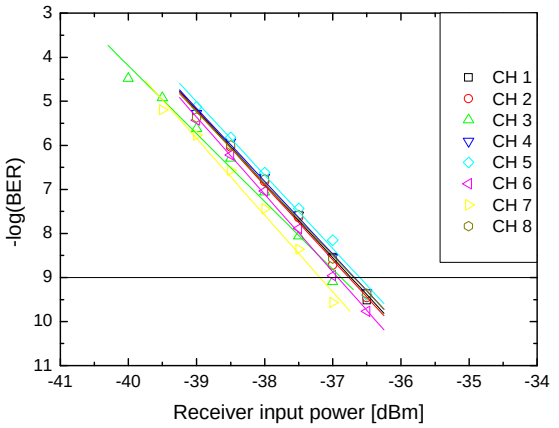

Figure 3.22: BER measurements of the 8 channels sliced from the supercontinuum generated in the HNL-PCF described in section 3.4.1

using an autocorrelator and is found to have a FWHM of 5.5 ps and a Gaussian shape after filtering.

3.5.2 Results and conclusion of wavelength conversion using supercontinuum

Pulse durations smaller than 1 ps are used to generate a supercontinuum with a pump wavelength at 1550.5 nm. The influence of fiber birefringence is illustrated in figure 3.24 (a) and (b) where two supercontinuum spectra with different features are shown, depending on the state of polarization of the light at the HNL-PCF input. In the first case (figure 3.24 (a)), the supercontinuum extends over 60 nm in a 20 dB bandwidth, whereas for the orthogonal state of polarization shown in figure 3.24 (b), a larger supercontinuum bandwidth of 75 nm is obtained, at the expense of a deeper notch in the spectrum around 1585 nm. Such bandwidths cover the C and L bands used for optical communication. It is investigated whether the generated supercontinuum can be sliced using a tunable band-pass filter placed after the HNL-PCF. Figure 3.24 (c) and (d) show the clock signal obtained from the supercontinuum at wavelength of 1582 nm and 1574.1 nm, respectively, corresponding to the spectra of figure 3.24 (a) and (b), respectively. The top traces in those figures show the original

Table 3.3: Receiver sensitivity comparison between two HNL-PCF with flattened dispersion profile i.e. negative and positive.

Channel number	Negative dispersion (dBm)	Positive dispersion (dBm)	Difference (dB)
1	-36.7	-35.9	0.8
2	-36.8	-35.1	1.7
3	-36.9	-34.7	2.2
4	-36.7	-36.7	0.0
5	-36.6	-36.4	0.2
6	-36.9	-36.6	0.3
7	-37.2	-36.5	0.7
8	-36.7	-34.7	2.0

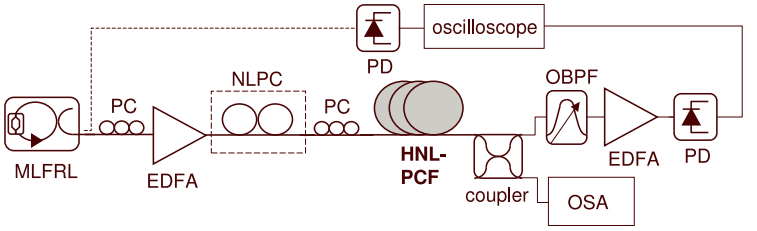

Figure 3.23: Experimental setup for wavelength conversion of an optical clock signal. PC: polarization controller, NLPC: nonlinear pulse compressor, OBPF: tunable optical bandpass filter, OSA: optical spectrum analyzer.

clock signal at 1550.5 nm, whereas the bottom traces correspond to the converted clock signal.

It should be noted that the pulse width of the pulses generating the supercontinuum is slightly different in the cases of figure 3.24 (a)(c) and (b)(d), with FWHM of the autocorrelation trace equal to 0.5 and 0.4 ps, respectively. It has therefore been demonstrated that, with such pulse durations, it is possible to translate an original clock signal to the L-band. The maximum wavelength for which clock translation is observed in the experiment is limited by the tunable optical band-pass filter and not by the extent of the supercontinuum.

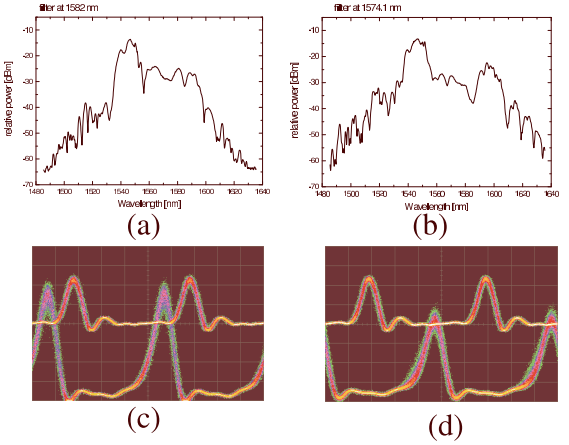

Figure 3.24: Supercontinuum spectra and converted clock signals when the pumping signal is launched parallel to the HNL-PCF principal polarization axes. In (c) and (d) the top trace corresponds to the original clock at 1550.5 nm, whereas the bottom trace shows the converted clock signal at 1582 and 1574.1 nm respectively. (a) and (c) are obtained with pump aligned to one of the fiber principal polarization axes, whereas (b) and (d) are obtained when the pump is aligned to the orthogonal principal axis.

3.6 Summary

Supercontinuum generation in HNL-PCF has been discussed. A number of characterization experiments have shown how different supercontinuum spectra can be achieved depending on the fiber parameters such as dispersion and nonlinear coefficient. Furthermore, it has been described how pulse parameters also play a crucial role in supercontinuum generation.

It was shown how a supercontinuum can be part of an optical system in both a wavelength conversion experiment and as a WDM source. A successful WDM experiment with a supercontinuum as the WDM source was performed and transmission on 2×44 km of SMF and 6 and 7 km of DCF as well as transmission on 5.6 km PCF without dispersion compensation were demonstrated. In both experiments 5 channels were transmitted with one channel carrying 10 Gbit/s data and the other channels carrying 10 GHz pulses. The power penalty when transmitting over SMF

varied with 1.5 dB between the best and worst case, while the power penalty when transmitting over 5.6 km of PCF varied with 3.6 dB.

Investigation of the pulses generating the supercontinuum was carried out. Two different lasers with slightly different pulse widths resulted in very different supercontinuum performance in system experiments. The pulse width of the lasers were 2.9 and 2.2 ps, respectively. The average power used in both cases was 24.5 dBm. It was seen how stability and noise of the sliced supercontinuum was improved when changing lasers.

Using the most stable laser with the most narrow pulses and comparing two different HNL-PCF with different dispersion profiles, but similar nonlinear coefficient, demonstrated the importance of dispersion in a fiber. It was seen that a HNL-PCF with flattened negative dispersion profile generated a supercontinuum with uniform performance characteristics of the 8 sliced channels. All 8 channels carrying 10 Gbit/s data signal showed a power penalty difference of 0.6 dB between the best and worst channel when a HNL-PCF with flattened negative dispersion profile was used. Using a HNL-PCF with positive flattened dispersion profile yielded a power penalty difference of 2.0 dB between the best and worst channels. For all 8 channels the HNL-PCF with negative flattened dispersion profile has lower receiver sensitivity than the HNL-PCF with positive dispersion. The overall picture is that better performance is obtained by using a HNL-PCF with flat negative dispersion.

Using RZ pulses when generating supercontinuum for a WDM source makes a combination of OTDM and WDM a possibility for future optical communication systems.

From all the experiments the importance of a stable pulse source is seen when generating a supercontinuum in optical communication systems. The future of supercontinuum generation is linked very closely to the stability of the pulse source. The most important parameter when discussing stability of a pulse source used to generate a supercontinuum is the intensity noise which has to be near zero. If a very stable pulse generator is used, supercontinuum is one attractive way of obtaining a WDM source or achieving wavelength conversion over a considerable wavelength range.

Chapter 4

Regeneration of high speed optical signals

4.1 Introduction

Regeneration is an integral part of a data transmission system and therefore a lot of effort has gone into research on regeneration, and in this context especially all-optical regeneration has been a research focus in recent years. Regeneration consists of three parts: Re-amplification, reshaping and re-timing of the data signal, where the first two ways combine to 2R-regeneration and including re-timing 3R-regeneration is achieved. Regeneration of an optical signal can be performed either all-optically or opto-electronically. Opto-electronic regeneration consists of three parts: detecting the optical signal, regenerating it electronically, and using this electronic signal to modulate a new optical carrier. The latest advances in the research on opto-electronic regeneration has increased the speed of opto-electronic regenerators to bit rates up to 40 Gbit/s [66].

Opto-electronic 3R-regeneration is a simplification over all-optical regeneration in terms of parameters that needs to be controlled. The implementation of opto-electronic 3R-regeneration in systems today is generally preferred by system providers over all-optical 3R-regeneration [67]. The choice of one technology over the other is not a simple one. Since regenerators will be implemented in future WDM systems, the number of regenerators increase with the number of channels in a WDM system. That means that besides the number of controllable parameters, also cost,

number of components, and power budget of the regenerator need to be considered. This is a complex task that can only be decided on a case by case basis.

For signals with higher bit rates of 80 or 160 Gbit/s all-optical regeneration is the only option. Therefore all-optical regeneration remains an important research tool and much investigation is put into that area of research. Some of the latest results using SOAs [68, 69] or fiber [40, 70] in a 3R-regenerator show a promising future for all-optical 3R-regeneration.

4.2 Regenerator performance

A misconception about regeneration has been that 3R-regeneration corrects the errors in the signal. This is not the case [71, 72]. A regenerator impedes the accumulation of errors during transmission by re-distributing noise on "1" and "0" levels, which may also aid in improving the receiver sensitivity.

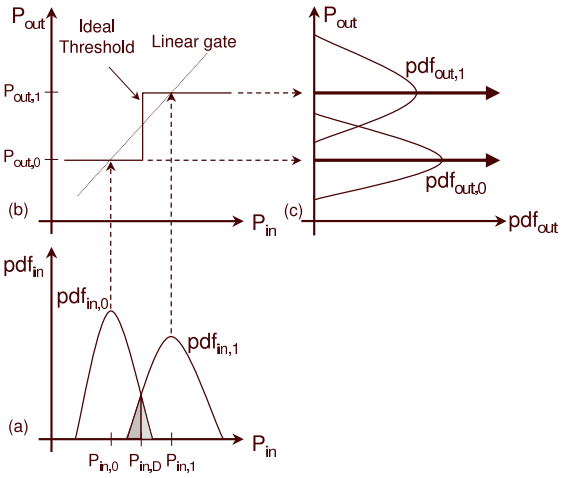

Figure 4.1: (a) Probability density functions (pdfs) of logic levels at the input of the regenerator, (b) transfer function of a nonlinear gate, (c) pdfs at the output of the regenerator (reprinted from [67]).

Figure 4.1 shows the principles behind 2R-regeneration. The probability density functions (pdf) describe the probability that the addition

of noise causes the power level to attain a certain value. The pdfs at the input of a regenerator for the "0" and "1" levels centered around the average logic level $P_{in,0}$ and $P_{in,1}$ are seen in figure 4.1(a). The probability of detection of a "0" as a "1" bit as a function of input power is determined as the integral of the $\mathrm{pdf}_{in,0}$ from the threshold $\mathrm{P}_{in,D}$ to infinity i.e. the tail of the pdf. For the detection of a "1" as a "0" bit the leading edge of the $\mathrm{pdf}_{in,1}$ until $\mathrm{P}_{in,D}$ is integrated i.e. the dark gray area in figure 4.1(a). The overlap between the two pdfs (the gray shaded area) in figure 4.1(a) correspond to the errors in the system where it can be seen how "0" will be detected as "1" (light gray) and how "1" will be detected as "0" (dark gray). It is impossible to distinguish between "1" and "0" bits in the overlap region and errors occur. Figure 4.1(b) shows the threshold of an ideal regenerator and a linear gate equivalent to no regeneration. The effect of the two different gates on the input pdfs are seen in figure 4.1(c). The linear gate keeps the shape of the pdfs and the ideal regenerator transforms the pdfs into delta functions clearly separated from each other. The errors already part of the signals are still there, but are now hidden in the delta functions and therefore a regenerator can not correct errors, but only makes the signal more resilient towards noise addition and deterioration.

4.3 2R-regeneration

Regeneration is normally classified into 2R-regeneration and 3R-regeneration. 2R-regeneration is often used in laboratories since omitting the re-timing, i.e. clock recovery circuit of a setup makes it a simpler setup with less parameters to control. Depending on the modulation format used for the signal, different all-optical regenerators are needed. A lot of work has gone into regeneration of RZ signals [68, 69, 40]. A theoretical proposition for NRZ [73] using FWM in DSF has been reported.

One of the first fiber-based all-optical 2R-regenerators for RZ pulses was proposed by Mamyshev [74]. The regenerator is using SPM in a fiber and spectral filtering to obtain 2R-regeneration. The basic idea is to substantially broaden the spectrum using SPM and subsequently slice the spectrum with an optical band-pass filter whose center frequency is offset with respect to that of the signal. The concept has many similarities with the generation of short pulses using supercontinuum in a fiber, but

since much lower input power is used, ideally only SPM should contribute to the spectral broadening of the pulse in the fiber. Using spectral filtering of a SPM-broadened optical spectrum as 2R-regenerator has been shown in both HNL-PCF, HNLF, and DSF [75, 76, 77], respectively. The method is not without issues that need consideration, namely that slicing of a broadened optical spectrum may result in a severe degradation of the signal to noise ratio (SNR) if only a very small noise component is present at the input [77]. Choosing the dispersion regime of the fiber when generating SPM broadening is one of the most important considerations to be taken. Working in the positive dispersion (anomalous dispersion) regime of the fiber, the filtered pulses often become noisy if the input pulses are not extremely stable in intensity and the SNR is very high. This is due to unstable excitation of higher order solitons either due to intensity fluctuations in the input pulse or to beating between the pulse and optical noise from an EDFA [78, 79]. Figure 4.2 shows the schematics of the setup used by Mamyshev in [74]. As can be seen a small wavelength conversion occurs since the filter has to be displaced from the input light in order to perform the re-shaping part of the 2R-regenerator.

Figure 4.2: Schematic of the setup used by Mamyshev [74].

4.4 Working principle of 3R-regenerator

An all-optical regenerator is a device that receives a noisy and distorted signal and transmits an undistorted and noise free signal. The method investigated in this chapter is based on a 3-stage NOLM setup [80], exploiting the Kerr effect in fibers in order to restore high-speed data signals. An incoming noisy data signal is transformed on to a clean locally generated clock pulse. The clock pulse characteristics (pulse width and pulse shape) should be suitable for transmission.

The regenerator consists of 3-stages each containing a NOLM as shown in figure 4.3. The 3-stages are two pedestal suppressors and one wavelength converter all based on nonlinear fibers. The first stage of the re-

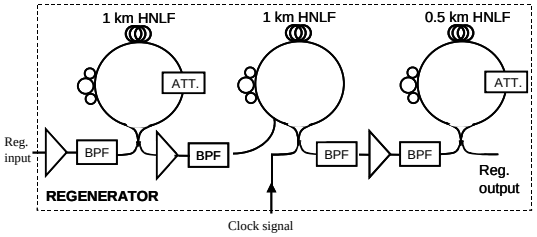

Figure 4.3: Schematic of the 3R-regenerator based on a 3-stage NOLM setup.

generator suppresses the noise on the "0" level by using a nonlinear fiber in a loss imbalanced NOLM. The second stage works as a wavelength converter that inverts the logic so "0" level becomes "1" level and vice versa also using a nonlinear fiber in a NOLM. That moves the clean "0" level to the "1" level and the noisy "1" level to the "0" level obtaining a clean "1" level and noisy "0" level at the output of the 2^{nd} NOLM. The third stage is again a "0" level noise suppressor similar to the first stage. The data signal after regeneration is wavelength converted and the logic is inverted compared to the original data signal.

The two "0" level noise suppressors are loss imbalanced NOLMs based on SPM in a nonlinear fiber. The wavelength conversion part is based on XPM in a nonlinear fiber using a NOLM. Results using both SPM and XPM in a NOLM containing dispersion shifted fiber has been reported [81, 82, 83, 84]

4.5 Evaluation of a HNLF-based NOLM for regeneration up to 160 Gbit/s

Recently, a 3-stage NOLM scheme was proposed as a way of performing 3R-regeneration in an all-optical manner [80]. The first NOLM in that setup works as a pedestal suppressor eliminating noise on the "0" bits by SPM [81]. The characterization of this NOLM is performed in this experiment when data bit rates of 80 Gbit/s and 160 Gbit/s are used. The use of HNLF in the NOLM reduces the power required for the experiment.

4.5.1 Experimental setup for pedestal suppression

The experimental setup used is shown in Figure 4.4 where the dashed NOLMs are only shown for future reference. The data pulses are generated by an external cavity mode-locked semiconductor laser (ECMSL) [85] running at a 10 GHz repetition rate. The wavelength of the ECMSL is 1546 nm and the pulse width is 2 ps. The pulses are multiplexed to 40 GHz by a polarization maintaining multiplexer and modulated with a $2^7 - 1$ PRBS sequence generating a 40 Gbit/s signal. In order to deteriorate the quality of the data signal on the "0" bits a sub-optimum setting of the bias to the modulator is used, increasing the noise level on the "0" bits. The 40 Gbit/s signal is multiplexed to an 80 Gbit/s or a 160 Gbit/s signal using a second polarization maintaining multiplexer. The signal is amplified and inserted into a loss imbalanced NOLM acting as suppressor of the noise on the "0" level. The fixed loss in the lossy arm in the loop is 5 dB and the non-linear medium is 1 km of HNLF. The HNLF has a zero-dispersion wavelength of 1553 nm and a dispersion slope of $S = 0.02$ ps/(nm^2·km) at 1550 nm with a non-linear coefficient, $\gamma = 10$ W^{-1}·km^{-1}. The use of HNLF enables a strong reduction of the required input power, allowing 15 dBm as average input power. The pulses at the output of the NOLM are attenuated and received. The receiver allows a demultiplexing from 80 to 40 Gbit/s, but in this case is not able to demultiplex from 160 Gbit/s to 40 Gbit/s. BER measurements are carried out on the 40 Gbit/s demultiplexed signal with a 40 Gbit/s error detector (ED).

The receiver is seen in figure 4.5 and consists of a pre-amplifier, a demultiplexer and a 50 GHz photodiode. The demultiplexer is based on an OKI electro absorption modulator (EAM) [86] running at 40 GHz and having a switching window of 5 ps. The demultiplexing from 160 Gbit/s can not be performed due to the lack of electrical amplification of the 40 GHz electrical drive signal into the EAM resulting in a too broad switching window. Therefore only demultiplexing of a 80 Gbit/s data signal is possible.

4.5.2 Results of pedestal suppression

Initially the data signal is kept at 80 Gbit/s. Figure 4.6 shows the 80 Gbit/s data signal at the input and at the output of the NOLM.

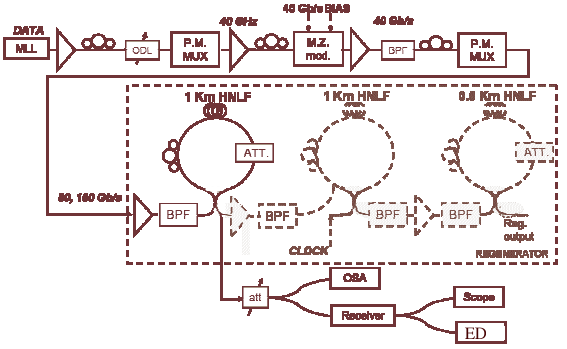

Figure 4.4: Schematic of the experimental setup used for pedestal suppression.

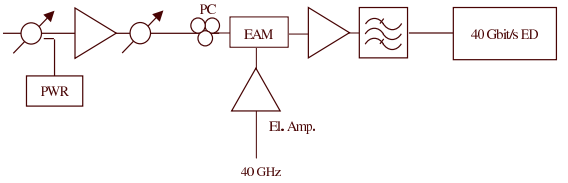

Figure 4.5: Schematic setup of the receiver used for detection of a 40 Gbit/s signal in characterizing a NOLM as pedestal suppressor.

The input 80 Gbit/s signal is noisy on the "0" level, but at the output of the NOLM the 80 Gbit/s data signal looks more clean on the "0" level and the eyes more open even though it looks like added noise on the "1" level.

Furthermore, the spectra and the autocorrelations are monitored during the experiment and the results are seen in Figure 4.7. From the spectra it is seen that the SPM-effect causes a spectral broadening, which in turn results in pulse compression, as seen on the autocorrelation trace. The pulses are compressed from a FWHM of 3.3 ps to 2.1 ps.

In order to carry out BER measurements, the 80 Gbit/s data signal is demultiplexed to a 40 Gbit/s signal in the receiver. In Figure 4.8 the eye-diagrams of the 40 Gbit/s demultiplexed signal at the input and at the output of the NOLM are presented. The input signal presents high noise on the "0" level, but the output signal shows that the noise on the

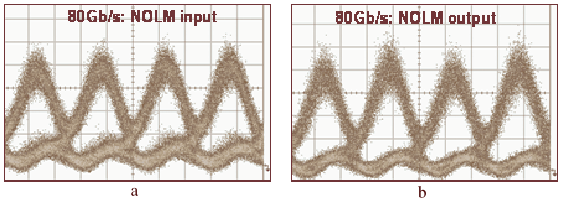

Figure 4.6: (a) eye-diagram of 80 Gbit/s data at NOLM input (b) eye-diagram of 80 Gbit/s data at NOLM output.

"0" level has been strongly reduced. Looking at the "1" levels the output signal appears to have more noise than the input signal.

Figure 4.8 shows the BER values at the input and at the output of the NOLM as a function of the receiver input power for one of the two multiplexed 40 Gbit/s channels. At the input of the NOLM the BER, in the best case, is 2.8×10^{-7} with receiver input power of -22.7 dBm. The BER curve at the output of the NOLM shows a receiver input power reduction of 6 dB for the same BER value. Moreover for a receiver input power higher than -27 dBm an error free data signal is obtained. This reduced receiver power is the fingerprint of noise suppression, and demonstrates that the noise on the "0" level in the signal has been cleaned considerably. Error free detection is defined as a BER better than 10^{-9}.

Figure 4.9 shows the results when a 160 Gbit/s signal is input to the NOLM. Due to the inability to demultiplex from 160 to 40 Gbit/s with this setup, an analysis is carried out on the basis of looking at a 50 GHz oscilloscope and an optical spectrum analyzer. The eye-diagram of the signal at the output of the NOLM (Figure 4.9 top right) appears clearer than the eye-diagram of the input signal (Figure 4.9 top left). This is in part aided by the pulse compression and in part by the suppression of the noise on the "0" level. A spectral broadening of the signal is also observed in figure 4.9 and that results in a pulse compression of the signal to a FWHM of 2.1 ps.

4.5.3 Conclusion

The experiment shows an improvement in the receiver sensitivity when an imbalanced NOLM is used for noise suppression on the "0" level. The

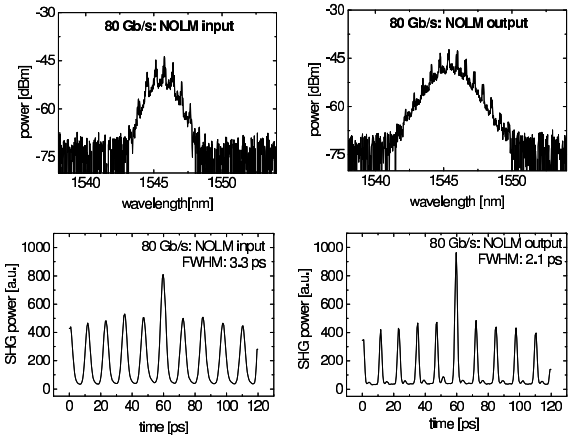

Figure 4.7: Left: Spectrum and autocorrelation of the 80 Gbit/s signal at the input to the NOLM. Right: Spectrum and autocorrelation at the output of the NOLM, revealing spectral broadening due to SPM and the resultant pulse compression from 3.3 ps to 2.1 ps.

combination of noise suppression and pulse compression improves the receiver sensitivity by 6 dB, when an 80 Gbit/s signal is investigated. A complete BER curve is obtained after applying the pedestal suppressor to the 80 Gbit/s signal, giving rise to an improvement of the receiver sensitivity. Due to receiver limitations, BER measurements can not be performed when investigating a 160 Gbit/s signal and clear conclusions can not be stated. Based on the conclusions made when an 80 Gbit/s signal is investigated it is believed that an improvement of a 160 Gbit/s signal will also be feasible.

4.6 Experimental investigation of a 3R-regenerator based on a 3-stage NOLM scheme

An experimental investigation of the entire 3-stage NOLM setup is performed when data rates of 80 and 160 Gbit/s are considered. Q-factors are estimated using the sampling oscilloscope in order to give a qualitative performance evaluation.

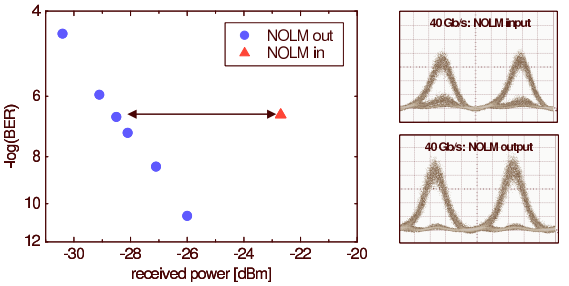

Figure 4.8: Left: BER measurements of the 80 Gbit/s data demultiplexed to 40 Gbit/s at the input and the output of the NOLM, with the output being error free. Right: The corresponding eye-diagrams of the demultiplexed data.

4.6.1 Experimental setup of 3R regenerator

The experimental setup is seen in figure 4.10. The regenerator is the central part of the setup and consists of 3 NOLMs all using HNLF with a nonlinear coefficient of ~ 10 W^{-1}·km^{-1} and zero dispersion wavelength at 1553 nm for the HNLFs used in the first two NOLMs and a zero dispersion wavelength of 1559 nm for the HNLF used in the last NOLM. The dispersion slope of all the HNLFs at 1550 nm is $S = 0.02$ ps/(nm^2·km). The HNLF used in the experiment are 1 km, 1 km and 500 m long, respectively for the 3 NOLMs. The principle of operation of the regenerator is described in section 4.4 and leads to a cleaning of the entire data signal and a wavelength conversion during the regeneration process.

Since the NOLM is not polarization maintaining, the problem of the reduced efficiency due to the counter propagating pulses is overcome by an opportune setting of the polarization controller in the 2^{nd} NOLM [87, 88].

The signal pulses are generated by a MLFRL and compressed at the output of the MLFRL in order to keep the pulses in the 160 Gbit/s time slot. The wavelength of the signal is 1547 nm and pulses have a width of ~ 1 ps after compression. The signal is modulated using a Mach-Zehnder (MZ) modulator resulting in a 10 Gbit/s signal with a $2^7 - 1$ PRBS. The signal is multiplexed to 80 or 160 Gbit/s using a polarization maintaining multiplexer and transmitted through a dispersion compensated fiber span consisting of 44 km SMF, 6 km DCF and an EDFA. The imperfect dispersion compensation and the noise from the EDFA helps deteriorate the signal before regeneration.

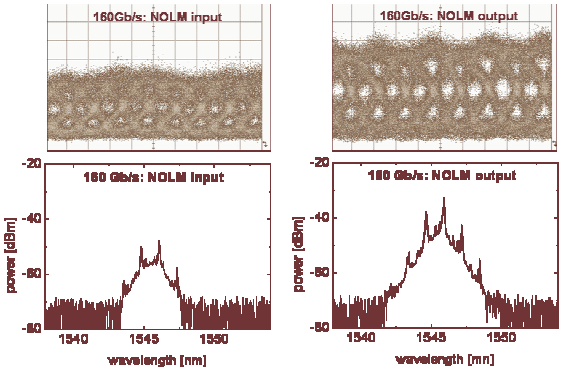

Figure 4.9: Left: 160 Gbit/s eye-diagram and spectrum at the input to the NOLM. Right: 160 Gbit/s eye-diagram and spectrum at the output. Eyes measured on 50 GHz scope. Spectral broadening results in a 2.1 ps wide output pulse.

The clock signal pulses are generated by a semiconductor monolithic mode-locked laser (MMLL). The clock signal and the data signal are synchronized to 10 GHz. The wavelength of the clock signal is 1560 nm in order to avoid walk-off between the clock pulses and the data signal in the second NOLM. The clock pulses are 3.5 ps wide and are multiplexed to 80 GHz or left at 10 GHz.

The relative short length of HNLF helps reduce the instability of the NOLMs from mechanical vibrations which can cause polarization fluctuations.

4.6.2 Results of 3R-regeneration experiment

In order to keep the setup simple and useful when characterizing the performance of the regenerator, the clock is kept at 10 GHz making the second NOLM a combination of a regenerator and a demultiplexer and only a single 10 Gbit/s channel of the original multiplexed signal will be regenerated.

With an 80 Gbit/s data signal transmitted, the investigated signal has a pulse width of 5.6 ps and a Q-factor of 3 when entering the regenerator. The Q-factor is estimated measuring histograms, and thereby getting probability density functions (pdf) for the ”1” and ”0” levels, using a

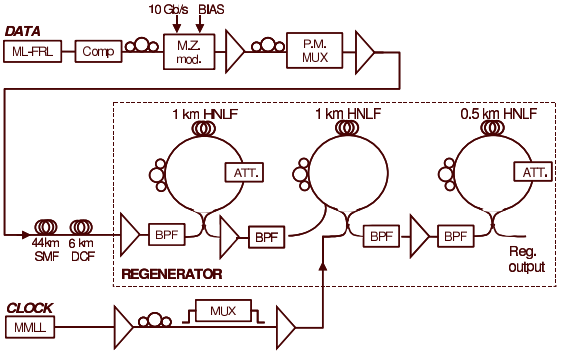

Figure 4.10: Schematic of the experimental setup of the 3R-regenerator based on a 3 stage NOLM configuration.

50 GHz sampling oscilloscope. Determining the "1" and "0" levels is done by looking at the scope in order to set the boundaries for the histogram measurements. That leads to considerable uncertainty on the Q-factor measurements.

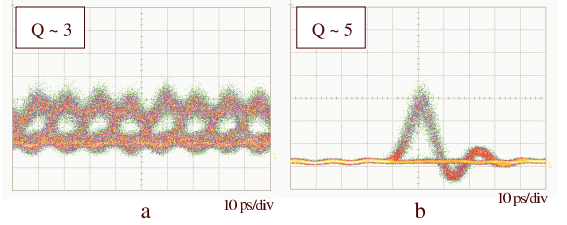

Figure 4.11: (a) The 80 Gbit/s input signal, (b) 10 Gbit/s regenerated and demultiplexed signal.

Figure 4.11 shows the eye-diagram of the 80 Gbit/s signal at the input to the regenerator and after regeneration and demultiplexing. The eye-diagram of the regenerated 10 Gbit/s eye looks well-behaved with the "0" level clean and the "1" level having intensity noise which is believed to come from the clock signal. Looking at the eye-diagram of the 80 Gbit/s signal in figure 4.11 gives an indication of the difficulty in determining where to set the boundary conditions in order to measure histograms and get the pdfs for the "0" and "1" levels. If an 80 GHz clock is used

the only difference will be a very small XPM contribution from the other clock pulses, but this can be made small by using small power. Mostly one would be limited by the quality of the clock pulses. Figure 4.12 shows the result when an 80 Gbit/s signal is regenerated using an imperfect 80 GHz clock. Figure 4.12 shows the regenerated 80 Gbit/s signal and an oscilloscope picture of the 80 GHz clock signal. The clock multiplexer could not be aligned properly, so the clock pulse train is very uneven. The signal at the output of the regenerator follows the pattern of the clock, so the conversion is fast and efficient enough. The estimated Q-factor measured on the scope is improved to 3.6 for the best eye-diagram. This is a small improvement of 0.6.

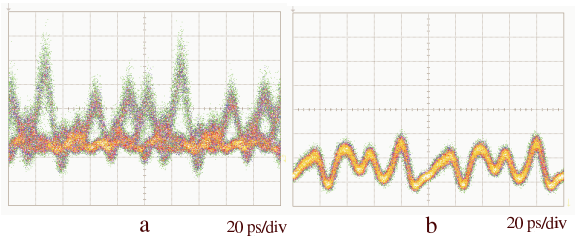

Figure 4.12: (a) Regenerated 80 Gbit/s signal, (b) waveform of 80 GHz clock.

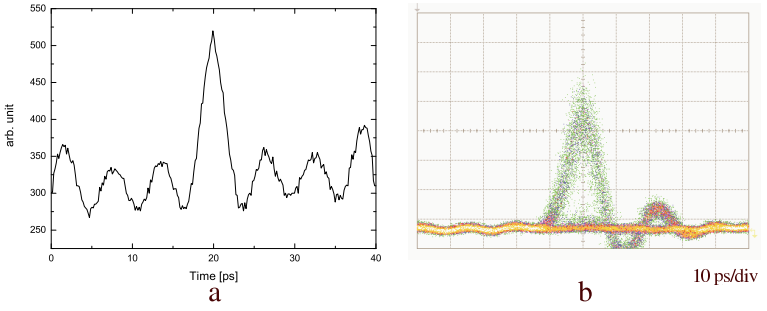

Figure 4.13: (a) Autocorrelation of 160 Gbit/s signal at input of regenerator, (b) 10 Gbit/s regenerated and demultiplexed eye-diagram.

Figure 4.13 shows an autocorrelation trace of the input 160 Gbit/s signal and a regenerated eye-diagram when a 10 GHz clock is used. The Q-factor is found to be 4.6.

Table 4.1: Q-factors

Input/output signal (Gbit/s)	Q-value dB
80/input	3.0
80/80	3.6
80/10	5.0
160/10	4.6

A comparison between eye-diagrams obtained when an 80 Gbit/s signal (figure 4.11(b)) and a 160 Gbit/s signal (figure 4.13(b)) is input to the regenerator and a 10 GHz clock signal is used in the second NOLM is performed. The two eye-diagrams have little noise on the "0" level and considerable intensity noise on the "1" level, especially for the eye-diagram shown in figure 4.13(b).

Table 4.1 shows an overview of the Q-factors found depending on the speed of the incoming signal and the clock. A more rigorous comparison of the Q-factor improvement when an 80 Gbit/s signal is input and regenerated shows an increase in Q-factor of 0.6, which considering the uncertainty associated with using the uneven 80 GHz clock pulses is nearly identical to the incoming signal. The noise on the "1" level does not change from input to output in the regenerator as it should according to the principle described in section 4.4. The noise on the "0" level is reduced and results in the small improvement of the Q-factor. The difference in Q-factor when a 10 GHz clock is used and the input data signal is either 80 Gbit/s or 160 Gbit/s is believed to be due to the peak power of the signal in the first NOLM being higher for the 80 Gbit/s signal. Each channel in the 80 Gbit/s case has higher peak power in the first stage because the same average power is used and therefore better noise suppression on the "0" level is achieved.

4.6.3 Conclusion of 3R-regenerator experiment

An experimental investigation of the 3-stage NOLM regenerator has been performed at data rates of 80 Gbit/s. A small improvement in the obtained Q-factor is seen when an 80 Gbit/s signal and an 80 GHz clock is input to the regenerator. A combination of regeneration and demultiplex-

ing for data rates of 80 Gbit/s to 10 Gbit/s and 160 Gbit/s to 10 Gbit/s have also been investigated.

Precise conclusions can not be made based on the vague results obtained in this investigation.

4.7 Summary

In this chapter a presentation and an experimental investigation of a 3R-regenerator based on a 3-stage NOLM has been performed. Experimental characterization of the first NOLM (pedestal suppressor) in the 3R-regenerator showed an improvement when an 80 Gbit/s signal is input to the NOLM. Based on the findings for the 80 Gbit/s signal and the inability to demultiplex from 160 Gbit/s to 40 Gbit/s in the receiver, it is believed that the pedestal suppressor will also work at higher bit rates i.e. 160 Gbit/s. The attained results when using one NOLM as a pedestal suppressor and noise eliminator showed one way of improving the receiver sensitivity for error free detection in an optical system.

The principle of a 3R-regenerator based on a 3-stage NOLM setup shows one approach to all-optical 3R-regeneration of high speed optical data signals. The experimental investigation of the 3R-regenerator shows the difficulty in making it work. The stability of a 3-stage NOLM setup is very limited due to the high number of parameters that needs to be controlled to a very high degree when a 160 Gbit/s signal is to be regenerated. The high requirements on the control of the polarization and power levels associated with NOLM experiments, makes it increasingly difficult to manage when several NOLMs are used in an experiment.

One way of improving the experimental results and thereby clarify the conclusions is to use a better multiplexer for the clock pulses in the 3R-regenerator, and to be able to demultiplex from 160 Gbit/s to 40 Gbit/s in the pedestal suppressor experiment.

Chapter 5

Wavelength conversion

5.1 Introduction

A high speed wavelength converter is an essential part within a high capacity all-optical WDM system and thus considerable interest in the development of a practical wavelength converter exists [89, 90]. An all optical wavelength converter satisfies the high speed requirement of modern communication systems and can be used for single channel wavelength conversion [91] and wavelength conversion of a WDM signal [89]. Reports on optical wavelength conversion using various methods already exist: XPM in a NOLM [83, 91, 92, 93], supercontinuum generation and spectral slicing [39], FWM in a fiber [94, 95] and interferometric SOA wavelength conversion [90], just to name a few. A preferred optical wavelength converter is transparent to both data rate and modulation format. One method to get such an optical wavelength converter is to use FWM in a nonlinear fiber.

Modern high speed optical systems are likely to use advanced modulation formats such as differential phase shift keying (DPSK) and return to zero DPSK (RZ-DPSK) due to their various advantages compared with conventional on-off keying (OOK) format, for example better receiver sensitivity associated with balanced detection, larger dispersion tolerance and better resilience to fiber nonlinear effects [96]. With the recent interest in phase modulated signals for optical communication systems, it is interesting to look at wavelength conversion methods suitable for such signals. Conventional methods, such as those relying on cross

gain modulation (XGM) in a SOA or XPM in a NOLM [83, 97] or in an interferometric SOA wavelength converter [90], disregard the phase information as they depend on the intensity of the signals. FWM in a fiber is a phase and intensity modulation preserving process that is furthermore independent of the bit rate owing to the virtually instantaneous response of the Kerr nonlinearity of fused silica, therefore satisfying the major requirements for transparent wavelength conversion in all-optical systems [98, 99, 100]. So far, wavelength conversion of phase modulated signals has been demonstrated using FWM in a nonlinear fiber for simultaneous amplitude shift keying ASK/DPSK modulation [101] at 2.5 Gbit/s, or in a SOA for RZ-DPSK signals [102] at 10 Gbit/s.

The design freedom offered by the crystal fiber technology makes HNL-PCFs very suitable for special applications where the fiber parameters should be tailored to satisfy specific demands, namely a flat dispersion profile, a high nonlinearity coefficient and low loss. The dispersion of HNL-PCFs can be tailored to satisfy the phase matching requirements for FWM. FWM wavelength conversion in a HNL-PCF has been reported for NRZ modulated signals at 10 Gbit/s [14, 103], as well as for phase conjugation at 40 Gbit/s [104].

In this chapter we will discuss FWM in HNL-PCFs and show how they can be used to make a transparent optical wavelength converter for both single channel systems and WDM systems. An experiment using FWM in a HNL-PCF for optical phase conjugation will also be discussed.

5.2 FWM as a way of wavelength conversion

The FWM process used in the following experiments can be described by considering the interaction of three co-propagating waves at frequencies f_i, f_j and f_k as shown in figure 5.1. The process gives rise to a new optical wave at f_{FWM} [48]:

$$f_{FWM} = f_j + f_i - f_k \tag{5.1}$$

It is this wave that is used in wavelength conversion experiments as the wavelength converted signal.

The new wave is called the FWM product or sideband and the power of this product is:

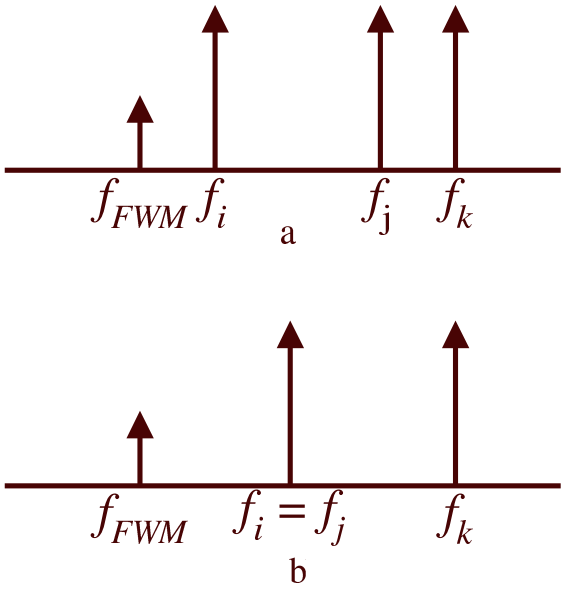

Figure 5.1: Schematic of a FWM process. f_i, f_j and f_k are the incident waves and f_{FWM} is the FWM generated wave. (a) shows the nondegenerate case and (b) shows the degenerate case with $f_i = f_j$. The degenerate case is the method used in the wavelength conversion experiments discussed later in this chapter.

$$P_{FWM}(L) \propto \gamma^2 L_{eff}^2 P_i(0) P_j(0) P_k(0) e^{-\alpha L} \eta \tag{5.2}$$

where η is the conversion efficiency and given by $\eta = \frac{\alpha^2}{\alpha^2+\Delta\beta^2}(1 + \frac{4e^{-\alpha L}\sin^2(\frac{\Delta\beta L}{2})}{(1-e^{-\alpha L})^2})$ where α is fiber attenuation, $\Delta\beta$ is difference between propagation constants, L is the length of the fiber, L_{eff} is the effective length of the fiber and $P_i(0)$, $P_j(0)$ and $P_k(0)$ are the input power of the three waves. The product is maximized if the phase matching condition $\Delta\beta = 0$ is satisfied [48].

$$\Delta\beta = \beta(f_i) + \beta(f_j) - \beta(f_k) - \beta(f_{FWM}) \tag{5.3}$$

Equation 5.2 shows the importance of the fiber parameters in the FWM process. The nonlinear coefficient, the effective length, the dispersion and the attenuation of the fiber are all parameters that need to be controlled

very accurately to get the most efficient possible FWM product. The difference between the propagation constants depends on the dispersion of the fiber [94, 95].

By having only two co-propagating waves, a very strong pump and a signal, the pump supplies two photons to the FWM process while the signal supplies one, equivalent to setting $f_i = f_j$ in equation 5.1. This situation is shown in figure 5.1(b). Both ways of describing the FWM process are discussed in details in [94, 95].

5.3 Fiber parameters

Photonic crystal fiber technology has made considerable progress in recent years and it is possible to tailor a fiber to satisfy very specific demands. This has resulted in production of a low loss dispersion flattened highly nonlinear photonic crystal fiber (HNL-PCF) [18]. Using such a fiber it becomes feasible to implement nonlinear telecommunication devices with reduced length/power requirements. Most of the experimental work presented in this chapter is based on a 50 m long HNL-PCF with a nonlinear coefficient, $\gamma = 11.2$ W^{-1}·km^{-1} [18]. The dispersion curve is shown in figure 5.2 and it can be seen that the fiber has no zero dispersion wavelength and the dispersion is always negative in the telecommunication range. The inset in figure 5.2 shows a microscopic picture of the microstructured region of the HNL-PCF. The HNL-PCF has a core diameter of 1.5 μm and a three-fold symmetric core region. The dispersion of the fiber can be flattened over a wide range (less then -3 ps/(km·nm) over 1500-1600 nm) [18] by choosing the appropriate pitch and hole size. The dispersion variation is less than 1.3 ps/(km·nm) in the range of 1500-1650 nm with a dispersion slope of less than 1×10^{-2} ps/(km·nm^2) at 1550 nm. The total insertion loss of the fiber is 2.6 dB for this 50 m fiber.

5.4 Wavelength conversion of a 40 Gbit/s RZ-DPSK signal

5.4.1 Introduction

In this experiment a demonstration of wavelength conversion of a 40 Gbit/s RZ-DPSK signal using FWM in a HNL-PCF as described in

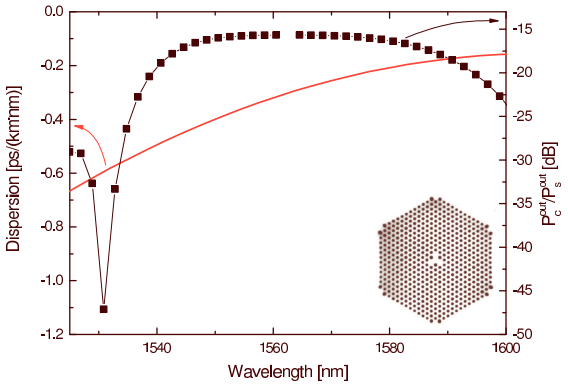

Figure 5.2: Dispersion curve (left) of the 50 m HNL-PCF and simulated conversion efficiency (right) when the signal is fixed at 1562.5 nm. The inset shows the microstructured region of the HNL-PCF where the three-fold symmetry is obtained from three missing holes.

section 5.3 is presented. The conversion efficiency and conversion bandwidth are shown and a discussion of the signal quality of the converted signal is performed.

5.4.2 Experimental setup

A schematic of the experimental setup used in this experiment is shown in figure 5.3. Light from a continuous wave (CW) laser is modulated using a Mach-Zehnder (MZ) modulator biased at peak in the transmission curve, driven with a 20 GHz clock signal to generate a 40 GHz pulse train with a pulse width of 33% of the time slot, or 8.3 ps. Then a second MZ modulator biased at null point and driven with a 40 Gbit/s $2^{31}-1$ PRBS adds phase modulation resulting in a 40 Gbit/s RZ-DPSK signal. The signal is merged with a pump signal from another CW laser using a 3 dB coupler before amplification and entering the HNL-PCF. The average power entering into the HNL-PCF is 25 dBm, total pump and signal power. Stimulated Brillouin scattering (SBS) measurements performed on the HNL-PCF yield a SBS threshold of ~ 21 dBm.

The state of polarization of both the signal and the pump is optimized in order to ensure optimum phase matching and thus best conversion efficiency. At the fiber output the converted signal is filtered out using a

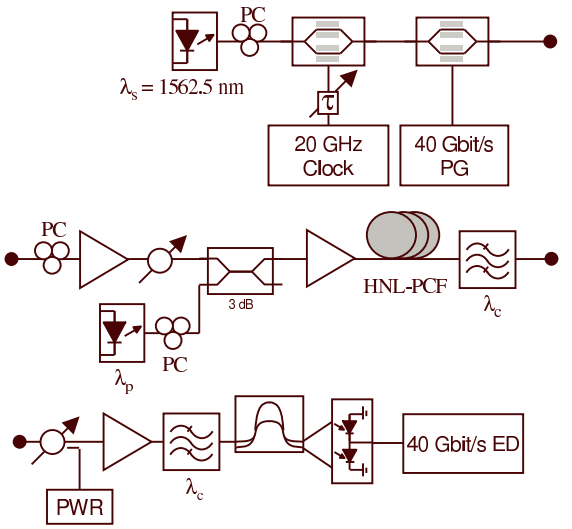

Figure 5.3: Schematic of the experimental setup. PC: polarization controller, λ_s: signal wavelength, λ_p: pump wavelength, λ_c: converted signal wavelength, PWR: optical power meter, PG: pattern generator and ED: error detector.

tunable optical bandpass filter with a 3 dB bandwidth of 0.9 nm. After the filtering the converted signal is detected in a balanced pre-amplified receiver. At the receiver the signal is amplified by an EDFA, filtered by an optical bandpass filter with a 3 dB bandwidth of 0.9 nm, and then demodulated using a 1 bit delay interferometer. The converted signal is detected using two photodiodes both with a bandwidth of 45 GHz in a balanced configuration. Signal quality is quantified by measuring the BER using a 40 Gbit/s error detector. The signal is fixed at 1562.5 nm and the pump is swept from 1559.8 nm to 1545.2 nm allowing wavelength conversion of the signal to shorter wavelengths. The limitation on the conversion range is the gain bandwidth of the pre-amplifier in the receiver and the tuning range of the optical bandpass filters, limiting the wavelength of the converted signal to be above ∼1530 nm.

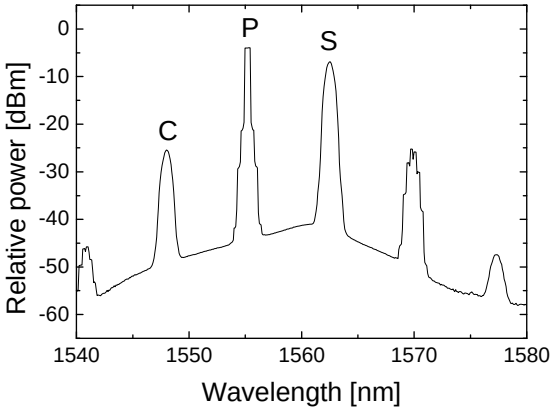

Figure 5.4: Spectrum at the HNL-PCF output, with the pump at 1555.2 nm (P), the signal at 1562.5 nm (S) and the converted signal at 1548.0 nm (C). The second generation sidebands are also clearly seen. (Resolution bandwidth 1 nm)

5.4.3 Results

Figure 5.4 shows the spectrum at the HNL-PCF output with the signal located at 1562.5 nm and the pump at 1555.2 nm and the converted signal at 1548.0 nm. The first and second order sidebands of the FWM process are clearly seen. The optical signal-to-noise (OSNR) of the converted signal is seen to be better than 25 dB in a 1 nm resolution bandwidth. Figure 5.5 shows the conversion efficiency, defined as the ratio between the power of the converted signal and the original signal, at the output of the HNL-PCF versus wavelength when the signal is fixed at 1562.5 nm. These results demonstrate a 3 dB bandwidth of the conversion efficiency as broad as 31 nm.

Note that the conversion efficiency becomes high for small detuning. It is believed to be due to overlap between the converted signal and the pump wavelength. The optical bandpass filter can not suppress the pump completely when the signal and pump are placed close together. The longer the wavelength detuning, the better the suppression of the pump and the better the sensitivity of the converted signal.

Figure 5.6 shows the BER versus receiver input power measurements for the converted signals. The receiver sensitivity, defined as the receiver

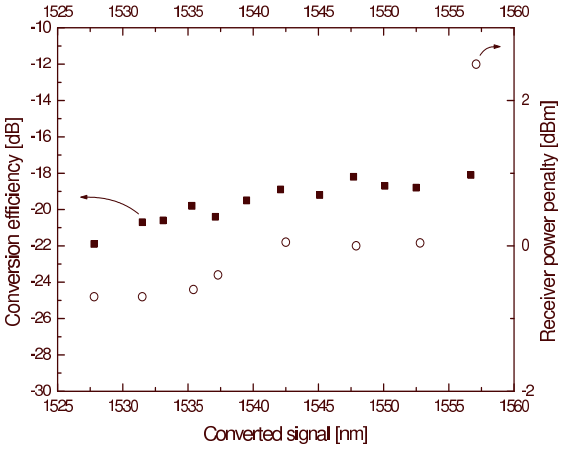

Figure 5.5: Conversion efficiency and conversion power penalty versus wavelength. The signal is fixed at 1562.5 nm and the pump moves from 1559.8 nm to 1547.0 nm. A 3 dB bandwidth conversion efficiency of more than 31 nm is obtained.

input power at a BER of 1.0×10^{-9}, of the converted signal is seen to improve with larger signal and converted signal separation. This is partly due to the filter effect and partly because the receiver becomes more sensitive for shorter wavelength. Even if the wavelength dependence of the receiver is taken into account, the receiver power penalty is seen to become smaller towards short wavelengths when wavelength conversion is performed. Figure 5.5 shows how the receiver power penalty improves and becomes better for wavelength conversion to shorter wavelengths. The power penalty becomes zero for short wavelengths, meaning that optical wavelength conversion can be performed without system degradation.

Figure 5.7 shows the waveforms of the transmitted signal at 1562.5 nm and the converted signal at 1537.4 nm and 1531.5 nm. The demodulated eye-diagrams obtained after single-ended detection of the two converted signals are also seen. It is seen how the optical waveform of the converted signals retains its shape compared to the transmitted waveform.

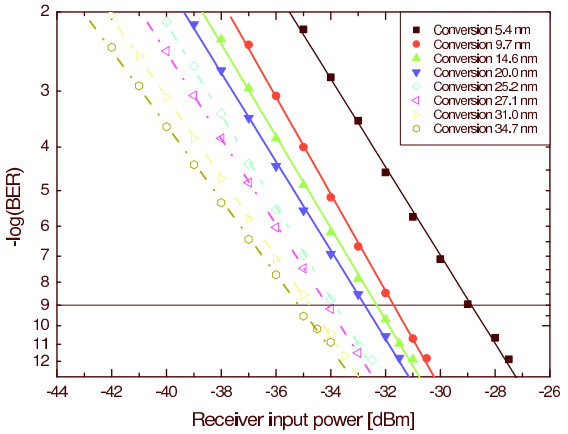

Figure 5.6: BER curves of converted signals for several values of wavelength separation. (Conversion in corresponds to wavelength conversion.)

5.4.4 Conclusion of 40 Gbit/s RZ-DPSK experiment

A demonstration of wavelength conversion of a 40 Gbit/s RZ-DPSK signal has been successfully performed using a 50 m HNL-PCF in a simple FWM scheme. The conversion efficiency is found to be better than −20 dB in a 31 nm conversion band. The wavelength conversion to shorter wavelengths was limited by the bandwidth of the EDFA in the receiver and the tunability of optical bandpass filters. It was also shown how the quality of the signal was maintained during the wavelength conversion process. The HNL-PCF used has been proven to be a very good candidate for wavelength conversion of high speed RZ-DPSK signals in the C-band using FWM.

5.5 Wavelength conversion of a 6 × 40 Gbit/s DPSK WDM signal

5.5.1 Introduction

So far, wavelength conversion of single channel phase modulated signal has been demonstrated using FWM in a nonlinear fiber for simultaneous ASK/DPSK modulation at 2.5 Gbit/s [101], or in a SOA for return to

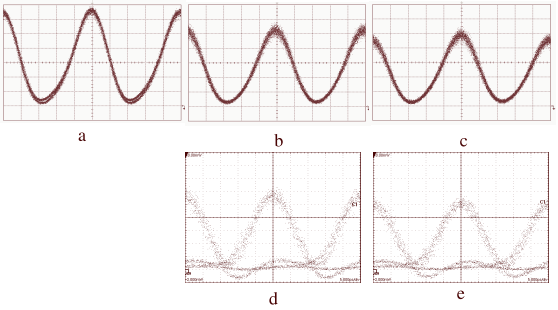

Figure 5.7: Eye-diagrams for the transmitted signal at 1562.5 nm (a) and for the converted signal 1537.4 nm (b) and 1531.5 nm (c) respectively. The single-ended demodulated eye-diagrams of the two converted signal is also seen in (d) and (e).

zero DPSK signals [102] at 10 Gbit/s and as demonstrated in section 5.4. Wavelength conversion of a WDM DPSK signal in a highly nonlinear photonic crystal fiber (HNL-PCF) is a new and unexplored area of research.

In this section, wavelength conversion of a 6×40 Gbit/s DPSK WDM signal using FWM in a dispersion flattened HNL-PCF is shown. A conversion efficiency of ~ -20 dB for 24.8 dBm pump power and a power penalty varying between 2 and 4 dB is shown. Cross talk between channels is less than ~ 31 dB.

5.5.2 Experimental setup

Figure 5.8 shows a schematic of the setup used in this experiment. All 6 channels are polarization optimized in order to achieve phase matching before being multiplexed in an arrayed waveguide grating (AWG) with 200 GHz spacing. The polarization of all 6 channels is then controlled by one polarization controller before the signal is modulated in a MZ modulator to obtain a 40 Gbit/s DPSK signal on all 6 channels. The 6 channels have wavelengths of 1552.0 nm (channel 1) to 1560.0 nm (channel 6) with 200 GHz spacing. The AWG has a 3 dB bandwidth of 0.8 nm.

A MZ modulator biased at a null point and driven with a 40 Gbit/s $2^{31} - 1$ PRBS adds phase modulation resulting in a 40 Gbit/s DPSK signal. The signal is polarization controlled and amplified before being combined with a pump signal from a CW laser using a 3 dB coupler and

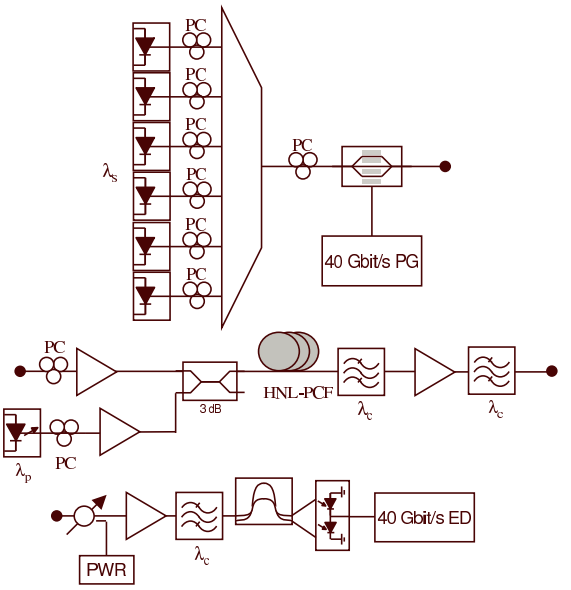

Figure 5.8: Schematic of the experimental setup. λ_s: signal wavelengths, λ_p: pump wavelength, λ_c: converted signal wavelength, PC: polarization controller, PWR: power meter, PG: pattern generator, ED: error detector.

entering the HNL-PCF with a power of 20 dBm. The pump signal enters the HNL-PCF with a power of 24.8 dBm.

The state of polarization of both the signal and the pump is optimized in order to ensure the best conversion efficiency on all 6 channels. When a polarization state is selected it is not changed during the entire duration of the experiment. At the fiber output one of the 6 converted channels is filtered out using two tunable optical bandpass filters each with a 3 dB bandwidth of 0.9 nm. At the receiver the signal is amplified by an EDFA, filtered by an optical bandpass filter with a 3 dB bandwidth of 0.9 nm and demodulated using a 1 bit delay interferometer. The converted channel is detected using two 45 GHz photodiodes in a balanced configuration. Signal quality is quantified by measuring the BER using a 40 Gbit/s error detector. The pump is fixed at 1544.3 nm.

5.5.3 Results of WDM experiment

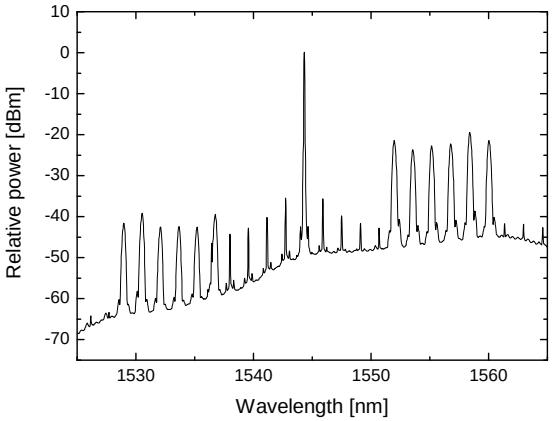

Figure 5.9: Spectrum at the HNL-PCF output. The pump and the 6 channels as well as the 6 converted channels are seen. The small peaks next to the pump are due to FWM between two signal channels and the pump.

Figure 5.9 shows the spectrum at the output of the HNL-PCF. The pump, the 6 signal channels and the 6 converted channels are clearly seen. The pump is fixed at 1544.3 nm. The converted channels are located at 1528.9 nm (channel 6) to 1536.8 nm (channel 1) with 200 GHz spacing. The OSNR of each channel at the converted wavelength is seen in figure 5.10 and varies between -24.0 dB to -17.4 dB in a 0.1 nm resolution bandwidth. The conversion efficiency for each channel versus converted wavelength (measured on a 0.1 nm resolution bandwidth) is also shown in figure 5.10 and seen to vary between -17.6 dB and -20.5 dB. Each point in figure 5.10 corresponds to a specific channel with channel 1 located at the converted wavelength 15.2 nm (wavelength 1536.7 nm) and channel 6 located at the converted wavelength 31.5 nm (wavelength 1528.9 nm).

Narrow peaks on both sides of the pump can also be seen in figure 5.9. These peaks are spaced 200 GHz apart and 200 GHz from the pump due to FWM between two signal channels and the pump. The FWM process generates a wavelength conversion of the pump depending on the spacing between the two signal channels according to $f_{FWM} = f_p + f_s^i - f_s^j$ [94], where f is the frequency and the schematic process is seen in figure 5.1(a).

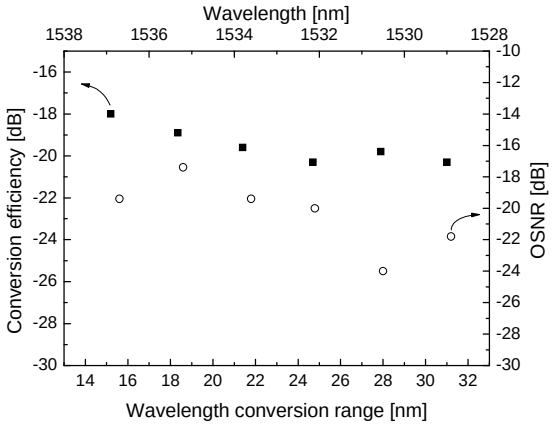

Figure 5.10: Conversion efficiency versus detuning between signal and converted signal. The open circles show the OSNR versus the wavelength of the channel at the top and right axes.

Figure 5.11 shows the spectrum when the pump is detuned to shorter wavelength, (1540.8 nm), effectively wavelength converting the 6 signal channels to even shorter wavelengths. The presence of the converted channels and the converted pump, i.e. the small peaks, is now more clear.

The converted signals are results of the degenerate FWM process as shown in figure 5.1(b) and the small peaks are the result of the nondegenerate FWM process as shown in figure 5.1(a).

By performing simulations of the setup and using the same parameters as in the experiment, good agreement between experimental and numerical results are obtained. Figure 5.12 shows the calculated output spectrum from the HNL-PCF. Comparing to the spectrum from figure 5.9, good agreement is observed. The simulations are performed using VPI software. Figure 5.12 shows the spectra at the HNL-PCF output when the pump is at 1544.3 nm.

All 6 wavelength converted channels shown in figure 5.9 are analyzed and BER curves are obtained. BER curves are measured for all 6 wavelength converted channels and 3 of them are shown in figure 5.13 together with the corresponding back to back curves for the original signals. The

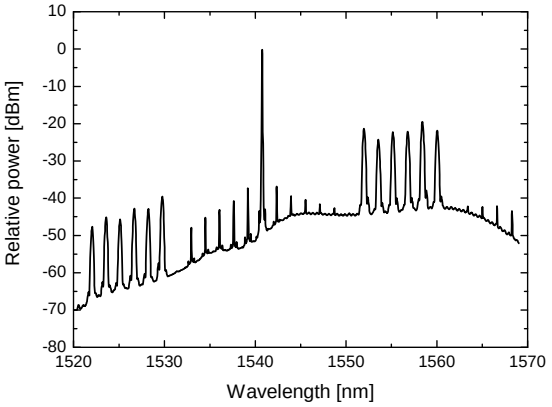

Figure 5.11: Output spectrum from the HNL-PCF. The pump and the 6 channels as well as the 6 converted channels are seen. FWM between the pump (1540.8 nm) and the combined 6 signal channels generate 5 peaks with 200 GHz spacing.

figure shows the BER for channel 1, channel 3, and channel 5. Back-to-back measurements are performed after multiplexing and demultiplexing of the 6 channels but without wavelength conversion. The power penalty due to the wavelength conversion process for each channel is shown in figure 5.14.

The power penalty for including the AWG multiplexer in the back to back BER measurements is measured to be ∼0.7 dB.

It is seen that the power penalty varies between 4.1 dB and 2.0 dB becoming smaller for longer wavelength separation. The two channels with the higher power penalty are at 1535.2 nm and 1536.8 nm and are the channels most effected by the wavelength conversion of the pump. A closer look at figure 5.9 shows that the fifth peak of the wavelength converted pump nearly coincides with the wavelength converted channel 1 at 1536.8 nm. The peak has a phase different from the signal and therefore deteriorates the wavelength converted channel performance, leading to higher power penalty for that channel. In figure 5.15 both the optical and electrical eyes from the back to back case and the converted case are seen. A comparison of the optical eye-diagrams shows added noise to the converted eye. That translates into noise on the electrical eye-diagram

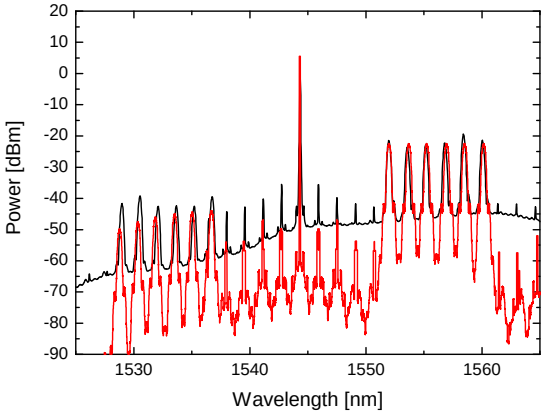

Figure 5.12: Simulation (red) and data (black) at the output from the HNL-PCF when the pump is at 1544.3 nm.

and causes deterioration to the received signal causing an increase in power penalty.

The cross talk is estimated by simulations of the WDM wavelength conversion when one of the channels in the WDM signal is turned off and wavelength conversion is performed. Figure 5.16 shows the simulated spectrum at the HNL-PCF output. The cross talk is defined as the ratio between the power of the missing channel and the neighboring FWM product channels and is better than 38 dB.

5.5.4 Conclusion

A successful wavelength conversion of a 6 × 40 Gbit/s DPSK signal has been demonstrated in a 50 m long HNL-PCF with a nonlinear coefficient $\gamma = 11.2\ \mathrm{km}^{-1}\cdot\ \mathrm{W}^{-1}$. The converted channels do all have a conversion efficiency better then −20.6 dB and the deviation is less than 3 dB. The power penalty attained by the system due to the wavelength conversion process of the WDM signal is between 2.0 dB to 4.1 dB. The cross talk in the WDM signal in the HNL-PCF is also evaluated to be better than 38 dB.

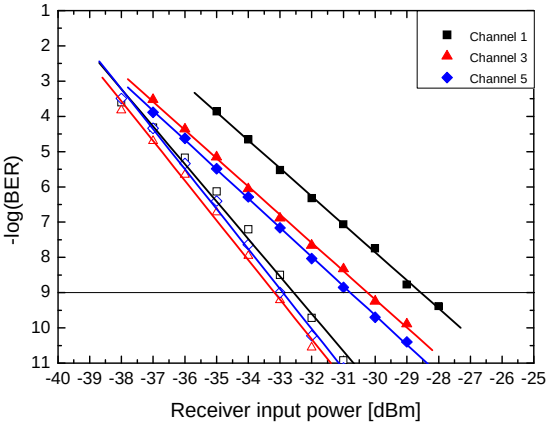

Figure 5.13: BER curve for 3 channels. The back to back measurements are represented by open symbols and the wavelength converted measurements are represented by full symbols. Channel 1, 3 and 5 are shown.

5.6 Wavelength conversion of an 80 Gbit/s RZ-DPSK-ASK signal

5.6.1 Introduction

Multilevel modulation formats have been suggested for optical communication systems [105, 106]. Multilevel modulation can be implemented by combining phase and intensity modulation [107]. Generation of 40 Gbit/s signals using 10 Gbit/s equipment has been demonstrated by combining differential quadrature phase shift keying (DQPSK) and four level amplitude shift keying (ASK) [107]. This opens a new door for generation of high speed signals using electronics. Another very attractive feature of multilevel modulation formats is that they allow the generation of signals with higher bit-rates than state of the art electronic and opto-electronic equipment can deliver. This has already been demonstrated using DQPSK where signals with channel rate of 80 Gbit/s have been generated using 40 Gbit/s equipment [108].

In the following experiment, the generation of an 80 Gbit/s signal using a combination of DPSK with ASK and RZ pulse carving at a symbol rate of 40 Gbaud is performed. The 80 Gbit/s RZ-DPSK-ASK signal is

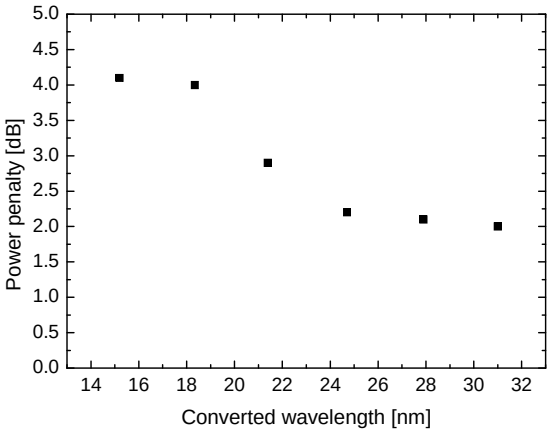

Figure 5.14: Power penalty versus wavelength when the pump is fixed at 1544.3 nm.

wavelength converted using FWM in a HNL-PCF and transmitted over 80 km of SMF and DCF fiber span.

5.6.2 Results and discussion

The setup used in this experiment can be seen in figure 5.17 where 3 MZ modulators are used to generate the signal. Light from a CW laser is modulated in the first MZ modulator driven with a 20 GHz clock signal with $2V_\pi$ voltage, where $2V_\pi$ is the voltage required to achieve π phase shift. The MZ modulator is biased at peak in the transfer function generating a 40 GHz pulse train with a FWHM pulse width of 8.3 ps (33% of bit slot at 40 Gbit/s). The pulse train is then phase modulated using the second MZ modulator biased at null point and driven with a PRBS of $2^{31}-1$ data signal having an amplitude equal to $2V_\pi$. A third MZ modulator driven with a $2^{23}-1$ PRBS data signal is used to intensity modulate the 40 Gbit/s signal, resulting in a 80 Gbit/s RZ-DPSK-ASK signal. The driving amplitude signal on the third MZ modulator were adjusted to obtain the desired extinction ratio on the ASK signal. The extinction ratio on the ASK signal is a trade-off between good eye-opening for the ASK signal and good eye-opening for the DPSK signal after demodulation. An extinction ratio of 6 dB resulted in equal BER for both tributaries, and

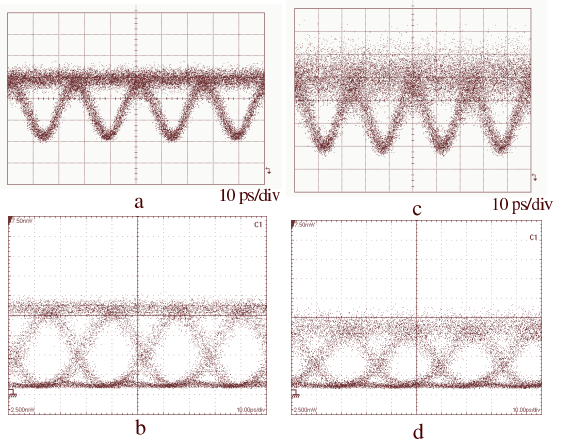

Figure 5.15: a) and b) show the optical and electrical eye-diagrams of the back to back of one of the channels in the WDM signal, respectively. c) and d) show the optical and electrical eye-diagram of the converted signal, respectively.

thus the lowest total BER. Therefore an extinction ratio of 6 dB is used for all measurements.

At the receiver, the signal is pre-amplified and filtered with an optical band-pass filter with a 0.9 nm 3 dB bandwidth. The signal is then split using a 3 dB coupler for detection of the ASK and DPSK signals, respectively. The DPSK signal is detected as described in previous sections and the ASK signal is detected using direct detection with a 50 GHz photodiode. Two 40 Gbit/s error detectors allowed for measurements of the BER of both ASK and DPSK simultaneously. The signal quality is quantified by BER measurements. The signal is fixed at 1556.4 nm and the CW pump is fixed at 1550.6 nm. The signal and pump are coupled together using a 3 dB coupler and amplified to 25 dBm total power before wavelength conversion in the HNL-PCF. The spectrum at the output of the HNL-PCF is seen in figure 5.18, where the FWM products are clearly seen.

The output of the HNL-PCF is filtered using an OBPF with a 3 dB bandwidth of 0.9 nm to filter out the converted signal located at 1544.8 nm. The conversion efficiency is estimated from figure 5.18 to be -18.8 dB in a 0.01 nm resolution bandwidth. The wavelength converted

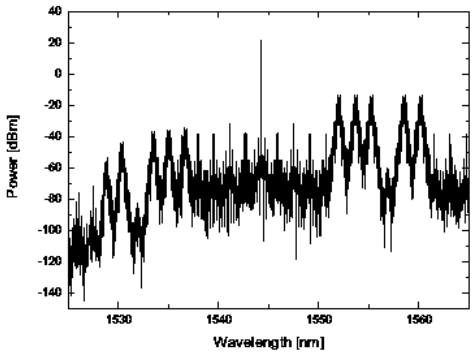

Figure 5.16: Simulated output spectrum from the HNL-PCF when one of the channels in the WDM signal is turned off. The cross talk is seen as the ratio between the missing channel and the other FWM products. It is seen to be better than 38 dB in the worst case.

signal is transmitted over a 80 km fiber span consisting of 80 km SMF and 13 km DCF.

Eye-diagrams of the generated ASK signal and the demodulated DPSK tributary are seen in figure 5.19 for the back-to-back case, the wavelength converted signal and the transmitted wavelength converted signal. Six distinct traces are visible in the demodulated DPSK tributary, due to differential demodulation of high-high, low-high, and low-low amplitude signals with either 0 or π relative phase shift.

The signal quality is quantified by BER measurements. Figure 5.20 shows results of BER measurements for the back-to-back signals, the wavelength converted signals, and the transmitted wavelength converted signals for both ASK and DPSK modulated signal. In all three cases, the ASK and DPSK BER curves are nearly identical. The receiver sensitivity of the back-to-back signal is -22.5 dBm, and -13.6 dBm for the wavelength converted signal, and after transmission the receiver sensitivity is seen to be -13.2 dBm. The primary degrading factor is believed to be the OSNR degradation after the conversion stage. From figure 5.19(c) and (d) it is seen how the signal waveform is very well preserved after conversion. From the eye-diagrams after transmission shown in figure 5.19(e)

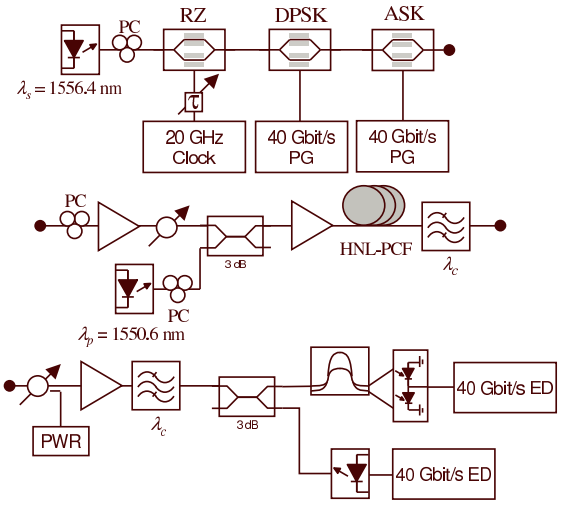

Figure 5.17: Experimental setup. The transmitter (top), the wavelength converter and fiber span (center), and the receiver (bottom).

and (f) it should be noted that the waveform is well maintained, but some degradation to the demodulated DPSK eye is observed. The degradation is due to cross talk from the ASK tributary to the DPSK tributary by SPM in the fiber, as symbols with high amplitude result in a much higher phase change due to SPM than low amplitude symbols.

5.6.3 Conclusion

The direct generation of an 80 Gbit/s RZ-DPSK-ASK signal with a symbol rate of 40 Gbaud, wavelength conversion in a HNL-PCF using FWM and transmission over 80 km SMF+DCF fiber span is demonstrated.

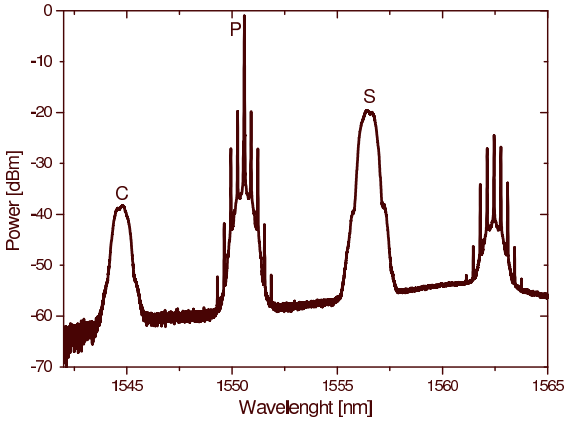

Figure 5.18: Optical spectrum at the output of the HNL-PCF, showing signal (S), the pump (P) and the wavelength converted signal (C). Resolution bandwidth 0.01 nm

5.7 Wavelength conversion in a 40 Gbit/s signal transmission over PCF

5.7.1 Introduction

By using FWM for wavelength conversion in a fiber, optical phase conjugation of the signal can be achieved. Optical phase conjugation has been used for dispersion compensation in fiber links [109].

An all crystal fiber dispersion compensated transmission link is demonstrated using a combination of transmission PCF [59] and a HNL-PCF [19]. A 40 Gbit/s NRZ signal is transmitted over 5.6 km of transmission PCF with a PRBS $2^{31} - 1$. The transmission PCF consists of two spools of PCF (2.6 km and 3.0 km) each with 1.7 dB/km loss and 32 ps/(nm·km) dispersion at 1550 nm [59]. The transmission length is beyond the dispersion limit for 40 Gbit/s signals, thus some form of dispersion compensation is needed. The two spools are separated by an optical phase conjugator (OPC) based on FWM in a HNL-PCF in order to realize mid-span spectral inversion [48]. The HNL-PCF used is 50 m long and has a nonlinear coefficient, $\gamma \sim 17$ W^{-1}·km^{-1}, and a zero dispersion wavelength at 1552.5 nm [19].

Based on the conversion bandwidth of the HNL-PCF the signal wave-

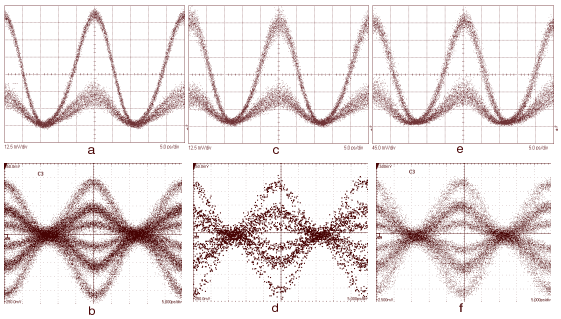

Figure 5.19: Eye-diagrams of the back-to-back signal (a)(b), after wavelength conversion (c)(d) and after transmision (e)(f), showing the ASK and DPSK signal components, respectively.

length, $\lambda_S = 1548.86$ nm, and the pump wavelength, $\lambda_P = 1555.24$ nm are selected. The conversion bandwidth of the HNL-PCF is seen in figure 5.21. The maximum conversion efficiency for a 25 dBm pump power is -20 dB and the 3 dB conversion bandwidth is 15 nm, primarily limited by the dispersion slope of the HNL-PCF.

5.7.2 Experimental setup

The setup is shown in figure 5.22. It can be seen how the signal is generated using a MZ modulator and a CW laser before it is transmitted over the first transmission spool. The optical phase conjugator (OPC) consists of a CW laser working as a pump, a high power EDFA, an optical bandpass filter (OBF) for noise reduction and a 3 dB coupler. The pump power delivered to the HNL-PCF is 25 dBm and both the signal and the pump are polarization controlled in order to obtain the best conversion efficiency. The converted signal is selected at the output of the HNL-PCF using an OBF having a 3 dB bandwidth of 1 nm. After transmission in the second spool the signal is detected in the receiver consisting of an EDFA with 4 dB noise figure followed by an OBF with a 3 dB bandwidth of 1 nm and a 50 GHz photodiode.

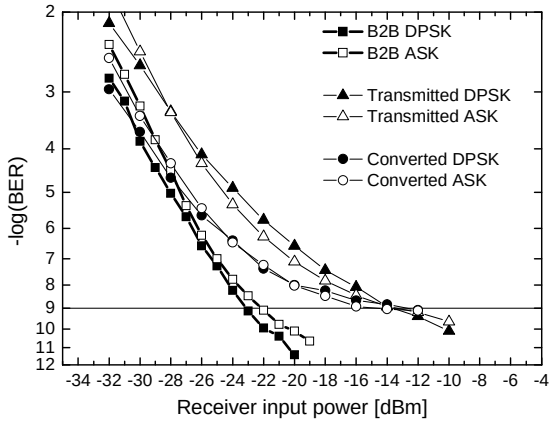

Figure 5.20: BER versus receiver input power. The BER is shown for both ASK and DPSK in back-to-back, wavelength converted and transmitted configuration.

5.7.3 Results and discussion

The eye-diagrams along the transmission link are seen in figure 5.23. The eye-diagrams at the transmitter, before the OPC and at the receiver are all seen. A strong deterioration of the eye-diagram due to the accumulated dispersion is seen after transmission over the first spool before the OPC. It can be seen how a clear and open eye is recovered at the receiver after transmission of the signal over the entire system. Some reshaping of the received eye-diagram compared to the transmitted is seen and attributed to the filtering necessary to select the converted signal.

BER measurements are performed in order to determined the power penalty. The receiver sensitivity of the back-to-back signal is -26.6 dBm and a power penalty of 0.7 dB is measured. The two BER curves of the back-to-back and transmission signals can be seen in figure 5.24. The inset in figure 5.24 shows the output spectrum of the HNL-PCF. The power penalty is attributed to the different amounts of dispersion accumulated before and after the OPC, based on the length difference of the two spools. The dispersion slope of the PCF, of the order 0.067 ps/(nm^2·km) does not contribute much to the difference in accumulated dispersion by the signal and the converted signal spaced 6.4 nm apart.

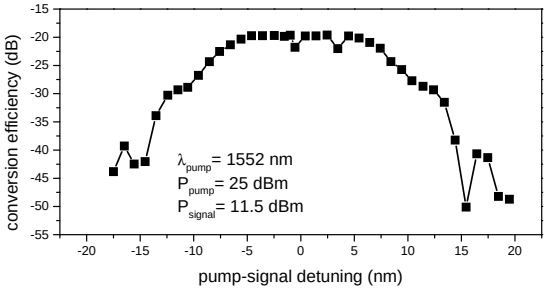

Figure 5.21: Conversion efficiency against pump-signal detuning.

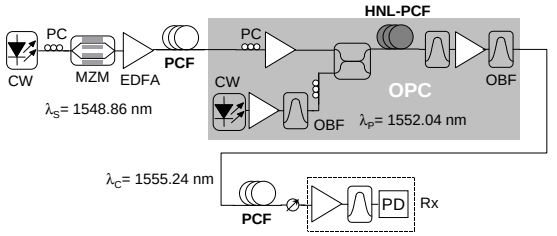

Figure 5.22: Schematic of the experimental setup. CW: continuous-wave laser, PC: polarization controller, OBF: optical bandpass filter, OPC: optical phase conjugator, Rx: receiver

5.7.4 Conclusion

A demonstration of 40 Gbit/s signal transmission through 5.6 km of PCF has been performed. Simultaneous wavelength conversion and dispersion compensation are achieved by using a HNL-PCF and FWM to realize optical phase conjugation of the signal. A power penalty of 0.7 dB is measured after transmission over the 5.6 km PCF transmission link. By optimizing the two PCF spools the power penalty could be reduced.

5.8 Summary

It has been shown how a 50 m long HNL-PCF works as a wavelength converter for a 40 Gbit/s RZ-DPSK signal using FWM with a conver-

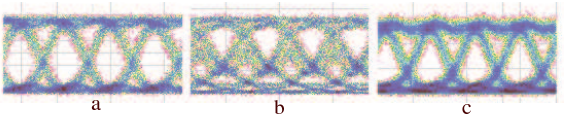

Figure 5.23: Eye diagrams (a) at modulator output, (b) after 2.6 km PCF (c) after 2.6 km PCF, OPC and 3 km PCF. Horizontal scale is 10 ps/division

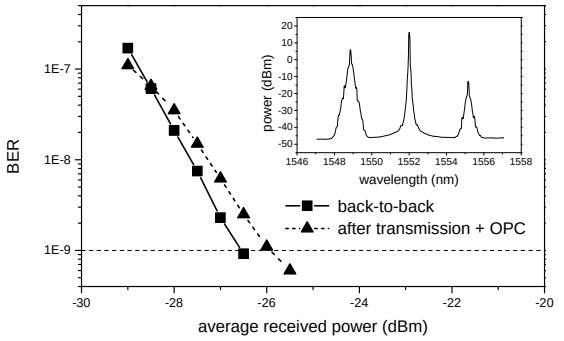

Figure 5.24: BER curves for back-to-back and after transmission through 5.6 km link. Inset: Spectrum at output of HNL-PCF (0.1 nm resolution bandwidth)

sion efficiency of −20 dB for a conversion band of 31 nm. The wavelength conversion to shorter wavelengths is limited by the performance of the EDFA in the receiver and the tunability of optical bandpass filters. It is also shown how the quality of the signal is maintained during the wavelength conversion process. Wavelength conversion of a 6×40 Gbit/s DPSK WDM signal has been demonstrated. The converted channels all have a conversion efficiency better than −20.6 dB and a deviation of less than 3 dB was achieved.

A multilevel modulation format experiment generating an 80 Gbit/s RZ-DPSK-ASK signal using 40 Gbit/s equipment is discussed. The HNL-PCF is also used in this experiment as the medium for wavelength conversion using FWM. The wavelength converted signal has been successfully transmitted over a fiber span consisting of 80 km SMF and 13 km DCF.

Again the eye-diagrams and waveforms were seen to be well maintained and BER measurements showed good performance of the system.

The HNL-PCF used has been proven to be a very good candidate for transparent optical wavelength conversion of RZ-DPSK signals, WDM DPSK signals and multi-level ASK-DPSK signals at high data rate using FWM in the C-band.

A HNL-PCF with a nonlinear coefficient of $\gamma \sim 17\ \mathrm{W}^{-1}\times\mathrm{km}^{-1}$ is used in an optical phase conjugator in order to dispersion compensate a PCF transmission link. The transmission of a 40 Gbit/s signal over 5.6 km of PCF is only possible when an OPC is used. Optical phase conjugation as a way of dispersion compensation is not very practical because the fiber link should be designed for this process. The wavelength conversion achieved on the basis of the OPC shows very little power penalty to the transmission. The design of the HNL-PCF makes it a good candidate for OPC and wavelength conversion by FWM.

The two HNL-PCF, used in this chapter in wavelength conversion experiments show a clear place for HNL-PCFs in optics. Wavelength conversion based on FWM is a powerful tool that is transparent to both modulation format and speed of the optical signal. The fiber used in an all-optical system has to be designed especially in order to accommodate the feasibility of wavelength conversion. It has been shown how the PCF technology makes it possible to achieve this by designing a HNL-PCF with the right dispersion profile and a nonlinear coefficient large enough to accommodate the FWM process and thereby achieve the desired result.

Chapter 6

Conclusion

The increased capacity demands placed on telecommunication systems might transform the current telecommunication networks into all-optical systems where signal data rates surpass the electronic boundary that currently exists at 40 Gbit/s [4]. In order to avoid electronic bottlenecks, existing electro-optical components must be changed into all-optical components. That means transforming components such as regenerators, wavelength converters and demultiplexers, just to mention a few.

The term "a transparent" system needs to be defined when an all-optical system is considered. An all-optical communication system is considered transparent when the system is independent of the bit rate and modulation format used. By increasing the bit rate the tolerance of the system becomes increasingly difficult to satisfy. A number of effects needs consideration by the network designer, such as chromatic dispersion or polarization mode dispersion. Different modulation formats have different chromatic dispersion tolerances e.g. a 40 Gbit/s NRZ signal provides a tolerance margin within ± 70 ps/nm for a 1 dB receiver sensitivity penalty (measured in a PIN receiver). In comparison to the NRZ modulation format a RZ modulation format has the tolerance reduced to ± 30 ps/nm for a 33% duty cycle transmitter [110].

The choice of modulation format puts strict limitations on the design of the all-optical components needed in order to build a fiber link. Increasing the bit rates beyond the electronic boundary can be done by using OTDM. In using OTDM RZ modulation is required in order to multiplex the data signals.

A phase preserving wavelength converter makes it possible to use different modulation formats such as DPSK, ASK or a combination of the two in the system. Choosing a modulation format for a system requires careful consideration [111] and can have an effect on which optical components can be used in the system.

6.1 Summary

The use of HNL-PCF in optical communication systems has been investigated in this thesis. The investigation has been done with respect to the future of telecommunications in an all-optical system. The PCFs used have all been used for all-optical signal processing as part of an optical component.

A large part of the work performed for this thesis has been on supercontinuum generation in a HNL-PCF and the use of such a supercontinuum in a system experiment. It has been shown how a supercontinuum generated by a HNL-PCF could form the basis for a multi-wavelength pulse source in a WDM system. The thinking behind using a supercontinuum in an optical system is the same whether the fiber is a HNLF or a HNL-PCF, but the extra possibilities given by the freedom of design of the PCF technology appeals to using a HNL-PCF for a WDM source. The possibility of single-mode guidance at all wavelengths and the possibility of large differences between the refractive indices of the core and the cladding by using air-holes, makes PCFs suited for custom made components. By testing a HNL-PCF as a medium for supercontinuum generation at various dispersion values and at the same time using that supercontinuum in an optical system showed the importance of the fiber design.

Different HNL-PCFs were tested for supercontinuum generation with the widest spectrum seen to be 210 nm (20 dB bandwidth). A comparison between two supercontinua generated by two different HNL-PCFs with different dispersion profiles, but similar nonlinear coefficient, showed the dependence of supercontinuum on the dispersion in the HNL-PCF. It is not only the generation of a supercontinuum that is dependent on the dispersion in the fiber, but also the slicing of the supercontinuum. An experiment using supercontinuum covering both the C- and L-band and having a 20 dB bandwidth of $\sim$ 70 nm was discussed.

A comparison between different pulse sources also showed the importance of low timing and amplitude jitter in the pulse source. The strict requirements on the pulse source and the fiber design in order to get a broad supercontinuum limits the choice of modulation format of the signal. The modulation format is also dependent on transmission in the optical system and dependent on the pulse source used to generate the supercontinuum.

It is believed that by satisfying strict demands on the pulse sources and the fiber design, could the use of a supercontinuum in a commercial optical system become a possibility in the near future. In this thesis the supercontinua have all been generated using a 10 GHz pulse train, but higher repetition rates such as 40 or 160 GHz are also possible due to the speed of the Kerr-effect [48].

For bit rates higher than 40 Gbit/s all-optical regeneration is the only possible way of regenerating a signal with the current technology. Transforming the current telecommunication network into an all-optical network will require an all-optical regeneration of the optical signal. At the current time (May 2005) all-optical regeneration is a tool only used in laboratory experiments for regeneration of signals with bit rates of 80 and 160 Gbit/s or higher. One method of 3R-regeneration was discussed in this thesis. The well known NOLM configuration was used as a part of the setup in an attempt of achieving regeneration of an optical signal. More successful 3R-regeneration experiments have been reported [40] for high speed signals.

An extensive investigation into using HNL-PCF as part of an all-optical wavelength converter has been performed in chapter 5. Especially FWM has been used in order to perform wavelength conversion since FWM is a transparent process. Using a HNL-PCF with a flattened dispersion profile, a 40 Gbit/s RZ-DPSK signal was wavelength converted over 31 nm. The same fiber was also used when showing the wavelength conversion of a 6×40 Gbit/s DPSK signal. The conversion efficiency was found to be better than -21 dB in both cases. Using a HNL-PCF as an integral part of a transparent all-optical wavelength converter shows one of the many possible applications for a HNL-PCF in optical systems.

A combination of a HNL-PCF and FWM generates a very powerful tool for all-optical wavelength conversion. The transparency of an optical system is tested by mixing different modulation formats. By using

40 Gbit/s equipment and combining two different modulation formats a signal rate of 80 Gbit/s is achieved. The 80 Gbit/s RZ-DPSK-ASK signal is wavelength converted in a HNL-PCF using FWM. With a conversion efficiency better than -19 dB and a wavelength conversion over ~ 10 nm a simple but efficient all-optical wavelength converter was realized.

The dispersion profile of a fiber remains one of the most important parameters to control for the fiber designer. The manufacturing of a HNL-PCF with negative dispersion slope and zero dispersion wavelength in the C-band made it possible to build an OPC using this fiber. Optical phase conjugation is one way of dispersion compensating a fiber span. The experiment performed in chapter 5 shows that, by using optical phase conjugation in a HNL-PCF, a successful transmission over a PCF fiber link is made possible. Without the optical phase conjugation component, transmission of a 40 Gbit/s signal would not have been possible due to dispersion in the fiber link.

Two methods of characterizing a fiber are also presented. An interferometric dispersion measurement technique and a technique for measuring the nonlinear coefficient of a fiber are used to obtain measurement results from various PCFs. The dispersion of a PCF was measured over 1100 nm and a zero dispersion wavelength at 1064 nm was found.

The results obtained in the work presented in this thesis show that PCF technology and especially HNL-PCF can be used in an all-optical system for signal processing.

6.2 Future work

When designing an all-optical telecommunication system a multitude of different problems needs to be addressed. The research in electronic equipment and the possibility of network vendors of getting an upgrade to 40 GHz components will force an increase in high speed optical research. The limits of the electronic components keep pushing the lower boundary of an all-optical system to higher bit rates. OTDM is one of the answers to getting higher bit rates and has been used extensively in laboratory experiments as a way of achieving bit rates exceeding 160 Gbit/s [62].

Using OTDM, different aspects of an optical system have been investigated at high bit rates [112] such as dispersion tolerance and polarization mode dispersion. With the lack of commercial investment in OTDM

technology it will remain a tool for testing high speed optical systems in laboratory environments. OTDM has a number of benefits compared to WDM such as, a reduced number of opto-electronic components, simplification of network maintenance due to reduced number of paths, more compactly terminals and consequent a reduction of terminal space costs.

The use of HNL-PCF in optical communication systems will mainly occur in components such as wavelength converters or as part of an multi-wavelength pulse source. The possibility of designing a HNL-PCF with very specific design parameters can help generate compact all-optical wavelength converters or a multi-wavelength pulse source. The future of PCFs in telecommunication systems is closely connected to the progress in fiber design.

Bibliography

[1] H. Ishio, J. Minowa, and K. Nosu, "Review and status of wavelength-division-multiplexing technology and its application," vol. LT-2, pp. 448–463, August 1984.

[2] J. Devaney, "The Great Telecoms Crash: Where did it all go wrong," *Fibresystems Europe*, pp. 40–42, September 2002.

[3] T. Enoki, "InP-based HEMT Technologies toward 100 Gbit/s ICs," in *Proceedings of Indium Phosphide and Related Materials Conference (IPRM) 2002*, 2002, pp. B6–1 (invited).

[4] "SHF Communication Technologies AG http://www.shf-communication.de," May 2005.

[5] S. Watanabe and F. Futami, "All-optical wavelength conversion using ultra-fast nonlinearities in optical fiber," *IEICE TRANS. ELECTRON.*, vol. E85-C, no. 4, pp. 889–895, April 2002.

[6] J. Knight, T. Birks, P. Russell, and D. Atkin, "All-silica single-mode optical fiber with photonic crystal cladding," *Optics Letters*, vol. 21, no. 19, pp. 1547–1549, 1996.

[7] J. C. Knight, T. A. Birks, P. S. Russell, and D. M. Atkin, "All-silica single-mode optical fiber with photonic crystal cladding:errata," *Optics Letters*, vol. 22, no. 7, pp. 484–485, April 1997.

[8] P. Russell, "Photonic crystal fibers," *Science*, vol. 299, no. 5605, pp. 358–362, January 2003.

[9] M. van Eijkelenborg, M. Large, A. Argyros, J. Zagari, S. Manos, N. A. Issa, I. M. Bassett, S. C. Fleming, R. C. McPhedran, C. M.

de Sterke, and N. A. P. Nicorovici, "Microstructured polymer optical fibre," *Opticics Express*, vol. 9, no. 7, pp. 319–327, Sept. 2001.

[10] M. Lehtonen, G. Genty, H. Ludvigsen, and M. Kaivola, "Supercontinuum generation in a highly birefringent microstructured fiber," *Applied Physics Letters*, vol. 82, no. 14, pp. 2197–2199, 2003.

[11] K. M. Hilligsøe, H. N. Paulsen, J. Thøgersen, S. R. Keiding, and J. J. Larsen, "Initial steps of supercontinuum generation in photonic crystal fibers," *Journal of the Optical Society of America - B - Optical Physics*, vol. 20, no. 9, pp. 1887–1893, 2003.

[12] Z. Yusoff, P. Petropoulos, K. Furusawa, T. M. Monro, and D. J. Richardson, "A 36-channel x 10-GHz spectrally sliced pulse source based on supercontinuum generation in normally dispersive highly nonlinear holey fiber," *IEEE Photonics Technology Letters*, vol. 15, no. 12, pp. 1689–1691, Dec. 2003.

[13] L. Boivin, S. Taccheo, C. Doerr, P. Schiffer, L. Stulz, R. Monnard, and W. Lin, "400 Gbit/s transmission over 544 km from spectrum-sliced supercontinuum source," *Electronics Letters*, vol. 36, no. 4, pp. 335–336, 2000.

[14] J. H. Lee, W. Belardi, K. Furusawa, P. Petropoulos, Z. Yusoff, T. M. Monro, and D. J. Richardson, "Four-wave mixing based 10-Gb/s tunable wavelength conversion using a holey fiber with a high SBS threshold," *IEEE Photonics Technology Letters*, vol. 15, no. 3, pp. 440–442, 2003.

[15] A. Siahlo, L. Oxenlowe, K. Berg, A. Clausen, P. Andersen, C. Peucheret, A. Tersigni, P. Jeppesen, K. Hansen, and J. Folkenberg, "A high-speed demultiplexer based on a nonlinear optical loop mirror with a photonic crystal fiber," *IEEE Photonics Technology Letters*, vol. 15, no. 8, pp. 1147–1149, August 2003.

[16] E. Yablonovitch, "Inhibited spontaneous emission in solid-state physics and electronics," vol. 58, no. 20, pp. 2059–2062, May 1987.

[17] S. John, "Strong localization of photons in certain disordered dielectric superlattices," vol. 58, no. 23, pp. 2486–2489, June 1987.

[18] K. P. Hansen, "Dispersion flattened hybrid-core nonlinear photonic crystal fiber," *Optics Express*, vol. 11, no. 13, pp. 1503–1509, June 2003.

[19] K. Hansen, J. Jensen, C. Jacobsen, H. Simonsen, J. Broeng, P. Skovgaard, and A. Petersson, "Highly nonlinear photonic crystal fiber with zero dispersion at 1.55 um," in *Technical Digest Optical Fiber Communication Conference, OFC'02*, vol. post-deadline, OFC2002-address, mar 2002, p. FA9.

[20] K. M. Hilligsøe, T. V. Andersen, H. N. Paulsen, C. K. Nielsen, K. Molmer, S. Keiding, R. Kristiansen, K. P. Hansen, and J. J. Larsen, "Supercontinuum generation in a photonic crystal fiber with two zero dispersion wavelengths," *Optics Express*, vol. 12, no. 6, pp. 1045–1054, March 2004.

[21] S. Diddams and J.-C. Diels, "Dispersion measurements with white-light interferometry," *Journal of the Optical Society of America - B - Optical Physics*, vol. 13, no. 6, pp. 1120–1129, 1996.

[22] P. A. Merritt, R. P. Tatam, and D. A. Jackson, "Interferometric chromatic dispersion measurements on short lengths of monomode optical fiber," vol. 7, no. 4, pp. 703–716, 1989.

[23] X. Yao and J. Feinberg, "Simple in-line method to measure the dispersion of an optical system," *Applied Physics Letters*, vol. 62, no. 8, pp. 811–813, 1993.

[24] B. Costa, D. Mazzoni, M. Puleo, and E. Vezzoni, "Phase shift technique for the measurement of chromatic dispersion in optical fibers using LEDs," *IEEE Transactions on Microwave Theory and Techniques*, vol. MTT-30, no. 10, pp. 1497–503, 1982.

[25] S. Ryu, Y. Horiuchi, and K. Mochizuki, "Novel chromatic dispersion measurement method over continuous Gigahertz tuning range," vol. 7, no. 4, pp. 1177–1180, 1989.

[26] G. P. Agrawal, *Fiber-Optic Communication Systems*, 2nd ed., K. Chang, Ed. John Wiley & sons, Inc., 1997.

[27] A. Boskovic, S. Chernikov, J. Taylor, L. Grüner-Nielsen, and O. Levring, "Direct continuous-wave measurement of n_2 in various types of telecommunication fiber at 1.55 μm," *Optics Letters*, vol. 21, no. 24, pp. 1966–8, December 1996.

[28] L. Grüner-Nielsen, A. Boskovic, S. Chernikov, and J. Taylor, "Measurement of nonlinear refractive index n_2 of dispersion compensating fibres," in *Proceedings European Conference on Optical Communication, ECOC'96*, vol. 2, Oslo, Norway, september 1996, pp. 249–252 vol.2.

[29] H. Cristiani, R. Tediosi, L. Tartara, and V. Degiorgio, "Dispersive wave generation by solitons in microstructured optical fibers," *Optics Express*, vol. 12, no. 1, pp. 124–135, January 2004.

[30] S. A. Diddams, D. J. Jones, J. Ye, S. T. Cundiff, J. L. Hall, J. K. Ranka, R. S. Windeler, R. Holzwarth, T. Udem, and T. W. Hansch, "Direct link between microwave and optical frequencies with a 300 thz femtosecond laser comb,," vol. 84, p. 51025105, 2000.

[31] I. Hartl, X. D. Li, C. Chudoba, R. K. Ghanta, T. H. Ko, J. G. Fujimoto, J. K. Ranka, and R. S. Windeler, "Ultrahighresolution optical coherence tomography using continuum generation in an air-silica microstructured optical fiber," *Optics Letters*, vol. 26, pp. 608–610, 2001.

[32] L. Boivin and B. C. Collings, "Spectrum slicing of coherent sources in optical communications," *Optical Fiber Technology*, vol. 7, pp. 1–20, 2001.

[33] H. Sotobayashi, W. Chujo, A. Konishi, and T. Ozeki, "Wavelength-band generation and transmission of 3.24-Tbit/s (81-channel WDM*40-Gbit/s) carrier-suppressed return-to-zero format by use of a single supercontinuum source for frequency standardization," *Journal of the Optical Society of America - B - Optical Physics*, vol. 19, no. 11, pp. 2803–9, 2002.

[34] H. Takara, T. hara, T. Yamamoto, H. Masuda, M. Abe, H. Takahashi, and T. Morioka, "Field demonstration of over 1000-channel

DWDM transmission with supercontinuum multi-carrier source," *Electronics Letters*, vol. 41, no. 5, pp. 270–271, March 2005.

[35] N. I. Nikolov, O. Bang, and A. Bjarklev, "Designing the dispersion for optimum supercontinuum bandwidth using picosecond pulses," in *Technical Digest Optical Fiber Communication Conference, OFC'03*, vol. 1, Atlanta, Georgia, U.S.A., March 2003, p. MF16.

[36] S. Taccheo and L. Boivin, "Investigation and design rules of supercontinuum sources for WDM applications," 2000, pp. 2–4.

[37] P. A. Andersen, B. Zsigri, C. Peucheret, P. Jeppesen, K. P. Hansen, and M. Dybendal Nielsen, "Photonic Crystal Fibers used in a Multi-Wavelength Source and as a Transmission Fiber in a WDM system," in *Proceedings Conference on Lasers & Electro-Optics*. CLEO, May 2004.

[38] Z. Yusoff, P. Petropoulos, K. Furusawa, W. Belardi, T. Monro, and D. Richarson, "24 channels x 10 GHz spectrally sliced pulse source based on spectral broading in a highly nonlinear holey fiber," in *Technical Digest Optical Fiber Communication Conference, OFC'03*, vol. 2, Atlanta, Georgia, U.S.A., March 2003, pp. 687–689.

[39] P. A. Andersen, C. Peucheret, K. M. Hilligsøe, K. S. Berg, K. P. Hansen, and P. Jeppesen, "Supercontinuum generation in a photonic crystastal fibre using picosecond pulses at 1550 nm," in *5th International Conference on Ttansparent Optical Networks*, vol. 1, Warsaw, Poland, June 2003, p. Mo.C1.6.

[40] S. Watanabe, F. Futami, R. Okabe, Y. Takita, A. Ferber, R. Ludwig, C. Schubert, C. Schmidt, and H. G. Weber, "160 Gbit/s optical 3R-regenerator in a fiber transmission experiment," 2003, pp. PD16–1–3.

[41] X. Gu, M. Kimmel, A. P. Shreenath, R. Trebino, J. M. Dudley, S. Coen, and R. S. Windeler, "Experimental studies of the coherence of microstructure-fiber supercontinuum," *Optics Express*, vol. 11, no. 21, pp. 2697–2703, October 2003.

[42] S. Coen, A. H. L. Chau, R. Leonhardt, J. D. Harvey, J. C. Knight, W. J. Wadsworth, and P. S. J. Russell, "White-light supercontinuum generation with 60-ps pump pulses in a photonic crystal fiber," *Optics Letters*, vol. 26, no. 17, pp. 1356–1358, 2001.

[43] W. J. Wadsworth, A. Ortigosa-Blanch, J. C. Knight, T. A. Birks, T.-P. M. Man, and P. S. Russell, "Supercontinuum generation in photonic crystal fibers and optical fiber tapers: A novel light source," *Journal of the Optical Society of America - B - Optical Physics*, vol. 19, no. 9, pp. 2148–2155, 2002.

[44] S. Coen, A. H. L. Chau, R. Leonhardt, J. D. Harvey, J. C. Knight, W. J. Wadsworth, and P. S. J. Russell, "Supercontinuum generation by stimulated Raman scattering and parametric four-wave mixing in photonic crystal fibers," *Journal of the Optical Society of America - B - Optical Physics*, vol. 19, no. 4, pp. 753–764, 2002.

[45] A. V. Husakou and J. Herrmann, "Supercontinuum generation, four-wave mixing, and fission of higher-order solitons in photonic-crystal fibers," *Journal of the Optical Society of America - B - Optical Physics*, vol. 19, no. 9, pp. 2171–2182, 2002.

[46] J. Herrmann, U. Griebner, N. Zhavoronkov, A. Husakou, D. Nickel, J. Knight, W. Wadsworth, P. Russell, and G. Korn, "Experimental evidence for supercontinuum generation by fission of higher-order solitons in photonic fibers," *Physical Review Letters*, vol. 88, no. 17, pp. 173 901–1–4, 2002.

[47] A. L. Gaeta, "Nonlinear progagation and continuum generation in microstructured optical fibers," *Optics Letters*, vol. 27, no. 11, pp. 924–926, June 2002.

[48] G. P. Agrawal, *Nonlinear Fiber Optics*, third edition ed., P. L. Kelly, I. P. Kaminow, and G. P. Agrawal, Eds. Academic Press, 2001.

[49] A. Husakou and J. Herrmann, "Supercontinuum generation of higher-order solitons by fission in photonic crystal fibers," *Physical Review Letters*, vol. 87, no. 20, pp. 203 901/1–203 901/4, 2001.

[50] J. P. Gordon, "Theory of the soliton self-frequency shift," *Optics Letters*, vol. 11, no. 10, pp. 659–661, October 1986.

[51] J. M. Dudley, L. Provino, N. Grossard, H. Maillotte, R. S. Windeler, B. J. Eggleton, and S. Coen, "Supercontinuum generation in air-silica microstructured fibers with nanosecond and femtosecond pulse pumping," *Journal of the Optical Society of America - B - Optical Physics*, vol. 19, no. 4, pp. 765–771, 2002.

[52] A. Ortigosa-Blanch, J. C. Knight, and R. S. J. Russell, "Pulse breaking and supercontinuum generation with 200-fs pump pulses in photonic crystal fibers," *Journal of the Optical Society of America - B - Optical Physics*, vol. 19, no. 11, pp. 2567–2572, 2002.

[53] G. Genty, M. Lehtonen, H. Ludvigsen, J. Broeng, and M. Kaivola, "Spectral broadening of femtosecond pulses into continuum radiation in microstructured fibers microstructured fibers," *Optics Express*, vol. 10, no. 20, pp. 1083 – 1098, October 2002.

[54] Z. Zhu and T. G. Brown, "Effect of frequency chirping on supercontinuum generation in photonic crystal fibers," *Optics Express*, vol. 12, no. 4, pp. 689–694, Feb. 2004.

[55] J. Ames, S. Ghosh, R. Windeler, A. Gaeta, and S. Cundiff, "Excess noise generation during spectral broadening in a microstructured fiber," *Applied Physics B: Lasers and Optics*, vol. 77, pp. 279–284, 2003.

[56] N. R. Newbury, B. R. Washburn, K. L. Corwin, and R. S. Windeler, "Noise amplification during supercontinuum generation in microstructured fiber," *Optics Letters*, vol. 28, no. 11, pp. 944–946, June 2003.

[57] B. R. Washburn and N. R. Newbury, "Phase, timing, and amplitude noise on supercontinua generated in microstructure fiber," *Optics Express*, vol. 12, no. 10, pp. 2166–2175, May 2004.

[58] T. Hori, J. Takayanagi, N. Nishizawa, and T. Goto, "Flatly broadened, wideband and low noise supercontinuum generation in highly nonlinear hybrid fiber," *Optics Express*, vol. 12, no. 2, pp. 317–324, January 2004.

[59] M. D. Nielsen, A. Peterson, C. Jacobsen, H. R. Simonsen, G. Vienne, and A. Bjarklev, "All-silica photonic crystal fiber with large

mode area," in *Proceedings European Conference on Optical Communication, ECOC'02*, vol. 2, Copenhagen, Denmark, September 2002, p. 3.4.2.

[60] L. Krainer, R. Paschotta, G. Spuhler, I. Klimov, C. Teisset, K. Weingarten, and U. Keller, "Tunable picosecond pulse-generating laser with repetition rate exceeding 10 ghz," *Electronics Letters*, vol. 38, no. 5, pp. 225–227, February 2002.

[61] F. Futami and S. Watanabe, "All-optical data addition to a time slot in 160-Gb/s OTDM signal using wavelength conversion by supercontinuum in a nonlinear fiber," in *Proceedings European Conference on Optical Communication, ECOC'01*, Amsterdam, The Netherlands, September 2001, p. We.B.2.2.

[62] T. Yamamoto, E. Yoshida, K. R. Tamura, K. Yonenaga, and M. Nakazawa, "640-Gbit/s Optical TDM transmission over 92 km through a dispersion-managed fiber consisting of single-mode fiber and reverse dispersion fiber," *IEEE Photonics Technology Letters*, vol. 12, pp. 353–355, 2000.

[63] J. Seoane, A. I. Siahlo, A. T. Clausen, L. K. Oxenløwe, Z. Xu, and P. Jeppesen, "All optical 160 to 10 Gbit/s demultiplexing using co-propagating optical clock," 2004, p. CThQ4.

[64] M. Nakazawa, K. Suzuki, and E. Yamada, "NOLM oscillator and its injection locking technique for timing clock extraction and demultiplexing," *Electronics Letters*, vol. 32, no. 12, pp. 1122–1123, June 1996.

[65] H. Bulow, "Optoelectronic synchronisation scheme for ultrahigh-speed optical demultiplexer," *Electronics Letters*, vol. 31, no. 22, pp. 1937–1938, October 1995.

[66] W. Kuebart, B. Lavigne, M. Witte, G. Veith, and O. Leclerc, "40 Gb/s transmission over 80 000 km dispersion shifted fibre using compact opto-electronic-3R regeneration," in *Proceedings European Conference on Optical Communication, ECOC'03*, Rimini, Italy, September 2003, p. Mo.4.3.1.

[67] M. L. Nielsen, "Experimental and Theoretical investigation of Semiconductor Optical Amplifier (SOA) based All-Optical Switches," Ph.D. dissertation, Research Center COM, Technical University of Denmark, April 2004.

[68] B. Lavigne, E. Balmefrezol, P. Brindel, B. Dagens, R. Brenot, L. Pierre, J.-L. Moncelet, D. d. l. Grandière, J.-C. Remy, J.-C. Bouley, B. Thedrez, and O. Leclerc, "Low input power All-Optical 3R Regenerator based on SOA devices for 42.66 Ggit/s ULH WDM RZ transmission with 23dB span loss and all-EDFA amplification," in *Technical Digest Optical Fiber Communication Conference, OFC'03*, Atlanta, Georgia, U.S.A., March 2003, pp. PD15–1.

[69] B. Lavigne, E. Balmefrezol, P. Brindel, L. Pierre, B. Dagens, R. Brenot, B. Thedrez, M. Renaud, and O. Leclerc, "Operation margins of a SOA-based 3R regenerator for 42.66Gbit/s ULH transmission systems," in *Proceedings European Conference on Optical Communication, ECOC'03*, Rimini, Italy, September 2003, p. Mo. 4.3.4.

[70] C. Schubert, R. Ludwig, S. Watanabe, F. Futami, C. Schmidt, J. Berger, C. Boerner, S. Ferber, and H. Weber, "160 gbit/s wavelength converter with 3r-regenerating capability," *Electronics Letters*, vol. 38, no. 16, pp. 903–904, August 2002.

[71] P. Ohlen and E. Berglind, "Noise accumulation and BER estimates in concatenated nonlinear optoelectronic repeaters," *IEEE Photonics Technology Letters*, vol. 9, no. 7, pp. 1011–1013, 1997.

[72] J. Mørk, F. Ohman, and S. Bischoff, "Analytical expression for the bit error rate of cascaded all-optical regenerators," *IEEE Photonics Technology Letters*, vol. 15, no. 10, pp. 1479–1481, 2003.

[73] E. Ciaramella and S. Trillo, "All-optical signal reshaping via four-wave mixing in optical fibers," *IEEE Photonics Technology Letters*, vol. 12, pp. 849–851, July 2000.

[74] P. V. Mamyshev, "All-optical data regeneration based on self-phase modulation effect," in *Proceedings European Conference on Optical Communication, ECOC'98*, Madrid, Spain, sep 1998, p. 475.

[75] K. K. Chow, C. Shu, L. Chinlon, and A. Bjarklev, "All-Optical restoration by spectral filtering of Self-Phase Modulation in nonlinear photonic crystal fiber," in *Proceedings European Conference on Optical Communication, ECOC'04*, vol. 3, Stockholm, Sweden, September 2004, p. P104.

[76] T.-H. Her, G. Raybon, and C. Headley, "Optimization of pulse regeneration at 40 gb/s based on spectral filtering of self-phase modulation in fiber," *IEEE Photonics Technology Letters*, vol. 16, no. 1, pp. 200–202, 2004.

[77] B.-E. Olsson and D. Blumenthal, "Pulse restoration by filtering of self-phase modulation broadened optical spectrum," *Journal of Lightwave Technology*, vol. 20, no. 7, pp. 1113–1117, 2002.

[78] M. Nakazawa, K. Tamura, H. Kubota, and E. Yoshida, "Coherence degradation in the process of supercontinuum generation in an optical fiber," *Optical Fiber Technology: Materials, Devices, and Systems*, vol. 4, no. 2, pp. 215–223, 1998.

[79] M. Nakazawa, H. Kubota, and K. Tamura, "Random evolution and coherence degradation of a high-order optical soliton train in the presence of noise," *Optics Letters*, vol. 24, no. 5, pp. 318–320, 1999.

[80] A. Bogoni, in *Proceedings European Conference on Optical Communication, ECOC'03*, Rimini, Italy, September 2003, p. Th2.5.6.

[81] L. Chusseau and E. Delevaque, "250-fs optical pulse generation by simultaneous soliton compression and shaping in a nonlinear optical loop mirror including a weak attenuation," *Optics Letters*, vol. 19, no. 10, pp. 734–736, May 1994.

[82] P. K. A. Wai and W.-h. Cao, "Ultrashort soliton generation through higher-order soliton compression in a nonlinear optical loop mirror constructed from dispersion-decreasing fiber," *Journal of the Optical Society of America - B - Optical Physics*, vol. 20, no. 6, pp. 1346–1355, June 2003.

[83] G. Rauschenbach, K. Hall, J. Livas, and G. Raybon, "All-optical pulse width and wavelength conversion at 10 Gb/s using a nonlinear

optical loop mirror," *IEEE Photonics Technology Letters*, vol. 6, no. 9, pp. 1130–1132, September 1994.

[84] P. Kaewplung, in *APCCAS'02*, vol. 2, 2002, pp. 215–218.

[85] R. Ludwig, S. Diez, A. Ehrhardt, L. Kueller, W. Pieper, and H. G. Weber, "Tunable femtosecond modelocked semiconductor laser for applications in otdm-systems," *IEICE Transactions on Electronics*, vol. E81-C, no. 2, pp. 140–145, 1998.

[86] "http://www.okisemi.com/eu/," May 2005.

[87] M. Scaffardi, P. Ghelfi, A. Bogoni, and L. Poti, "Investigation and solution for undesirable counter-propagating effects in nonlinear optical loop mirrors," in *Proceedings Conference on Lasers & Electro-Optics*, San Francisco, USA, 2004, p. CThEE7.

[88] A. Bogoni, M. Scaffardi, P. Ghelfi, and L. Poti, "Nonlinear optical loop mirrors: investigation solution and experimental validation for undesirable counterpropagating effects in all-optical signal processing," *IEEE Journal of Elected Topics in Quantum Electronics*, vol. 10, no. 5, pp. 1115 – 1123, Sept.-Oct. 2004.

[89] S. Yoo, "Wavelength conversion technologies for WDM network applications," *Journal of Lightwave Technology*, vol. 14, no. 6, pp. 955–966, 1996.

[90] K. E. Stubkjaer, "Semiconductor optical amplifier-based all-optical gates for high-speed optical processing," *IEEE Journal on Selected Topics in Quantum Electronics*, vol. 6, no. 6, pp. 1428–1435, November/December 2000.

[91] P. Ohlen, B.-E. Olsson, and D. J. Blumenthal, "Wavelength dependence and power requirements of a wavelength converter based on xpm in a dispersion-shifted optical fiber," *IEEE Photonics Technology Letters*, vol. 12, no. 5, pp. 522–524, 2000.

[92] T. Sakamoto, F. Futami, K. Kikuchi, S. Takeda, Y. Sugaya, and S. Watanabe, "All-optical wavelength conversion of 500-fs pulse trains by using a nonlinear-optical loop mirror composed of a highly

nonlinear DSF," *IEEE Photonics Technology Letters*, vol. 13, no. 5, pp. 502–504, 2001.

[93] J. H. Lee, Z. Yusoff, W. Belardi, M. Ibsen, T. Monro, and D. Richardson, "A tunable WDM wavelength converter based on cross-phase modulation effects in normal dispersion holey fiber," *IEEE Photonics Technology Letters*, vol. 15, no. 3, pp. 437–439, 2003.

[94] K. Inoue, "Four-wave mixing in an optical fiber in the zero-dispersion wavelength region," *Journal of Lightwave Technology*, vol. 10, no. 11, pp. 1553–1561, November 1992.

[95] R. Tkach, A. Chraplyvy, F. Forghieri, A. Gnauck, and R. Derosier, "Four-photon mixing and high-speed WDM systems," *Journal of Lightwave Technology*, vol. 13, no. 5, pp. 841–849, May 1995.

[96] C. Xu, X. Liu, and X. Wei, "Differential phase-shift keying for high spectral efficiency optical transmissions," *IEEE Journal of Selected Topics in Quantum Electrinics*, vol. 10, no. 2, pp. 281–293, March/April 2004.

[97] K. J. Blow, N. J. Doran, B. K. Nayar, and B. P. Nelson, "Two-wavelength operation of the nonlinear fiber loop mirror," *Optics Letters*, vol. 15, no. 4, pp. 248–250, February 1990.

[98] K. Inoue and H. Toba, "Wavelength conversion experiment using fiber four-wave mixing," *IEEE Photonics Technology Letters*, vol. 4, no. 1, pp. 69–72, 1992.

[99] O. Aso, S.-I. Arai, T. Yagi, M. Tadakuma, Y. Suzuki, and S. Namiki, "Broadband four-wave mixing generation in short optical fibres," *Electronics Letters*, vol. 36, no. 8, pp. 709–711, 2000.

[100] O. Aso, S. Arai, T. Yagi, M. Tadakuma, Y. Suzuki, and S. Namiki, "Efficient FWM based broadband wavelength conversion using a short high-nonlinearity fiber," *IEICE Transactions on Electronics*, vol. 83, no. 6, pp. 816–823, 2000.

[101] N. Chi, J. Zhang, P. V. Holm-Nielsen, C. Peucheret, and P. Jeppesen, "Transmission and transparent wavelength conversion of an

optically labeled signal using ASK/DPSK orthogonal modulation," *IEEE Photonics Technology Letters*, vol. 15, no. 5, pp. 760–762, May 2003.

[102] Z. Li, Y. Dong, J. Mo, Y. Wang, and C. Lu, "Cascaded all-optical wavelength conversion for RZ-DPSK signal based on four-wave mixing in semiconductor optical amplifier," *IEEE Photonics Technology Letters*, vol. 16, no. 7, pp. 1685–1687, July 2004.

[103] K. K. Chow, C. Shu, L. Chinlon, and A. Bjarklev, "Widely tunable wavelength converter by four wave mixing in a dispersion-flattened nonlinear photonic crystal fiber," in *Proceedings European Conference on Optical Communication, ECOC'04*, vol. 2, Stockholm, Sweden, September 2004, pp. 188–189.

[104] C. Peucheret, B. Zsigri, P. Andersen, K. Berg, A. Tersigni, P. Jeppesen, K. P. Hansen, and M. D. Nielsen, "40 Gbit/s transmission over photonic crystal fibre using mid-span spectral inversion in highly nonlinear photonic crystal fibre," *Electronics Letters*, vol. 39, no. 12, pp. 919–921, 2003.

[105] M. Ohm and J. Speidel, "Quaternary optical ASK-DPSK and receivers with direct detection," *IEEE Photonics Technology Letters*, vol. 15, no. 1, pp. 159–161, 2003.

[106] R. A. Griffin, R. I. Johnstone, R. G. Walker, J. Hall, S. D. Wadsworth, K. Berry, A. C. Carter, M. J. Wale, P. A. Jerram, and N. J. Parsons, "10 Gb/s optical differential quadrature phase shift key (DQPSK) transmission using GaAs/AlGaAs integration," in *Technical Digest Optical Fiber Communication Conference, OFC'02*, Anaheim, California, U.S.A., mar 2002, p. FD6.

[107] K. Sekine, N. Kikuchi, S. Sasaki, S. Hayaseand, C. Hasegawa, and T. Sugawara, "Proposal and demonstration of 10 Gsymbol/sec 16-ary (40 Gbit/s) optical modulation / demodulation scheme," in *Proceedings European Conference on Optical Communication, ECOC'04*, vol. 3, Stockholm, Sweden, September 2004, p. We3.4.5.

[108] N. Yoshikane and I. Morita, "1.14 b/s/Hz spectrally-efficient 50×85.4 Gb/s transmission over 300 km using copolarized CS-RZ

DQPSK signals," in *Technical Digest Optical Fiber Communication Conference, OFC'04*, Los Angeles, California, U.S.A., Febuary 2004, p. PDP38.

[109] C. Peucheret, B. Zsigri, P. A. Andersen, K. S. Berg, A. Tersigni, P. Jeppesen, K. P. Hansen, and M. D. Nielsen, "Transmission over photonic crystal fiber at 40 Gbit/s using mid-span spectral inversion in a highly nonlinear photonic crystal fiber," in *Technical Digest Conference on Lasers and Electro-Optics, CLEO'03*, Baltimore, Maryland, U.S.A, 2003, pp. post–deadline paper CThPDB4.

[110] A. B. Azcoaga, "40 Gb/s optical transmission systems," Ph.D. dissertation, Research Center COM, DTU, Technical University of Denmark, Kgs. Lyngby DK-2800, Denmark, October 2003.

[111] T. Tokle, "Optimised dispersion management and modulation formats for high speed optical communications systems," *Research Center COM, DTU*, vol. 2004, pp. Technical University of Denmark, Kgs. Lyngby, DK–2800, Denmark, September.

[112] A. T. Clausen, L. K. Oxenløwe, A. I. Siahlo, J. Seoane, and P. Jeppesen, "Experimental and theoretical investigation of systems with potential for terabit capacity," in *SPIE International Symposium on Information Technology and Communication (ITCOM 2004)*, Philadelphia, Pennsylvania, USA, October 2004, pp. 5596–5609.